Università degli Studi di Genova

DITEN - Dipartimento di ingegneria navale, elettrica, elettronica e delle telecomunicazioni

Doctoral Thesis

Modelling energy efficiency of complex ship propulsion systems, considering sludge recycling, exhaust gas recovery and Flettner rotors.

Author:
Veronica Vigna

Supervisor:
Prof. Massimo Figari
Co-Supervisor:
Prof. Marco Altosole

A thesis submitted in fulfillment of the requirements
for the degree of Doctor of Philosophy in the

PhD Course of Science and technology for Electrical Engineering, Marine Engineering, Complex Systems for mobility
Curriculum: Marine Engineering

XXXIV Cycle 2018-2021

"We cannot change the wind but we can adjust the sails in the right direction."

Aristotle

]

Abstract

Energy efficiency has become increasingly important during the recent years due to the negative effects of the anthropogenic activities on the environment; in the maritime field IMO is leading a steep slope down policy on Greenhouse gas emission reduction by enacting stricter rules at a fast pace. In addition to the environmental and legal aspects, a key driver for increasing energy efficiency is operational cost savings due to fuel consumption reduction.

In this framework, the thesis focuses on the improvement of the energy efficiency of the ship propulsion plant by analysing different kind of innovative technologies. Modelling and simulation techniques and appropriate key parameter indicators have been extensively used to provide a suitable metric for bench-marking the different solutions. The reason behind the choice to analyse different technologies is because a well defined solution does not exist. Different ship types and different operational conditions may trigger different options.

The first way investigated to improve energy efficiency was by means of an innovative technology to transform sludge into new recycled marine fuel oil through a pyrolysis process carried out in a small reactor onboard. A passenger ship was chosen as a case study due to the advantageous large amounts of waste oil involved and the space availability. The feasibility study and the analysis of fuel consumption reduction and EEOI criticalities are reported: the results showed an easy integration of the system inside the incinerator and a reduction of time and costs; about the environmental aspect, the EEOI formula is not suitable for this innovative technologies and the attempt made to calculate it was unsatisfactory. The results are interesting but not good enough to justify the necessary expenditure investment, also in lieu of the non-calculable impact on the efficiency index.

The second investigated solution to further improve the ship efficiency was an innovative flexible propulsion and power system with recovery technologies, studied in collaboration with an Italian shipping company. In the propulsion plant there are dual fuel engines coupled with waste heat recovery systems, innovative hybrid turbocharger and electric power shaft motor/generators. In addition to the description of the propulsion plant and its various modes of use, different configurations are analysed in terms of efficiency and costs and the plant was tested with and without the various recovery systems and with natural gas and HFO, referring to the routes currently travelled by the model ship (a Ro-Ro ferry). The results are expressed as a function of the ship speed: for a given speed and a chosen plant configuration (which recovery systems to consider), the best plant mode of use, among the main three described, is chosen, which means the one associated with the minimum fuel expense. The results showed that the Normal Navigation scenario is the one associated with the lowest

fuel costs and highest plant efficiency, for all considered recovery systems. Moreover, they all allow considerable cost savings; in particular, the hybrid turbocharger is the more interesting because the low initial investment is paid off by considerable annual savings. On the other hand, the calculation of the EEDI for each plant configuration shows that only by combining WHRS and hybrid turbocharger together it is possible to respect the IMO limit.

After the analysis of said hybrid propulsion system, there was a need to go further to try to integrate renewable sources on board. Therefore the research moved to the wind assisted propulsion, which is gaining in popularity due to the expected benefit in emission reduction. A study was performed about the proper integration between the conventional diesel engine with controllable pitch propeller propulsion plant and the wind assisted plant with Flettner rotor. A mathematical model describing the behaviour of the rotor in terms of propulsive thrust and power is proposed; the rotor model was then integrated into a diesel propulsion model in order to evaluate the ship net fuel consumption for a given wind condition. The integrated propulsion model was written in parametric form. The methodology is intended to support the ship designer during the choice of the best possible propulsion diesel engine for a given rotor-propeller configuration, in addition it can be used to optimize the fuel consumption during the ship operation. A 3000 tons Ro-Ro/Pax ferry has been selected as case study; the results showed that a bigger rotor is always beneficial, that the best directions of incoming wind are from side to astern while the worst case is head wind, that the stronger the wind, the wider the range of suitable angle and that wind angle has a greater influence on the fuel consumption than the wind speed. With the optimized propulsion plant, remarkable double digit power savings can be observed in the whole range of ship speeds, while a 20% of fuel saving was achieved at the design ship speed.

The three developed numerical models allow to reduce the environmental impact of the ship and these simulators can be used as a tool to design or operate ships able to meet the present and future energy efficiency requirements. Decarbonisation and environmentally friendly innovations are the real challenges of our century. Therefore, the future of research is strongly linked to the improvement of the energy efficiency and the reduction of environmental impact.

Acknowledgements

I want to express my gratitude to Professor Figari for all the help, opportunities and kind support he has given me over the years and to Professor Altosole for conveying to me his curiosity about the subject and for the encouragement to undertake the path of research.

I want to thank Professor Campora, Professor Donnarumma, Professor Martelli and Professor Zaccone for their teaching and advice.

Grazie alla mia famiglia Laura, Mattia, Giorgio e Alberto per l'amore e il sostegno che sempre mi date.

Contents

List of Figures

List of Tables

List of Symbols

Abbreviations

Re   Reynolds number

AR   Aspect Ratio

B   Ship Beam

CAPEX CAPital EXpenditure

CII   Carbon Intensity Index

CO_2 Carbon dioxide

CPP   Controllable Pitch Propeller

DE   Diesel engine

DG   Diesel generator

ECA   Emission control area

EEDI   Energy Efficiency Design Index

EEOI   Energy Efficiency Operational Index

EEXI   Energy Efficiency Index for eXisting ships

EM/G Electric motor/generator

FPP   Fixed Pitch Propeller

FR   Flettner Rotor

GHG   Green House Gases

HFO   Heavy fuel oil

HRSG Heat Recovery Steam Generators

HTC   Hybrid turbocharger

KPI   Key Parameter Indicator

LNG   Liquefied natural gas

xvi

LOA   Ship Length OverAll

MCR   Maximum Continuous Rating

ME   Main engine

MEPC   Marine Environment Protection Committee

NO$_X$ Nitrogen oxides

SEEMP Ship Energy Efficiency Management Plan

SFOC   Specific Fuel Oil Consumption

SO$_X$ Sulphur oxides

SR   Spin Ratio

ST   Steam turbine

T   Ship draught

TC   Engine TurboCharger

UN   United Nations

WASP   Wind Assisted Ship Propulsion

WHRS   Waste heat recovery system

WHRS-ST Waste Heat Recovery System with Steam Turbine

Physics constants

ρ Sea water density = 1025 kg/m^3

ρ_{air} Air density = 1.225 kg/m^3

Symbols

α_{app} [deg] Incoming apparent wind direction in respect to the ship bow

α_{True} [deg] Incoming true wind direction in respect to the ship bow

$\dot{m}_{DG}$ [kg/s] Fuel mass flow rate in the diesel generator

$\dot{m}_{ME}$ [kg/s] Fuel mass flow rate in the main engines

η_g Gear efficiency

η_r Relative rotative efficiency

η_s Shaft line efficiency

η_{HS} Energy conversion efficiency of the high speed plant configuration

η_{LS} Energy conversion efficiency of the low speed plant configuration

η_{mr} Rotor transmission efficiency

η_{NN} Energy conversion efficiency of the normal navigation plant configuration

Ψ [rad] Yaw angle

$\underline{b}_i$ body-fixed base

$\underline{f}_i$ apparent wind frame

$\underline{F}_S$ Rotor Sway force

$\underline{n}_i$ inertial base

$\underline{R}_N$ Effective Net Resistance

$\underline{R}_H$ Hull Resistance in calm condition

$\underline{R}_T$ Total ship resistance

$\underline{R}_W$ Added air Resistance

$\underline{T}_P$ Propeller thrust

$\underline{T}_T$ Total ship thrust

$\underline{T}_{FR}$ Thrust generated by the rotor

a, b, c Coefficients of the engine power and torque equation

A_e/A_o Expanded blade area ratio of the propeller

$Area_S$ [m^2] Rotor lateral surface

C_D Drag Coefficient

C_f coefficient of Friction

C_L Lift Coefficient

D [N] Drag Force

d [m] Rotor diameter

d_e [m] Rotor end plate diameter

D_p [m] Propeller diameter

H_{DG} [MJ/kg] Diesel generator fuel lower heat value

H_{ME} [MJ/kg] Main engines fuel lower heat value

H_{rotor} [m] Rotor Height

i Gear ratio

J Wageningen propeller advance coefficient

K_Q Wageningen propeller torQue coefficient

K_T Wageningen propeller Thrust coefficient

L [N] Lift force

m_F [kg/s] Engine fuel flow

$m_{F_{MCR}}$ [kg/s] Engine fuel flow at maximum continuous rating

m_{Fd} [kg/s] Engine fuel flow at design conditions

n_e [rpm] Engine speed

n_p [rpm] Propeller rotational speed

n_{cyl} Engine's number of cylinders

$n_{e_{MCR}}$ [rpm] Engine speed at maximum continuous rating

n_{ed} [rpm] Engine speed at design conditions

n_{prop} Number of propellers

n_{rotor} Number of rotors

P/D Propeller Pitch over Diameter ratio

P_B [kW] Engine Break Power

P_O [kW] Openwater propeller Power

$P_{absspin}$ [kW] Mechanical Power Absorbed to Spin the rotor

$P_{B_{cyl}}$ [kW] Break Power per engine's cylinder

$P_{B_{MCR}}$ [kW] Engine brake power at maximum continuous rating

$P_{B_{propeller}}$ [kW] Power required by the propeller

$P_{B_{rotor}}$ [kW] Effective Power required to spin the rotor

P_{Bd} [kW] Engine brake power at design conditions

P_{hel} [kW] Ship hotel electrical power

P_{ME} [kW] Power of the main engines

P_{rec} [kW] Electric power of the energy recovery system

P_{TOT} [kW] Total ship propulsive Power

q_h [t/h] Engine hourly fuel consumption

Q_{Bd} [N m] Engine torque at design conditions

S_L [m^2] Longitudinal Ship projected area above waterline

S_T [m^2] Transverse Ship projected area above waterline

S_{rotor} [m^2] Longitudinal Rotor projected area

$sfoc$ [$\frac{kg}{kWh}$] Engine specific fuel oil consumption

t thrust deduction factor

U_{tan} [m/s] Flow tangential velocity

V_A [m/s] Advance velocity

w wake coefficient

x, y, z Exponents of the engine power and torque equation

V_{app} [m/s] Apparent wind speed

V_{ship} [knots] Ship speed

V_{True} [m/s] True wind speed

1 Introduction

1.1 Why is energy efficiency important?

During the last decades, the exponential population growth and the related increase in energy demand have led to over-exploitation of natural sources and uncontrolled environmental pollution.

An estimation of the impact of said over-exploitation is given by the evaluation of the "Earth Overshoot Day", which marks the date when humanity's demand for ecological resources and services, in a given year, exceeds what Earth can regenerate in that year.

We maintain this deficit by liquidating stocks of ecological resources and accumulating waste, primarily carbon dioxide in the atmosphere.
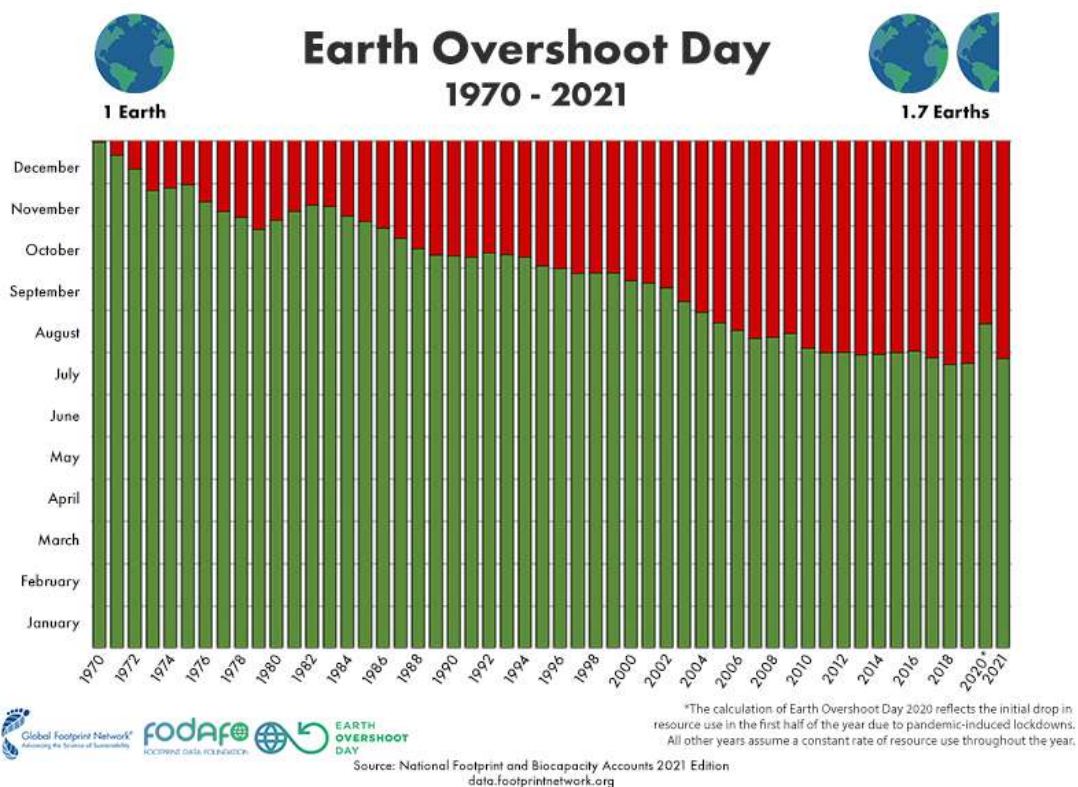
FIGURE 1.1: Past Earth Overshoot Days 1970-2021.
Source: [47]

The graph of Figure 1.1 shows the "Earth overshoot days" from 1970 to 2021: the

red part of each vertical bar represents the months of that year when humanity's demand for ecological resources and services has exceeded what Earth could have regenerated in that year: in 2021, it fell on July 29; the worsening of the situation over the years is very clear. In 2021 the humanity demand required the use of resources comparable to those that 1.7 Earths could give. It is very clear that this situation is non sustainable.

Among all the possible solutions to stop and to reverse this negative trend, the more glaring one is the reduction of the demand. Unfortunately, this seems to be a non viable option since it would involve the complete change of lifestyle of the majority of the population.

A good compromise seems to be the increasing efficiency of the technologies and processes. By this approach the demand can be met, however the use of natural resources is reduced and waste minimized. Increasing energy efficiency means using less energy to get the same result. This means reducing exploitation of resources and reducing pollution.

FIGURE 1.2: UN Sustainable development goals.

The goal is to to combat climate change and pollution without jeopardizing the quality of life. This ambitious goal requires a shared effort all over the world and the strategy must be common among all the players. In order to create this common path, the United Nations (UN) has developed the renowned 17 Sustainable Development Goals (SDGs), as reported in Figure 1.2. In particular goal n. 7, 12, 13, 14, 15 are related to environmental protection, and international regulations have been written by the various specialized UN agencies regarding their specific areas. The International Maritime Organization (IMO) is the UN specialized agency with responsibility

for the safety and security of shipping and the prevention of marine and atmospheric pollution by ships. In this framework, IMO produces rules and documents that are applicable to international shipping. IMO's work supports the UN SDGs.

1.2 Environmental impact of the maritime sector

1.2.1 Air pollution

IMO Green House Gas (GHG) Study 2020 [55] evaluated the share of shipping Carbon Dioxide (CO_2) emissions in global anthropogenic emissions to 2.89% in 2018. The same study reported an improvement of the energy efficiency of the ships, measured by means of the Energy Efficiency Operational Index (EEOI), between 2012 and 2018 for international shipping as a whole. However the pace of carbon intensity reduction has been slowed since 2015, with average annual percentage changes ranging from 1 to 2%. The projection to 2050 indicated a 90-130% of 2008 emissions, far away with respect to UN emission reduction goals of Net zero emissions by 2050.

Apart from CO_2, ships are responsible also for other air pollutants such as sulphur oxides (SO_X), nitrogen oxide (NO_X) and particulate matter (PM). Sulfur oxides are harmful to the lungs and make it difficult to breathe; they can cause asthma and bronchitis, burns to the skin and organs. SO_X also reacts with water droplets in the air to make sulfuric acid, causing acid rain. Since sulfuric acid is also corrosive and, thus, harmful for the exhaust gas plant components, the implementation of measures to reduce it is welcomed by the industry. Fuels with very low content of sulfur are the best option but also scrubbers to wash exhaust gas before emitting them, are now widely applied.

NO_X, the nitrogen oxides, contribute to the formation of smog (which leads to adverse effects such as asthma, damage to lung tissue and reduction in lung function) and acid rain, as well as affecting troposphere ozone. They are produced from the reaction among nitrogen and oxygen during combustion of fuels, especially at high temperatures. Selective catalytic reduction (SCR) can reduce post combustion NO_X by reacting the exhaust with urea or ammonia to produce nitrogen and water.

Exhaust particulates form a very complex aerosol system which is responsible for the black smoke traditionally associated with diesel powered vehicles. The basic fractions of PM are carbonaceous solids and heavy hydrocarbons derived from the fuel and lubricating oil. In cases where the fuel contains significant sulfur, hydrated sulfuric acid can also be a major component. PM contains a large portion of the polynuclear aromatic hydrocarbons (PAH) found in engine exhaust. [77] PM is one of the major harmful emissions produced by diesel engines. Due to the highly toxic health effects of particulate matter, most governments have created regulations both for the emissions allowed and for the ambient concentration of particulates. WHO designates particulates as Group 1 carcinogen: they are the deadliest form of air pollution due to their ability to penetrate deep into the lungs and blood streams unfiltered, causing respiratory diseases, heart attacks, and premature death [122]. In addition to the

health issues, PM Atmospheric aerosols affect the climate by changing the amount of incoming solar radiation and outgoing terrestrial radiation. The aerosol climate effects are the biggest source of uncertainty in future climate predictions.

1.2.2   Water pollution and marine wildlife

The presence of the ship in the sea has an impact on the marine environment and wildlife. The more blatant effect that comes to mind are the oil spills from scandalous exceptional disasters. Unfortunately, traditional everyday activities are responsible for most of the marine pollution even if they pass more unnoticed. About 80% of the total pollution from ships is estimated to be originated from operational discharges (such as discharges of waste oils or tank cleaning operations), made deliberately and in violation of international rules due to several reasons, including: lack of adequate facilities in ports to receive ships' waste, cost-savings (the costs for delivery to shore may be prohibitive and may cause significant delays to ships), or mere convenience of the ship's crew [39].

The major impact on marine environment is given by oil pollution and other chemicals released into water. Among others, antifouling paint was proven to be a great issue [116]. Antifouling paints were developed to reduce drag, and consequently fuel consumption on ship hulls by preventing the buildup of barnacles and other organisms. However their propensity for wider impacts on the marine environment had been grossly underestimated. Today these paints and their components are heavily regulated.

Another heavily underestimated aspect is the transfer of seawater and related microorganisms from one port to another and from one continent to another. This phenomenon occurs when the ship embarks and, subsequently, discharges untreated ballast water. Ballast water can contain thousands of aquatic or marine microbes, plants and animals, which are then carried across the globe. Untreated ballast water released at the ship's destination could potentially introduce a new invasive marine species. Hundreds of such invasions have already taken place, sometimes with devastating consequences for the local ecosystem. The IMO International Convention for the Control and Management of Ships' Ballast Water and Sediments (BWM Convention) was adopted in 2004 to introduce global regulations to control the transfer of potentially invasive species. With the treaty now in force, ships need to properly manage their ballast water [54].

A problem that is recently coming to attention is the noise pollution from ships, which can cause serious problems to marine wildlife and in particular to marine mammals. Marine animals depend on their hearing to navigate, communicate and hunt. But sound levels in the oceans are rising constantly [90]. Shipping, offshore oilrigs and the use of airguns in seismic oil explorations all add to the noise pollution but military sonar used to locate submarines is particularly dangerous, as its sound waves can interfere with hearing within a radius of about 3000 km. The most striking consequence

is the stranding of whales and dolphins and strandings have been observed to be particularly frequent after naval sonar manoeuvres [29]. Moreover, extremely loud sound may cause in marine animals hearing damages, illnesses and death [109].

1.2.3 Land pollution and ship recycling

Ships have always been recycled and the good news is that, today, about 95-98% of the ship by weight is reused [75]. But the bad news is that, even if steel and other metals are re-used, ship demolitions are widely associated with dangerous practices and pollution.

Ship dismantling activities are generally carried out at ship recycling yards in the dock or on the beach. The beaching method is especially used in developing countries. This is a dangerous system which lacks the ways of managing the hazardous materials and protecting the environment and workers' safety. The hazardous, including solid waste, chemicals (like polychlorinated biphenyls PCBs), asbestos, glass fiber etc., will result in environment pollution and affect human health and safety if they are not handled properly [124]. Moreover, oil spills and remaining are swept out to sea by tides and waves.

There are significant amounts of materials that should be handled carefully and appropriately but the beaching method make extremely difficult to ensure safety and manage pollutant.

Of course regulations play a big role in improving the present scenario but also better ship design, a recycling friendly ship design with an eye on the ship end of life, could give a big help.

1.3 Regulatory framework

Despite the increasing environmental concern worldwide and some selected proactive initiatives in the shipping sector, generally the environmental aspect has not been considered a sufficient drive for innovation in emission reduction technologies. Hence there is an urgent need for legally binding regulations.

1.3.1 International regulations

IMO MARPOL

In 1973, IMO adopted the International Convention for the Prevention of Pollution from Ships, known as MARPOL, which has been amended by the Protocols of 1978 and 1997 and kept updated with relevant amendments. The Convention includes regulations aimed at preventing and minimizing pollution from ships, both accidental pollution and that from routine operations, and currently includes six technical Annexes [59]. The year of entry into force of each annex is reported between brackets.

Annex I (1983): regulations for the prevention of pollution by oil. Covers prevention of pollution by oil from operational measures as well as from accidental discharges; it made it mandatory for oil tankers to have double hulls.

Annex II (1983): regulations for the control of pollution by noxious liquid substances in bulk. Details the discharge criteria and measures for the control of pollution by 250 noxious liquid substances; the discharge of their residues is allowed only to reception facilities until certain concentrations and conditions are complied with. In any case, no discharge of residues containing noxious substances is permitted within 12 miles of the nearest land.

Annex III (1992): prevention of pollution by harmful substances carried by sea in packaged form. Contains general requirements for the issuing of detailed standards on packing, marking, labelling, documentation, stowage, quantity limitations, exceptions and notifications of "harmful substances", in other words those substances which are identified as marine pollutants in the International Maritime Dangerous Goods Code (IMDG Code) or which meet certain criteria.

Annex IV (2003): prevention of pollution by sewage from ships. The discharge of sewage into the sea is only allowed if the ship has in operation an approved sewage treatment plant or if the ship is discharging comminuted and disinfected sewage using an approved system at more than three nautical miles from the nearest land; sewage which is not comminuted or disinfected has to be discharged at a distance of more than 12 nautical miles from the nearest land.

Annex V (1988): prevention of pollution by garbage from ships. Deals with different types of garbage and specifies how to manage each of them and the way they may be disposed of; it is fundamental for the complete ban imposed on the disposal into the sea of all forms of plastics.

Annex VI (2005): prevention of air pollution from ships. Sets limits on sulphur oxide SO_X, nitrogen oxide NO_X and particulate matter (PM) emissions from ship exhausts and prohibits deliberate emissions of ozone depleting substances; emission control areas, where it is mandatory to be compliant with even stricter emission limits to sail in, are here defined. About CO_2 and other greenhouse gases emissions, the calculation of energy efficiency indexes and parameters is imposed; their value must be compliant with the given thresholds. MARPOL applies to 99% of the world's merchant tonnage.

In June 2021 IMO's Marine Environment Protection Committee (MEPC 76) adopted amendments to MARPOL Annex VI that will require ships to further reduce their carbon intensity and greenhouse gas (GHG) emissions by improving their energy efficiency, as stated in [56]. These new amendments, which will enter into force in November 2022, introduce, among others, the calculation of the energy efficiency index for existing ships EEXI and threshold values to achieve. Furthermore the carbon intensity index CII has been introduced, in order to drive a progressive CO_2 emissions reduction of existing ships in the coming years.

IMO BWM Convention

Ballast Water Management Convention is an internationally binding instrument to address the transfer of harmful aquatic organisms and pathogens in ships' ballast water. It entered into force in 2017 but the Guidelines are kept under review by the MEPC and updated as new technologies emerge and additional knowledge becomes available.

Under the Convention, all ships in international traffic are required to manage their ballast water and sediments to a certain standard, according to a ballast water management plan. All ships have to carry a ballast water record book and an international ballast water management certificate. Most ships will need to install an on-board ballast water treatment system [54].

IMO AFS: International convention on the control of harmful anti-fouling systems on ships

It entered into force in 2008. This convention prohibits the use of harmful organotin compounds in anti-fouling paints used on ships and established a mechanism to prevent the potential future use of other harmful substances in anti-fouling systems. Anti-fouling systems to be prohibited or controlled are listed in Annex 1 to the Convention, which is updated as and when necessary [53].

IMO Guidelines for the reduction of underwater noise MEPC.1/Circ.833 7 April 2014

In an early stage, not yet ratified. In 2014, IMO's Marine Environment Protection Committee (MEPC) approved the "Guidelines for the reduction of underwater noise from commercial shipping to address adverse impacts on marine life", which focus on primary sources of underwater noise, namely on propellers, hull form, on-board machinery, and various operational and maintenance recommendations such as hull cleaning.

IMO noted a significant knowledge gap and that sound levels in the marine environment and the contribution from various sources was a complex issue; thus setting targets for underwater sound levels emanating from ships was premature and more research was needed, in particular on the measurement. IMO invited interested Member Governments to submit proposals to a future session.

IMO recommendations for the reduction of underwater noise could probably be submitted to MEPC 80 in 2023 [62].

IMO adopted "Particularly Sensitive Sea Areas" (PSSAs), considered to deserve special protection and which may be vulnerable to damage by ships. Ship routeing measures can be proposed in the future for adoption in connection with a PSSA, to protect marine life. IMO has also adopted a series of routing measures to protect whales and other cetaceans from ship strikes during breeding seasons, by keeping ships away from specified areas.

IMO Honk Kong Convention

The Hong Kong International Convention for the Safe and Environmentally Sound Recycling of Ships has not yet entered into force since it is not yet ratified.

It intends to address all the issues around ship recycling, including environmentally hazardous substances in ships (such as asbestos, heavy metals, hydrocarbons, ozone depleting substances and others) and concerns about working and environmental conditions in many of the world's ship recycling facilities.

It covers the design, construction, operation and preparation of ships, to facilitate safe and environmentally sound recycling without compromising safety and operational efficiency of ships, and the operation of ship recycling itself. Ships will be required to carry an inventory of hazardous materials. Ship recycling yards will be required to provide a ship recycling plan, to specify the way each individual ship will be recycled, depending on its particulars and its inventory [61].

1.3.2   EU regulations

European Green Deal. GHG and CO_2

In 2019 the European Commission adopted a set of proposals to make the EU's climate, energy, transport and taxation policies fit for reducing net greenhouse gas emissions by at least 55% by 2030, compared to 1990 levels and to achieve no net emissions of greenhouse gases by 2050. These goals are written into law by the European Climate Law, which sets a legally binding target of net zero greenhouse gas emissions by 2050. It entered into force on 29 July 2021 [42].

The EU Commission set out a strategy towards reducing GHG emissions from the shipping industry, consisting of three consecutive steps:

1. MRV Monitoring, reporting and verification of CO_2 emissions from large ships using EU ports; MRV shall be done in conformity with **Regulation 2015/757** (as amended by Delegated Regulation 2016/2071). In force from 2018 for large ships over 5 000 gross tonnage loading or unloading cargo or passengers at ports in the European Economic Area (EEA).
2. Greenhouse gas reduction targets for the maritime transport sector by at least 50% by 2050 compared to 2008 levels; short-term measures are to be decided in 2023, considering data collected by IMO and Intergovernmental Panel on Climate Change.
3. Further measures, including market-based measures, in the medium to long term.

EU SO$_X$

The codified legislation, in force, addressing sulphur oxides emissions from shipping in the EU is Directive (EU) 2016/802 regulating the sulphur content of certain liquid

fuels. It contains the latest limits for marine fuels as stated by IMO [41].

EU MSFD Descriptor 11 Underwater noise

The EU Marine Strategy Framework Directive (MSFD) identifies noises as pollution and it also dedicates one of the specific qualitative descriptors (descriptor 11) to define good environmental status of marine waters. Commission Decision (EU) 2017/848 of 17 May 2017 defines good environmental status, and lays down criteria, specifications and standardized methods for their monitoring and assessment, in particular for anthropogenic impulsive sound sources in D11 criteria 1 and for continuous low-frequency sound in D11 criteria 2 [43].

Member States shall establish threshold values for these levels through cooperation at Union level. In order to steer this work and advise EU Member States on the operational implementation of descriptor 11, a technical group of experts on underwater noise (TG Noise) was set up in 2011. So far, the work done by TG Noise focused on monitoring issues and included the publishing of monitoring guidance for underwater noise in the European Seas [98]. Now, TG Noise is focusing on the assessments of impacts of noise and the development of thresholds; this work is expected to be finalized by 2022.

2013 EU Ship recycling regulation SRR

Regulation (EU) No. 1257/2013 of the European Parliament and of the Council of 20 November 2013 on Ship Recycling (EU SRR) entered into force in 2020. By 31 December 2020, all ships entering a European Union port or anchorage will require a valid and certified Inventory of Hazardous Materials (IHM) on board [74].

1.4 Decarbonisation

Decarbonisation is the terminology used to identify the process of reducing greenhouse gasses output to the atmosphere through the use of low carbon power sources. This involves the use of renewable energy sources like wind power, solar power, and biomass.

Greenhouse gases include Carbon Dioxide (CO_2), Methane (CH_4), Nitrous Oxide (N_2O), Chlorofluorocarbons (CFCs) and Hydrofluorocarbons (HFCs and HCFCs). These gases allow incoming (short wave) radiation from the sun but block infrared (long wave) radiation from leaving the earth's surface. The trapped radiation from the sun warms the earth's surface.

The regulatory framework is pushing the marine sector toward the right path of decarbonisation. Consequently, the study of greener technologies and solutions, capable of improving the energy efficiency of ships, becomes even increasingly important.

EU MRV Regulation addresses carbon emission from the shipping sector. Since 2018, ships have to monitor several parameters such as CO_2 emissions, fuel consumption, travelled distance, time at sea and cargo carried, on a per voyage basis. Data are submitted to an accredited MRV shipping verifier for consistency checks and performance analysis. Moreover, since 2019, companies shall ensure that all their ships carry on board a document of compliance. Every year, the EU Commission publishes a report to inform the public about the CO2 emissions and energy efficiency information of the monitored fleet [44]. Moreover, EU set a GHG reduction targets for the maritime transport sector by at least 50% by 2050 compared to 2008 levels.

IMO has followed a similar path: in 2016 IMO adopted, by resolution MEPC.278(70), the mandatory IMO Data Collection System (DCS) for ships to collect and report fuel oil consumption data from ships over 5000 gt, which entered into force in 2018 (first data collection completed in 2019, report of 2020 available [65]); in June 2021, IMO adopted short-term measures (EEXI and CII) with the vision to reduce carbon intensity of all ships by 40% by 2030, compared to 2008 and by 70% by 2050.

MARPOL Annex VI regulation 13, addresses nitrogen oxides (another GHG); emission limitations are set, together with the definition of the emission control areas (ECAs). Three limits were set Tier I, II and III: Tier I is obsolete: since 2011 Tier II is mandatory everywhere, except for the ECAs zone where the stricter Tier III applies. North American sea, Caribbean Sea and, from 2021, also Baltic Sea and the North Sea are ECAs.

The same ECAs applies in Regulation 14 where threshold values for sulfur content in fuels are set. Sulfur is not a greenhouse gas (it is responsible for acid rains), however it is related to high carbon intensity fuels. Since 2020, the sulfur content in fuel should be less than 0.5% worldwide, while in ECAs the limit is 0.1%.

In Annex VI, the control of greenhouse gases emissions is made through the calculation of some indexes. CO_2 emissions are limited by regulating the ship energy efficiency, which is monitored applying the following indexes: EEDI, EEOI, SEEMP and, from 2022, EEXI and CII. In Section 1.5 they are explained in detail.

To conclude, the route to decarbonisation chosen by IMO is not only the reduction of carbon emissions in absolute term, as per EU, but also their relative reduction, obtained through the improvement of the ship energy efficiency.

1.5   Energy efficiency

In 2013 Energy Efficiency Design Index (EEDI) and the Ship Energy Efficiency Management Plan (SEEMP) entered into force, the first ever mandatory global GHG reduction regime for an entire international transport sector [52].
EEDI was made mandatory for new ships and SEEMP for all ships at MEPC 62 (2011)

with the adoption of amendments to MARPOL Annex VI resolution MEPC.203(62). This was the first legally binding climate change treaty to be adopted since the Kyoto Protocol.

EEDI is the Energy Efficiency Design Index. The value calculated for the ship ("attained EEDI") must be under a threshold value ("required EEDI") given by the regulation for the specific ship type and size segment. This threshold is tightened incrementally every five years to stimulate innovation and technical development. Phase 1, where CO_2 reduction level was set to -10% in respect to reference line of 2015, finished in 2020 and Phase 2 started with CO_2 reduction level of -20%. The next step will be -30% in Phase 3 from 2025.

The EEDI is a performance-based mechanism where the designer has the freedom to choose the best technology for achieving the target. That means, finding the most cost-efficient solutions for the ship to comply with the regulations, as long as the required energy efficiency level is attained.

The EEDI provides a specific figure for an individual ship design, expressed in grams of carbon dioxide (CO_2) per ship's capacity·mile. It represents the amount of CO_2 generated by the ship while doing one ton·mile of transport work; the smaller the EEDI the higher the energy efficiency. It is calculated with the design parameters for a given ship, as per Equations 1.1.

$$EEDI \left[gCO_2 / (tons \cdot nm) \right] = \frac{CO_2 \ emission}{transport \ work} \tag{1.1}$$

The actual formulation, reported in Equation 1.2, is more complex and accounts for main and auxiliary engines, innovative power generation systems and innovative propulsion systems, as can be seen in Figure 1.3.

$$EEDI = \frac{\left(\prod_{j=1}^{M} f_j \right) \left(\sum_{i=1}^{nME} P_{MEi} \cdot C_{FMEi} \cdot SFC_{MEi} \right) + \left(P_{AE} \cdot C_{FAE} \cdot SFC_{AE} * \right) +}{f_i \cdot f_c \cdot f_w \cdot Capacity \cdot v_{ref}}$$
$$+ \frac{\left(\left(\prod_{j=1}^{M} f_j \cdot \sum_{i=1}^{nPTI} P_{PTI(i)} - \sum_{i=1}^{neff} f_{eff(i)} \cdot P_{AEeff(i)} \right) \cdot C_{FAE} \cdot SFC_{AE} \right) +}{f_i \cdot f_c \cdot f_w \cdot Capacity \cdot v_{ref}}$$
$$\frac{- \sum_{i=1}^{neff} f_{eff(i)} \cdot P_{eff(i)} \cdot C_{FME} \cdot SFC_{ME}}{f_i \cdot f_c \cdot f_w \cdot Capacity \cdot v_{ref}} \tag{1.2}$$

EEDI represents the ratio of a ship's "cost to society" in the form of its CO2 emissions, divided by its "benefit to the society" represented by the transport work done by the ship.

SEEMP, the Ship Energy Efficiency Management Plan is an operational measure to improve the energy efficiency of a ship during operating life. The SEEMP urges
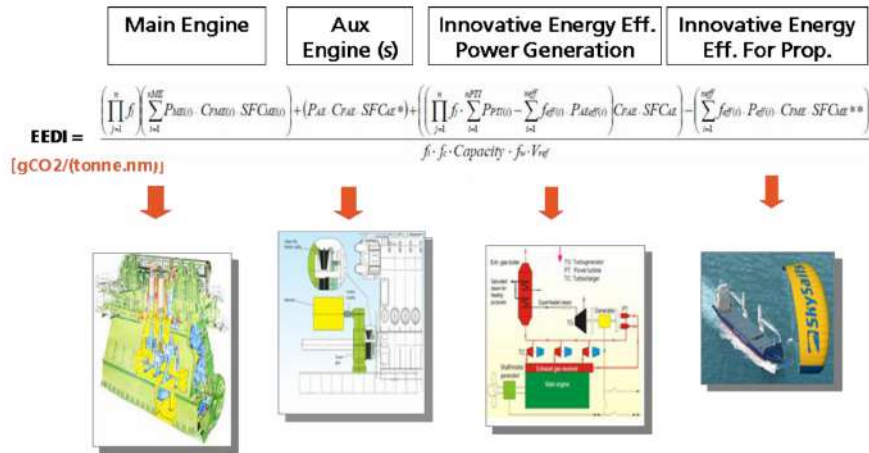
FIGURE 1.3: EEDI formula. Source: [58]

ship owners and operators to consider new technologies and practices to optimize the performance of the ship.

The SEEMP is a plan which is ship specific and has to be implemented according to the ship type, cargoes carried, ship routes, and other relevant factors; it also provides the Energy Efficiency Operational Indicator (EEOI) as a monitoring tool.

The guidance on the development of the SEEMP for new and existing ships incorporates best practices for fuel efficient ship operation, as well as guidelines for voluntary use of the EEOI for new and existing ships (MEPC.1/Circ.684). The EEOI enables operators to measure the fuel efficiency of a ship in operation and to gauge the effect of any changes in operation, e.g. improved voyage planning or more frequent propeller cleaning, or introduction of technical measures such as waste heat recovery systems or a new propeller.

EEOI, the energy efficiency operational indicator, is the most important performance indicator. It quantifies the ship's CO2 emissions in relation to its operational activities, measuring a ship's energy efficiency for each voyage or over a certain period of time. EEOI, like EEDI, represents the amount of CO2 emissions from a ship per unit of cargo-mile transport service. However, if the EEDI is defined for one operating point of a ship, EEOI represents the actual CO2 emission from combustion of all types of fuels on board a ship during each voyage in respect to the performed transport work, calculated by multiplying the actual mass of cargo (tonnes, number of TEU/cars, or number of passengers) and the corresponding actual distance in nautical mile travelled by the vessel.

In June 2021, IMO MEPC 76 adopted amendments to MARPOL Annex VI that will require ships to further reduce their greenhouse gas emissions. The new measures will require all ships to calculate their Energy Efficiency eXisting ship Index (EEXI) following technical means to improve their energy efficiency and to establish their annual operational Carbon Intensity Indicator (CII) and CII rating. These measures are expected to enter into force on 1 November 2022, with the requirements for EEXI

and CII certification coming into effect from 1 January 2023.

The EEXI is a one-time certification, concerning design parameters of the vessels, equivalent to the EEDI (phase 2 or 3) but for already existing and operating ships.

The CII is an operational indicator that will be assessed annually from 2023 with yearly stricter limits. It links the GHG emissions to the ship capacity over distance travelled and it will be a mandatory part of the enhanced SEEMP. It can appear to be the mandatory version of the EEOI, but it is slightly different: in fact EEOI is calculated with the actual cargo transported during the specific ship voyage (and doing so, being these data commercially confidential, the index could only be voluntary), on the contrary, CII is calculated considering the design ship cargo capacity and thus the index can be mandatory [73].

CII is calculated as CO_2 emitted per cargo-carrying capacity and nautical mile (the full formulation is not yet available since some correction factors will be developed during 2022-2023) as per Equation 1.3.

$$CII = \frac{Annual\ fuel\ consumption \cdot CO_2\ factor}{Annual\ distance\ travelled \cdot Capacity} \cdot Correction\ factors \qquad (1.3)$$

Ships will get a rating from A to E (where A is the best) and a ship rated D for three consecutive years, or E, is required to submit a corrective action plan, to show how the required index (C or above) would be achieved.

All these Energy efficiency indexes and carbon intensity are evaluated in terms of ratio between the ship CO_2 emissions with respect to the performance output (i.e., transport work).

Because CO_2 is proportional to fuel consumption, a way to improve the ship efficiency is to adopt propulsion technologies able to reduce the installed engine power and lower the fuel consumption for the same transport work. This way of thinking is also economically beneficial because it has the advantage to lower ship running costs (fuel bill) with moderate CAPEX increase.

1.6 Emerging energy efficiency strategies onboard

In recent years, various technical solutions are emerged to cope with the problem of emission reduction and ship energy efficiency improvement.

It is possible to identify three main paths:

- Reduce, reuse, recycle: trying to lower the power required onboard or reuse wastes to generate free energy.

  These solutions are excellent to lower well to propeller emissions[1].

---

[1]If carbon emissions are calculated by considering only the actual CO_2 derived from onboard combustion, they are called "tank to propeller emissions"; if the entire life cycle is considered, including the emissions to produce the energy carrier (fuel, electric power, hydrogen etc.), the total amount is called emissions "well to propeller"; the remaining component, the emissions emitted only to generate the energy carrier, is called "well to tank".

An example is the slow steaming where significant savings in fuel oil consumption and CO_2 emissions can be obtained reducing ship speed [36].

Technologies that enhance efficiency of propeller and hull (such as anti fouling-coatings [89] or better design) are worthy to be cited.

Very good results are possible thanks to waste heat recovery systems [6] [7] [10], but also other kind of wastes could be investigated to see if they could help to improve the energy efficiency of the ship.

A last example is carbon capture that allows to reduce EEDI ([111] reports a reduction of 50%) by reducing after combustion emission into the atmosphere; on the other hand it arises the problem of how to use the stored CO_2.

- Hybrid power plants [66]: to integrate some kind of electric energy technology onboard such as batteries, fuel cells [69] [103] or electric motors to lower pollutant emission onboard, from tank to propeller.
  Also the use of alternative fuels, such as LNG, biofuels, ammonia, hidrogen and methanol is often considered for their reduced emissions [96] [114] [49].

- The harvesting of renewable sources such as wind or solar power to achieve zero the emissions.

During this research one technology for each group was studied: a sludge recycling plant for the onboard generation of new fuel oil, an hybrid propulsion with waste heat recovery technologies and the wind assisted propulsion with Flettner rotors.

1.7 Aim of this study

This research aims to study emerging innovative solution to improve the energy efficiency of the ship power plant and the propulsion system.

Three main innovative solution are studied:
- First the focus is on a technology able to recycle the onboard oily waste to transform them into new fuel oil;
- then, a flexible hybrid power plant with electric motors-generators and heat recovery systems is investigated and
- lastly, the use of renewable sources, and in particular wind, is simulated to be integrated in an hybrid plant onboard.

The common thread among all those solutions is the energy efficiency of the ship, in particular the possibility to exploit energy that, without the proposed technology, would be wasted.

For each of these possibilities, a numerical simulator is developed, to evaluate the energy efficiency improvements in different scenario.

The key parameter indicator chosen to assess the potential of every technology is the fuel consumption.

This choice was made because fuel consumption calculation allows to simultaneously evaluate the potential reduction of pollutant emissions and the benefits in terms of cost.

The thesis is organised as follows:

Chapters 2 reports the study about an innovative sludge recycling technology to be installed onboard for the conversion of oily wastes into new fuel for the main engines. In Chapter 3, a flexible hybrid propulsion and power plant with waste heat recovery systems is proposed.

Wind assisted ship propulsion is introduced in Chapter 4. Among the alternatives presented, the Flettner rotor is selected to be studied in more details. The research about a rotors-propellers propulsive plant is reported in Chapters 5 and 6. Being this study the more extensive and detailed, it was divided in two chapters for sake of clarity. Conclusions are expressed in Chapter 7.

2 Sludge recycling

2.1 Waste production onboard

A variety of different wastes is produced onboard. Their classification and management is regulated by the UNO (United Nation Organization) specialized agency IMO (international Maritime Organisation) convention MARPOL 73/78 [60]. More in details, hhe following annexes describe waste regulations in detail:

- Annex I - Regulations for the Prevention of Pollution by Oil: the crude oil waste, sludge and slops (from tank draining and washing) are described here;
- Annex II - Regulations for the Control of Pollution by Noxious Liquid Substances in Bulk: for slops and chemical wastes;
- Annex IV - Regulations for the Prevention of Pollution by Sewage from Ships: about the discharge of sewage;
- Annex V - Regulations for the Prevention of Pollution by Garbage from Ships: all kinds of victual, domestic and operational waste, generated during the normal operation of the ship are covered here.

The summarised information on waste production on board is given in the Table 2.1

	Waste	Ann.	Source
Liquid	Slop	I	From oily tank washing
	Sludge	I	Muddy residue from fuel and oil depuration
	Oily bilge water	I	Seawater with oil dripping from machinery
	Waste oils	I	From oil change and maintenance
	Sewage	IV	From toilets and showers
Solid	Food waste	V	From the kitchen
	Paper	V	From living spaces
	Plastic	V	Same as per domestic use
	Glass	V	Miscellaneous
	Metal waste	V	Miscellaneous
	Rags	V	From cleaning and maintenance
Special	Chemicals	II	From tanks washing or maintenance
	Sanitary and ph.	V	Cleaning product or medical waste
	Cargo residues	V	From tanks, cargo bays and deck
	Ashes	V	From incinerator

TABLE 2.1: Waste production onboard

The most relevant information provided by MARPOL is about the waste management onboard.

In Annex V the general solid garbage, similar to "municipal waste" is covered: on-board separate collection is required and it is very important that they are not mixed with all the other wastes (hazardous, oily, chemical, etc.).

Special wastes must be collected in predetermined and differentiated containers or separated tanks.

Liquid wastes must be stored onboard in designated tanks and treated; in particular sewage must be treated with filters and UV disinfection to be discharged outboard (not in protected areas). Oily wastes must be treated even more carefully: sludge and other oils are stored onboard while bilge water can be treated to separate oil to store from water that can be discharged at sea after ensuring that the oil content is less than 15ppm. Also food waste can be discharged at sea (beyond 12 miles from the coast) or it can be incinerated. The onboard incinerator can be used also for paper, cardboard and wood.

Unfortunately, despite IMO rules, marine pollution from ships is still a reality, as it accounts for around 20% of the total sea pollution, and it can be caused both by accidents and ships daily activities. About 80% of the total pollution from ships is estimated to be originated from operational discharges (such as discharges of waste oils or tank cleaning operations), made deliberately and in violation of international rules due to several reasons, including: lack of adequate facilities in ports to receive ships' wastes, costsavings (the costs for delivery to shore may be prohibitive and may cause significant delays to ships), or mere convenience of the ship's crew [39].

2.2   Sludge and the purpose of this work

As just stated, sludge and other oils must be collected and properly stored onboard to be later unloaded in port upon payment of a fee. This process results in a double waste of money: load-related space wasted onboard and the fee to be paid in port.

The idea behind this research work was to turn sludge from waste into a new source of energy. As a result, wasted space is reduced and also better utilised: from storage of a waste to a space used to increase the ship energy efficiency.

Said space would be used to house an innovative plant capable of transforming useless and inconvenient sludge into new usable fuel.

To clearly study the effect of this idea, large quantities must be involved, so the passenger ship was chosen as the type of vessel to be analysed.

The wastes produced specifically by a passenger ship are a wide variety: paper, plastic, glass and aluminium are effectively recycled on land; food is discharged at sea or burned in the incinerator with paper, cardboard, wood, rags and dried bio-sludge derived from the water treatment plant.

Waste oils, mainly consistent of sludge from fuel and oil purifiers and exhaust lubricating oil and cooking oil, are stored onboard and unloaded in port, as previously reported.

Waste oil is often transformed into recycled fuel at reception facilities.

Theoretically, there is no reason why this process cannot be carried out directly on board; the "new" recycled marine fuel could be burnt in the propulsion engines or in the diesel generators, leading to environmental benefits and energy savings.

2.2.1 Literature review

The process chosen to transform sludge into fuel is called pyrolysis.

Pyrolysis process can be applied to biomass, solid waste and oils. In literature there are some studies about its use for fuel production from waste oils: from waste cooking oil [100], from waste automobile lubricating oil [68] and from oil sludge from petroleum industry [26] [50] [97] [106] [107] [121] but no study was found about the chemical process of ship sludge recycling. Therefore, the main innovation of this research consists in the new field of application of the cited process.

Some preliminary study at the University of Genoa [22] [118] showed a possible conversion factor into fuel of about 32% for sludge, while the remaining products are water (30%), gas (17%), and solid waste (21%). In this regard, it is important to point out that these results were achieved through a thermocatalytic pyrolysis process. But, to simplify the installation onboard, a pyrolysis without the use of a catalyst is chosen.

The present study focuses on the feasibility study of an onboard sludge treatment plant, based on the pyrolysis process. It is desired that such a system is simple to install and operate, efficient and compatible with the characteristics of the ship, knowing that the main challenge is the space.

A similar onboard plant has been proposed by [40] but this research is different: the cited paper suggests the use of a specially designed and built vessel to collect and recycle sludge from other merchant ships transiting the Suez Canal and analyses the economic benefits of investing in such an application. On the contrary, in the case of this work, the pyrolysis plant is intended to be built and integrated onboard a ship already engaged in another trade, to treat the waste produced exclusively by itself.

2.3 Sludge transformation technology

As previously stated, the goal of this research was the installation onboard of an innovative plant, able to transform sludge back into fuel. To achieve this goal, the means is a chemical process called catalytic pyrolysis.

2.3.1 Catalytic pyrolysis

The catalytic pyrolysis process is the thermal decomposition of organic materials that occurs in the absence of oxygen and that produces gaseous, liquid and solid compounds.

Thanks to heat, this process enables to transforms sludge into water, gas, solid waste part and recycled "new" fuel oil.

This recycled fuel oil is suitable to be burnt inside the main propulsion engines or into the diesel generators because it is compliant with the ISO standard 8217:2010 that regulates fuel oil chemical characteristics [67]. The gaseous part could be used to fed the boilers and the solid waste could be sent to incinerator.

The chemical analysis of the process, its numerical simulation with the software Aspen Plus (one of the leading process simulation software in the field of chemical industry) and the laboratory analysis and verification on the recycled fuel was made by Prof. Michela Mazzoccoli, Prof. Barbara Bosio and Prof. Elisabetta Arato of the chemical department of the University of Genova (DICCA). Their methodology and results are reported in full details in [83].

In few words the pyrolysis process involves the following steps: at first, sludge has to be de-watered, thus it has to be stored in a decanter where almost all the water is removed; after that, the mostly oily sludge is heated by a heat exchanger and then it can be sent to a jacketed agitated reactor where the actual transformation takes place. Here the sludge is converted into three separate fractions: gas, liquid, and solid.

The solid residue is discharged from the bottom of the reactor and separated from liquid and gaseous products. These are cooled and sent to a condenser (to eliminate all the water) and, then, to a flash drum to separate the condensable compounds (liquid) from the incondensable (gas) ones.

2.3.2 Sludge characteristics

To determine the precise composition of the chemical components of the sludge produced onboard, a chemical analysis of a sample kindly provided by an italian ro-ro ferry company was performed by the Renewable Energy Consortium for Research and Demonstration (RE-CORD), an external research center in Florence, Italy. To validate these results no references were found in literature. However, oil sludge from refinery plant (a stable emulsion of hydrocarbons compounds, water, solids and heavy metals) may be considered the most similar waste-to-oil residues on board. Thus, a validation of the experimental results was performed by comparison with the data reported in [50] and [121].

Among all the chemical components and information, that can be found in [83], the most relevant for our purposes is the water quantity in sludge, which is about 63%.

2.3.3 Chemical simulation: assumptions, results and validation

The numerical simulation of the chemical transformation of sludge into recycled fuel was performed by Prof. Michela Mazzoccoli, Prof. Barbara Bosio and Prof. Elisabetta Arato of the chemical department of the University of Genova (DICCA). For the complete and detailed description of the chemical simulation with the software Aspen Plus please refer to [83], since in this paragraph only the assumptions made and the obtained results of said simulation are reported.

Aspen simulation requires defining the components involved in the process and their specifications and to choose the property methods to calculate thermodynamic properties. Then it is possible to represent the process diagram regarding flows and main units (reactors, mixers, exchangers, etc.). Regarding the property method, the Peng-Robinson model has been chosen because it is recommended for hydrocarbon processing applications. With respect to the composition of sludge oil produced on-board and necessary for simulation, the exact values, validated by comparison with data available in literature, were found by means of experimental tests, as reported in Chapter 2.3.2. To quantify the quantity involved and in order to have a large amount of waste to study, a 5000 passenger ship was chosen as a case study. The sludge production of this ship was estimated in an average value of 1175 $m^3/year$ (data available on courtesy of Costa Crociere), corresponding to about 1000 $tons/year$. The pyrolysis process was assumed to take 4 hours a day, considering a sludge flow rate of 755 kg/h; but, after the decanting phase that separates approximately 60% of water from the sludge, the flow rate to the reactor is around 280 kg/h. Under these assumptions, a volume less than 1 m^3 is required for the system arrangement onboard. The reaction is assumed to take place at atmospheric pressure and 450°C of temperature [121] [28].

The results are reported in Table 2.2. From Table 2.2 it is possible to deduce a fuel conversion factor of 30% from sludge already separated from water. This factor drops to about 11% if wet (non-decanted) sludge is considered as the source.

		[t/year]	[% wt]
Decanter	Sludge to decanter	1.057	100
	Water from decanter	667	63
	Sludge from decanter	390	37
Reactor	Sludge to reactor	390	100
	Gas	67	17
	Liquid (fuel oil)	118	30
	Solid residue	124	32
	Water	81	21

TABLE 2.2: Pyrolysis simulation results

A series of laboratory experiments were carried out by the chemistry department of the University of Genoa to identify the real quantities involved in the pyrolysis process of the transformation of sludge into recycled fuel oil. The results of these experiments, reported in [22], are very similar to the numerical simulation results; therefore the latter were validated.

2.4 Innovative pyrolysis plant proposed

A schematic representation of the pyrolysis plant is reported in Figure 2.1. Firstly, sludge is sent to a decanter (DECANTER) where almost all water (H2O) is separated. After that, heater exchanger (HEATER) is used to raise the temperature reaction and, then, sludge (HEATOIL) is sent into a jacketed and agitated reactor (REACTOR) where
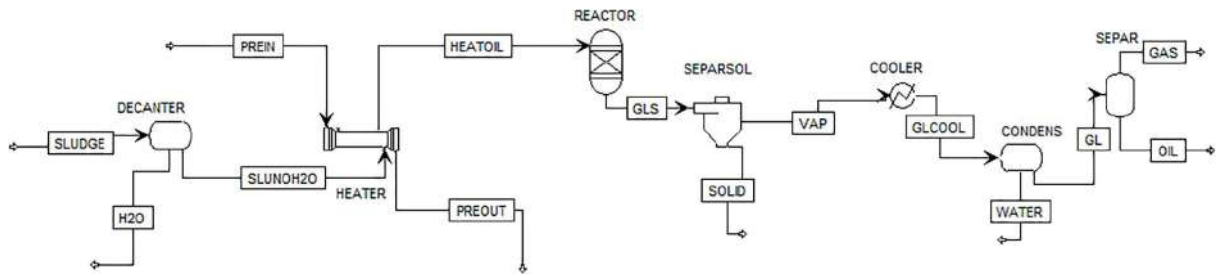
FIGURE 2.1: Scheme of the pyrolysis plant.

the feed is converted into three separate fractions: gas, liquid, and solid (GLS). The residue (SOLID) can be discharged from the bottom of the reactor (SEPARSOL) to be burnt in the onboard incinerator while liquid and gaseous products (VAP) are cooled (COOLER) and sent to a condenser (CONDENS) to eliminate water (WATER) and to a flash drum (SEPAR) in order to separate the condensable compounds (OIL) from the incondensable (GAS) ones. The latter can be sent to a burner, while the OIL is the newly obtained recycled fuel oil.

The bulkiest and more important component of this plant is the heated jacketed stirred reactor; therefore, the main challenge is to design said reactor in order to be space-saving, if compared to the sludge tanks, and powered by energy sources already available on board and, thus, "free". The main innovative aspect of the sludge transformation plant is its installation onboard. In fact, this kind of plant are already existent on land but they have never been applied onboard. Therefore, the novelty of this work is the integration of the sludge recycling technology onboard the ship.

In addition to the aforementioned advantage of better space management, there will be an immediate availability of free fuel a shorter chain of waste disposal, which leads to a reduction in costs and risk of pollution.

The technology proposed for the reactor is a cylindrical container and since, for the case study selected, a volume less than 1 m^3 is sufficient, space is not really a big deal. The issue of heat is totally different.

2.4.1   Heat source problem and solution

The reaction needs a temperature about 450°C to take place properly. More in details, the pyrolysis reaction is endothermic, therefore, a thermal power is needed to allow it. According to simulation results [83], the heat required is 146 kW: 90 kW to preheat sludge up to 450°C and 56 kW for the reaction.

The thermal power required by the pyrolysis process can be delivered by three different sources, each one with pros and cons:
- by means of a burner;
- by the exhaust gas of the main engines;
- by the incinerator already installed onboard.

Burner

Of course the burner is the most controllable option: it could be built to operate at the exact temperature required, but this is also a drawback: it must be built specifically for that purpose and requires a certain fuel consumption to work. As the reaction takes about 4 hours, the risk is that more fuel will be burnt to maintain the combustion needed to reach the temperature for the transformation than the amount of recycled fuel produced.

To avoid this uneconomic scenario, the proposed solution is to add a second purpose to a heat source already present onboard but not fully exploited and the choice falls between exhaust gas and incinerator.

Exhaust gas

The second option analysed was the main engines exhaust gas. The reactor should be a cylinder consisting of two concentric metal chambers: the most internal would contain the sludge and would be lapped externally by the exhaust gas flow through the second cylinder, insulated to minimize thermal exchanges with the engine room.

Here, the main problem is the identification of where to take the exhaust gases.

The following assumption was made: a 4000 passengers cruise ship powered by full electric propulsion whose electric generation is assumed to be entirely carried out by diesel engines of the type Wärtsilä 16V46C; the temperatures of the exhaust gases of said engine is known in various points. Three possible exhaust gas extraction locations have been identified:

(A) inside the exhaust manifold of each engine bank, before entering the turbine (of the turbocharger), the temperature reaches 540° C;

(B) after the turbine of the turbocharger the gas is usually at about 350°C in typical engines for passenger vessels;

(C) after the economizer there is 318°C of temperature.

It is clear that the best option, from the thermodynamic point of view, would be option (A). Unfortunately this is a very impractical choice because the modifications should be made by the engine manufacturer and the correct operation of the engine could be compromised.

Option (C) cannot be considered due to too low a temperature, even if it had the least impact on the already onboard systems.

Option (B) might be a good compromise: it is outside the engine so that the manufacturer does not have to be involved and, although some heat is subtracted from the economizer, the reactor is operated once in a while and may be chosen to turn it on when the heat load required by the ship is low. However, in this case, the temperature is a little low.

Then, another ship was tested: a 3000 passenger ferry with Wärtsilä 6R32LN diesel engines for electric generation. These engines are smaller and less efficient, so the

exhaust gas temperatures are higher. At point (B) it is 415°C, which is not optimal but acceptable for pyrolysis.

To verify the feasibility of the plant, simple formulation of heat transfer were applied [16] with the following assumptions:

- the reactor is perfectly insulated from the external environment, thus avoiding external heat exchange;
- exhaust gas temperature is constant over time;
- heat transfer takes place by:
  - natural convection between hot exhaust gas and inner tank wall,
  - conduction through the wall,
  - convection between the wall and the sludge.

The aim was to evaluate the temperature of the sludge and the result was that the temperature of the sludge was under the acceptability limit. Therefore, this heat source would be only suitable for a pre-heating phase.

Incinerator

The last chance to make this idea work was, then, the incinerator, which is already installed onboard passenger ships.

Firstly,the incinerator has the clear advantage to be often placed in the same room as the sludge tank so it is convenient to process the sludge oil here.

Secondly, it could supply all the required thermal power, since the power of a typical incinerator of, for instance, a Costa Crociere ship is around 1,600 kW, with a combustion temperature of about 850°C [35]. Being the temperatures reached inside the incinerator so high, it is, for sure, more than enough for the reaction.

Furthermore, the incinerator stays on for about 11 h/day, so its heat could be easily used during the entire pyrolysis process, whose duration is estimated in 4 h/day.

Under this conditions it seem convenient to build an integrated reactor-incinerator system, although the incinerator needs some small modifications in its geometry. An integrated reactor-incinerator system could be obtained by realizing a recess inside the incinerator and use its direct heat of combustion for the reaction. Another option is that the exhaust gas flow from the incinerator could be used for the reaction; then, the same gases could preheat the sludge.

Being the sludge tank and the reactor in the same room and the distance between the two so low, to move the oil sludge from the tank to the reactor, a small pump could be sufficient; in fact, in terms of height, even if the tank were on the bottom, the incinerator is almost always on the first deck and, about the longitudinal distance, it is not a problem, if the two are in the same room, the engine room.

Moreover, since the reactor is integrated with the incinerator, once the reaction is completed, the solid part is conveniently already on site to be directly incinerated, while the liquid product could be easily moved to the fuel tanks by gravity.

To sum up, in this case the correct temperature is guaranteed; the pyrolysis process can take as long time as needed and, with this configuration, this would not be a

problem as the incinerators are on 11 hours a day. In addition to that, since the sludge tank is already located in the incinerator room, it is also convenient to process the sludge oil here by an operational point of view.

The incinerator is the best choice as a heat source for the sludge transformation process.

2.5 Energy efficiency indices difficulties

The environmental impact of the ship is today very well monitored and the relevant legislation becomes more stringent every year.

If the sludge recycling technology were proven to improve the ship situation, it would be a further encouragement for the shipowner to install it onboard.

To measure the ship environmental impact, the main tools are the EEDI and EEOI.

In MARPOL Annex VI, the Energy Efficiency Design Index (EEDI) was made mandatory for new ships since 2011, the first legally binding climate change treaty to be adopted since the Kyoto Protocol. The EEDI is expressed in grams of CO_2 per ship's capacity by mile, which means that it is more a "specific emission factor" than an efficiency, in fact the smaller the EEDI, the more energy efficient ship design. It is calculated on the technical design parameters for a given ship, with a detailed formulation that represents the ratio between the environmental cost (CO_2 emitted) and the benefit produced for society (transport work) (Equation 2.1).

$$EEDI = \frac{CO_2 \text{ main and auxiliary engines} - CO_2 \text{ saved due to innovative technologies}}{\text{ship capacity} \cdot \text{ship speed}}$$

(2.1)

The maximum value acceptable for the EEDI is tightened incrementally every 5 years to stimulate innovation and technical development toward more energy efficient technologies.

Since EEDI only refers to design characteristics, the use of another index, more focused on operational aspects, is encouraged. This energy efficiency operational index is EEOI, which is a way, for shipping companies, to manage ship efficiency performance over time. It is a monitoring tool, defined as the ratio of mass of CO_2 emitted per unit of transport work; it has to be calculated for a specific journey as:

$$EEOI = \frac{\sum_j FC_j \cdot C_{Fj}}{m_{cargo} \cdot D}$$

(2.2)

where FC_j is the fuel (j) consumption per voyage; C_{Fj} is the conversion factor for fuel j to estimate CO_2 mass (e.g. diesel oil = 3.206); m_{cargo} is the cargo carried [tons] or work done [number of TEUs or passengers] and D is the distance [nm].

Unfortunately, neither formulation can take account of the innovative technology of sludge recycling.

In fact, the sludge conversion into fuel does not allow a real CO_2 emission reduction because it does not involve any consumption reduction for the ship engines. Therefore it was necessary to find an alternative way to attempt a calculation of a possible improvement in the efficiency index.

A proposal has been made for a way of taking account of this new technology in the EEOI, as this index was thought to be easier to adapt to the need. The new fuel produced from the sludge recycling plant is considered as an addition to the cargo. In this way the denominator of Equation 2.2 increases and the index decreases, as expected when a "green" technology is added.

This issue and the attempted proposal enlighten the problems that highly innovative technologies face when it comes to current pollution prevention regulation. The solutions currently being studied would become more attractive to shipowners if their undoubted environmental value were also recognized by current legislation.

2.6   Case study

A ro-ro ferry was chosen as a case study, as all information on diesel generators and propulsive power and fuel consumption for each ship speed and P/D of the propeller was available. Its geometrical characteristics are reported in Table 2.3.

Length [m]	Beam [m]	Draft [m]	Propulsive engines Wärtsilä 16V46C	Diesel generators Wärtsilä 6R32LN
193	30	7.4	4X 16.8 MW	4X 2.7 MW

TABLE 2.3: Case study ro-ro ferry characteristics

For various draught values, propulsive powers and main engines fuel consumption are available in tabular form. The design draught values (7.4m) are reported in Appendix A, together with the load diagram of the diesel engine for electric generation.

For a typical ship speed of 26.5 kn the values are reported in Table 2.4; the optimum P/D at this speed is 1.13. For the diesel generators the working point is hypothesized at 720 rpm and 70% of MCR power.

	Power P_B [kW]	Fuel consumption [kg/h]	Specific fuel consumption [g/kWh]
Propulsion (x 4)	10521	1975	187.8
Diesel generators (x4)	1890	367	194.0
TOTAL	49646	9369	190.9

TABLE 2.4: Case study power and fuel consumption of ME and DG

According to the conversion factors reported in Table 2.2 the sludge production can be treated to obtain the quantities of new fuel reported in Table 2.5.

Fuel consumption [t/h]	Sludge production [kg/h]	Sludge after decanter [kg/h]	New recycled fuel oil [kg/h]
9.369	141	52	16

TABLE 2.5: Case study sludge quantities

From the figures in Table 2.5 a fuel saving of more than 0.17% can be deduced. This was a promising result but, before proceeding with the economic analysis and the EEOI calculation, the positioning on board was verified.

2.6.1   Location onboard feasibility study

To verify the feasibility of positioning the system onboard, the engine room design is shown in Figure 2.2.

The incinerators are marked in orange, the sludge tank in blue.

As suggested in Section 2.4.1, the incinerator and the sludge tank are both in the engine room and they are even closer than estimated.

2.6.2   Economic evaluation

It was interesting to attempt an economic assessment of the proposed plant.

Considering the investment cost for the construction of the plant, deducted from the literature [99] and [27], the fuel oil price [20] and the cost of the no longer necessary disposal of oily waste (in the Italian ports an average of $65/m^3$ can be assumed) an annual saving of about 22% of the investment cost has been estimated.

Therefore, the investment cost for the construction of the plant can be recovered in about 4-5 years of operation.

Furthermore, this evaluation did not consider the time spent in port to discharge sludge: during the discharge of waste oil, fuel supply is prohibited. As the oily waste discharge is no longer necessary, said time is saved.

2.6.3   EEOI evaluation

For the evaluation of the EEOI, Equation 2.2 was used. EEOI shall be calculated for a specific voyage; for the examined case study, it was chosen a typical voyage of the ferry, at a medium cruise speed of 26.5 knots in even keel condition. The fuel consumption FC_j is reported in Table 2.4 for both main engines and diesel generators.

CF_j the conversion factor from fuel j to CO_2 mass, has the following values: Diesel: 3.206; LFO: 3.151; HFO: 3.114; LPG: propane: 3; butane: 3.03; LNG: 2.75. Either ME and DG are HFO engines.

The distance D is assumed to be 420 nm.

To estimate m_{cargo}, the cargo carried or work done, the IMO guidelines [63] report that for ro-ro vessels, which carry a mixture of passengers, cars and cargo, tons shall be used by multiplying the number of passengers by an average weight of 70kg and adding the "traditional" cargo to that.

(A) Cross section, looking forward

(B) Deck view

FIGURE 2.2: Position onboard

The innovative technology of sludge recycling is considered by adding the new recycled fuel to m_{cargo}.

All the inputs and the EEOI for the base case study are summarized in Table 2.6.

Fuel consumption [t/h]	9.369
voyage time [h]	15.8
FC_j fuel mass [t]	148
C_{Fj} HFO index	3.114
CO_2 mass [t]	**462**
Passengers	2900
Payload [t]	2500
m_{cargo} [t]	**2703**
D distance [nm]	**420**
EEOI	**4.0734E-04**

TABLE 2.6: Case study EEOI

The EEOI for the case with the sludge recycling technology onboard is evaluated in Table 2.7.

CO_2 mass [t]	**462**
Oil from sludge [t]	0.25
m_{cargo} [t]	**2703 + 0.25**
D distance [nm]	**420**
EEOI	**4.0730E-04**

TABLE 2.7: EEOI with sludge recycling technology

It can be noted that the reduction in the EEOI is barely visible. In this attempted interpretation of the index a reduction, which represent an improvement of efficiency, of less than 0.01 % is found.
This means that if these new recycling technologies are to be properly considered, the formulation of energy efficiency must be rethought.

2.7 Final remarks

The present study focused on the possible advantages for the ship system of an innovative solutions for sludge recycling. To sum up, the work done in this research area focused on the feasibility study of the onboard integration of the sludge recycling plant, with particular respect to the zero cost heat source analysis, and its economic and environmental assessment.

The study showed appreciable cost savings thanks to the elimination of the fee due to the port facilities for the proper disposal of sludge; also some time saving in port was found.
The study also showed a 0.17% of cost saving for the yearly purchase of fuel due to the

"self-production" of recycled fuel onboard; this is a modest quantity but not negligible, being the fuel bill of these companies very high. Moreover, since this recycled fuel is produced onboard, its carbon footprint is lower with respect to the bunkered fuel.

The most clear result was the optimisation of the onboard space, no more wasted to a useless tank but better used for recycled fuel production to be burnt onboard.

Finally, the environmental benefits are undeniable, considering the recycling of an otherwise pollutant oily waste and the bad practises related to its disposal. However, the energy efficiency index does not allow these benefits to be adequately addressed, as it is not yet suitable for these innovative waste recycling technologies and the attempt made to calculate it was unsatisfactory.

In conclusion, the small economic advantage and, for now, the impossibility of gaining benefits in the environmental index calculation do not encourage the adoption of this technological solution, despite the environmental advantage it can bring.

3 Hybrid propulsion with exhaust gas recovery systems simulation

3.1 Goal of this work and involvement of the shipping company

This research was born under the interest of a big Italian shipping company GNV. By the analysis of the operating profiles of their ferries, the idea of rethinking the propulsive plant to be more flexible and efficient was born.

The idea was to study an innovative propulsive plant that could be extremely flexible and cost effective, since a conventional propulsive system is usually convenient only in a limited range of ship speeds. To achieve the extreme flexibility desired the new plant proposed was made of dual fuel engines, electric propulsive motors/generators and recovery systems.

GNV was interested in the results of this research and so their technical office of Genova was involved in the project; their kind contribution was the transmission and sharing of relevant data and information.

The goals of the study were the improvement of the ship energy efficiency and the reduction of pollutant emissions. The use of dual fuel with LNG (a fuel with much less pollutant emission than traditional ones), recovery systems and fuel consumption reduction were identified as way to reach them.

To assess the performances, a numerical simulation model was written. This simulator is able to combine all the numerical models of the propulsion and power plant proposed (engines, electric motors, diesel generators and all the recovery systems) together with the ship characteristics (hull resistance and propellers) to evaluate power savings, fuel costs, efficiency and speed achievable the the ship in each and every configuration.

3.2 Literature review

A proper combination of thermal engines and electric propulsion motors, in addition to batteries (especially in small vessels), can offer significant benefits for the propulsion system, such as efficiency, environmental compatibility and flexibility.

Hybrid or electric propulsion systems in general, are not only able to reduce polluting emissions and optimise fuel consumption, but they are also lighter and take up less space, lowering noise and vibration levels together with maintenance costs.

Electric power plants can rely on the existence of technological solutions, now mature also in the maritime sector, such as gas engines [3], fuel cells [33], powerful batteries and energy recovery systems (e.g. energy recovery from engine exhaust gas [8] [72] [7] [6] or through particular turbochargers of the engine [10]).

This research presents the concept design of a flexible hybrid propulsion plant, suited to the design performance requirements of a typical Ro-Ro ferry operating in the Mediterranean Sea, where, due to the presence of numerous water cities, the problem of reducing emissions in port is becoming a high priority [85].

The advantages of the system are explained through the results of an energy efficiency analysis, carried out in the several propulsion modes allowed by the flexibility of the hybrid propulsion [84] [25] [80] [24].

3.3   Innovative hybrid propulsion plant with recovery systems

The propulsive plant proposed is schematically reported in Figure 3.1.

The power plant consists of a twin shaft configuration, where one turbocharged medium speed dual-fuel (DF) engine drives each shaft. The engine moves both a controllable pitch propeller (CPP) and an electric motor/generator (EM/G), with a clutch allowing the disconnection of the main DF engine from the plant. Each main engine is equipped with one hybrid turbocharger (HTC), while the waste heat recovery system (WHRS) of the exhaust gas is in common between the two main engines.
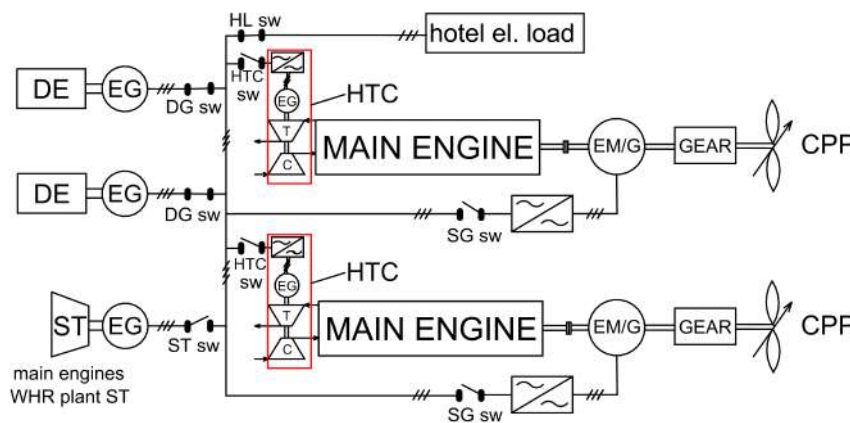
FIGURE 3.1: Flexible plant proposed. High Speed configuration.

The main innovative feature of this propulsive plant is the flexibility: it is adaptable to very different speed requirements, keeping its efficiency high.

The various operational configuration are described in the following chapter.

3.3.1 Operational configurations

Three main configurations can be identified: HS High speed, NN Normal navigation and LS Low speed.

High speed asset, the one represented in Figure 3.1, is comparable to a traditional ship propulsion plant; in fact, the main engine are used for propulsion, the EM/Gs are disconnected and the diesel generators are used for the other electric loads.
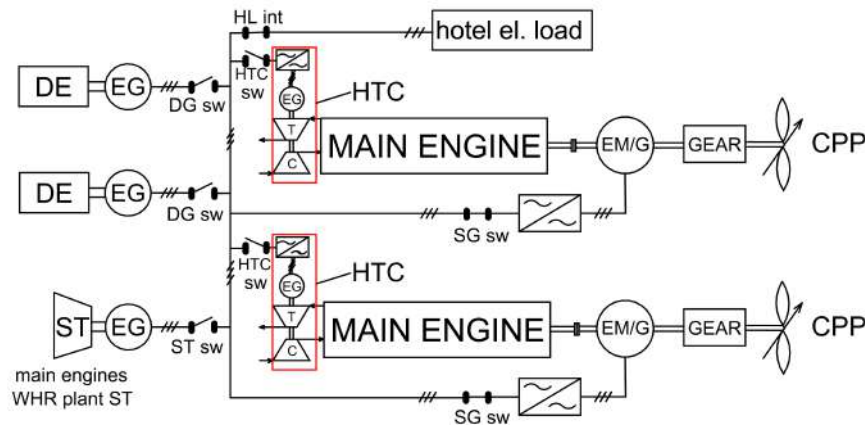
FIGURE 3.2: Normal Navigation configuration.

In **Normal Navigation** configuration, the maximum efficiency is achieved. This is the asset assumed for intermediate speeds and design speed. The main engines are running for propulsion but also to supply power to the shaft electric generators which provide the electric energy for the entire ship electric load (the diesel generators are disconnected in this case). The power subtracted from the propulsion by the shaft EG is variable depending on the requested electric load, which means that the maximum speed achievable in this asset varies from summer to winter, from day and night and so on, depending on electric load fluctuations.
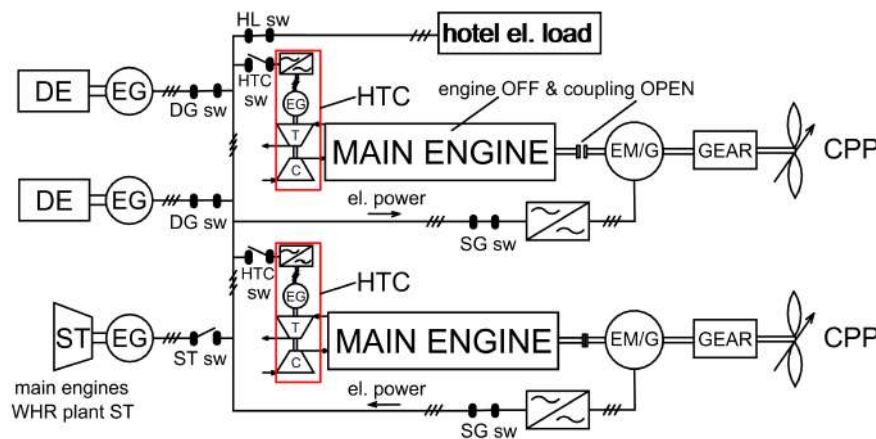
FIGURE 3.3: Low Speed configuration.

Low speed configuration is designed for, as the name suggests, lower speeds, keeping the efficiency high. In this case, only one of the two main engine is running and the other is turned off. The running engine, not only moves its own propeller, but also its shaft electric generator which is used to provide energy to the opposite shaft electric motor, responsible for the respective propeller rotation. The hotel electric load is supplied by the diesel generators.

In each configuration the recovery systems can be in function or they can be off: all the possible combinations were tested.

3.4   Main components of the propulsion plant

As already said, the power plant consists of a twin shaft configuration, with two hybrid-turbocharged medium speed dual-fuel (DF) engines, two controllable pitch propellers, two electric motor/generators (EM/G) and a waste heat recovery system.

3.4.1   Dual fuel engines

Dual-fuel engines can run on both gaseous and liquid fuels. In gas mode the engines work according to the Otto cycle where the lean air-fuel mixture is fed to cylinders during the suction stroke; when running in diesel mode, the engine works according to the Diesel process and the fuel is fed to cylinders at the end of compression stroke.

Usually these engines are optimised for gaseous fuels and diesel fuel is a back-up. They can run on a wide variety of fuels and the switch between gas and diesel mode can take place without turning off the engine.

The main gaseous fuel used is LNG, which is about 90% methane (CH_4).

LNG has the big advantage to have very low pollutant emission if compared to HFO: sulfur content and particulate matter are almost non existent, nitrogen oxides are reduced by 90% and CO_2 by about 20%. On the other end, recently, the problem of "methane slip" has emerged: some of the methane escapes into the atmosphere and, since it is a potent GHG, the risk is to undermine the effort made. This aspect was nearly overlooked since the use of LNG allows to be compliant with IMO Tier III (because of the very low nitrogen oxides) and with Regulation 14 (no sulfur content at all and almost zero particulate matter), thus in LNG mode, entering ECAs is permitted; moreover, LNG also allows to improve EEDI and other carbon intensity indexes since the carbon emissions are reduced. To sum up, conventional ways of looking at GHG, do not take into consideration the methane slip, thus, by the point of view of IMO environmental regulation compliance, LNG is thought to be a very green option, when in reality it is not entirely true [15].

Two more obstacles to its diffusion are the lack of bunkering infrastructures (they are easy to find in ECAs, since LNG allows compliance with IMO regulations, but not

elsewhere) and the low energy density of the LNG which leads to larger storage spaces required onboard (about three times the space is needed in respect to HFO ship).

3.4.2 Waste heat recovery system from exhaust gas

To improve ship energy efficiency, a very effective way is to exploit to the full the fuel burnt. Exhaust gases, in particular, are still full of energy and, to not waste it, it is possible to introduce a waste heat recovery system (WHRS) into the onboard power plant.

A WHRS with steam turbine (WHRS-ST) mainly consists of a recovery boiler, where the heat from exhaust gas is used to transform water into steam to send to a steam turbine, used to move an electric generator.

WHRS are a well-known technology, widely applied in land based power plants. Unfortunately, WHRS plants are usually bulky and heavy, two huge limitations to onboard application. However, with the increase of fuel prices and the introduction of stricter emissions regulation, WHRS started to be installed onboard, primarily to be used as free steam source for onboard use (heating, hot water, laundry etc.). But for ferries and passenger ships, that have a huge electrical demand, the installation of a steam turbine to further exploit main engines exhaust gas, seems a good idea; also because the four stroke diesel engines of these ships have, usually, a lower efficiency compared to the two stroke diesel engines and, therefore, higher exhaust gas (EG) temperature. In LNG mode the EG temperature is even higher and also, since LNG does not need to be heated (as, instead, HFO does), more steam is available to be sent to the ST; moreover, LNG exhaust gas is almost free of particulate matter, hence the WHRS do not get dirty quickly.

In this research two WHRS-GT were considered: with single and dual pressure steam generator, as proposed, studied and extensively reported by professors Altosole, Campora and Zaccone in [11], specifically for the use with marine dual fuel engines. A schematic representation of the two alternatives is reported in Figure 3.4.

The WHR steam plant of Figure 3.4a is made of a heat recovery steam generator(HRSG), composed by an economizer (E) and an evaporator (EV), that feeds a steam turbine (ST) to drive an electric generator (EG). The turbine exhaust steam is extracted by a condensing pump (SCP) from the condenser (SCO), and preheated in the Jacket Water (JW). Then it is delivered to the Heat Water Tank (HWT), from which it is moved by the main feed pump (MFP) to the HRSG economizer (E). Meanwhile the water is warmed in the engine scavenger (SC) by the turbocharger compressor outlet hot air. Meanwhile, a saturated steam part is taken from the HRSG steam drum (SD) to satisfy the ship steam services.

The high pressure part, the superheater (SH hp), of the dual pressure steam plant of Figure 3.4b is the exact WHR single pressure configuration of Figure 3.4a. To improve the efficiency, the authors of [11] proposed to add a low pressure saturated steam system (in blue) with a low pressure economizer (E lp), an evaporator (EV lp) and one more steam drum (SD lp), in order to reach a greater cooling of the exhaust gas.

(A) Single pressure

(B) Double pressure
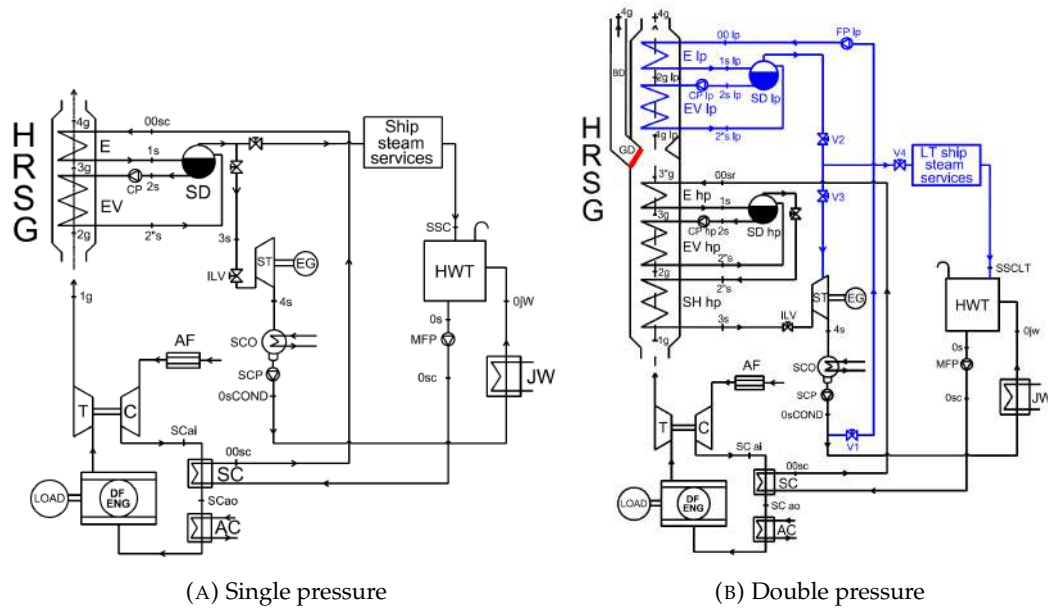
FIGURE 3.4:   Waste heat recovery system with steam turbine.
Source:[11]

3.4.3   Hybrid turbocharger

Another way to fully exploit exhaust gas is the hybrid turbocharger (HTC). In [10] the simulation of the hybrid turbocharger application on a marine natural gas engine was presented and the improvement of the overall efficiency of the engine was proven.
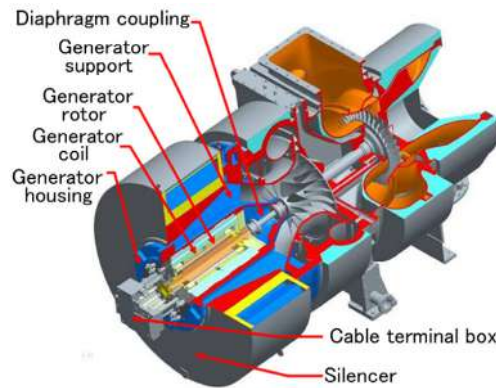
FIGURE 3.5: Cross section of an hybrid turbocharger. Source:[92]

In Figure 3.5 an HTC is represented.

When the turbine of the engine turbocharger (TC) provides more torque than what it is needed by the compressor, a common practice is to divert a portion of the exhaust gas to reduce the mass flow and balance turbine's torque to that of the compressor.

Obviously, this solution is at the expense of overall efficiency. To solve this problem, an interesting solution was proposed and developed by Mitsubishi Heavy Industries [51], for marine applications: a hybrid turbocharger (HTC) with an integrated high-speed electric motor-generator, installed in the TC, as represented in Figure 3.5.

The HTC uses the "extra" portion of the turbine torque to drive an electric generator, thus it is a particular type of exhaust gas waste heat recovery system.

The use of the HTC increases the efficiency of the power plant. Moreover, it can be used together with other kind of recovery system such as the WHRS-ST of Section 3.4.2, since the presence of the HTC does not affect the possibility to install other exhaust gas recovery systems.

3.4.4 Shaft electric motor-generator

A shaft electric motor-generator is added to each shaft. It can be used in both ways: to convert part of the shaft torque, provided by the main dual fuel engine, into electric energy to supply to the ship electric load, but also as an electric motor to drive the propeller.

In the latter situation, the electric motor can be used as a booster or as the only propulsion prime mover.

In fact, it can work together with the DF engine to provide a boost to the propulsion, in order to achieve the top speed of the vessel, but it can also spin the propeller on its own if requested, which is the perfect solution for lower speeds: here the main engine would run outside its optimal range of consumption and, thanks to the shaft electric motor, the DF engine can be turned off; instead, the diesel generators, working at a better condition, are used to supply power and the overall propulsion and power plant efficiency is increased.

3.5 Numerical simulation model

The plant has been numerically modelled by using MATLAB® software.

To evaluate the performances of the different plant operational configurations and choice of recovery components, the approach chosen was different from the conventional matching. In the traditional procedure, knowing the desired ship speed, the propulsive power needed to reach it is calculated (See Section 5.3.1 for the matching procedure explained in details). Instead, in this case, the exact opposite was done: starting from the amount of available total power generated onboard, it was possible to compute the achievable ship speed and use this information, together with information about efficiency, to compare the various possibilities.

To evaluate the ship speed, apart from the propulsive power available for the propellers, the hull resistance and open water diagram are needed. The hull resistance-ship speed curve was provided by the shipping company; about the propeller, Wageningen open water diagrams for CPP, as the one reported in Figure 3.6, were used; the values represented in the graph, one for each value of propeller pitch over diameter ratio (P/D), are: the dimensionless propeller thrust (K_T) with the black solid lines, ten times the dimensionless torque (K_Q) in blue and the openwater propeller efficiency (η_O) in red.
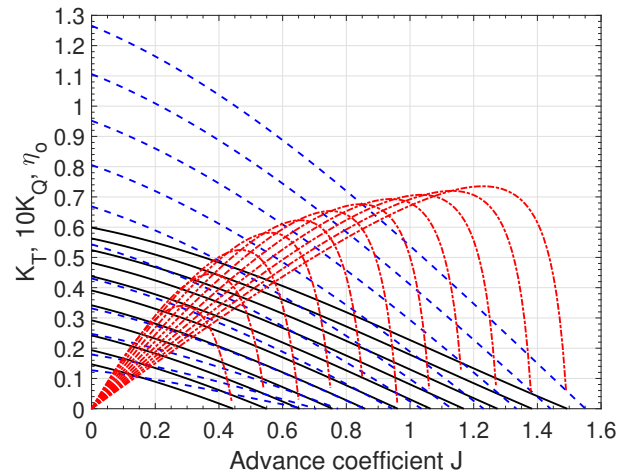
FIGURE 3.6: CPP openwater diagram.

The equilibrium point between the propeller thrust and the ship resistance is found using the ship resistance curve and the openwater diagram, through the matching procedure described in Section 5.3.1.

Doing so, the simulation code provides the propulsive power required to the engine by the propeller to reach a certain speed.

After that, knowing the available propulsive power provided by the power plant, that will be different for every operational configuration and recovery systems installation considered, the simulator is able to identify the powers equilibrium point, through interpolation.

This cited available propulsive power has been calculated as the difference between the total amount of power produced onboard and the power demand for the hotel loads, in different conditions (summer and winter, day and night) as registered by GNV, net of mechanical and electrical efficiency.

To simulate the total power produced onboard, information about main engines, shaft electric generators and different recovery systems are required.

The main engines data in five working conditions are assumed to be inputs, known from the engine project guide. These data are used to calculate engine fuel consumption and exhaust gas information relevant for the recovery systems simulators, in a process deeply analysed by [93].

The delivered power values of WHRS-ST and HTC were calculated for each engine working point as reported in [6] and [10] respectively.

The fuel consumption map provided by the engine manufacturer was used for DG representation.

To sum up, it was possible to obtain the total generated power, fuel consumption, efficiency and ship speed achievable at each engine load for every propulsion and recovery plant configuration.

For each operational configuration and recovery system arrangement the numerical code is slightly different. Each case is better described below.

But before going into more details about this, some important considerations have to be made:

- All the cases reported in Sections from 3.5.1 to 3.5.9 are simultaneously evaluated by the developed MATLAB® code in only one run.

- Common to all the cases there is the propeller-ship resistance equilibrium point evaluation, where required propeller P_B is determined; this procedure is described in full details in Section 5.3.1.

- The inputs to provide to the simulator are:

  - propeller characteristics: Diameter, A_e/A_O, number of blades, P/D interval;
  - ship resistance-speed curve, number of propellers, wake fraction and thrust deduction factor;
  - main engine fuel mode (between LNG and HFO) and power and speed in the desired specific working point;
  - shaft electric motor-generator power;
  - diesel generators power;
  - recovery systems (WHRS-ST 1 and 2 and HTC) powers obtained in the specific main engine working point;
  - hotel electric load for winter and summer, day and night and all the desired conditions;
  - efficiencies.

- The outputs obtained are: ship speed, powers involved and propeller optimum P/D for each case explained below.

- The propeller speed was not considered a relevant parameter in this study since CPP allows great flexibility: being the main engine speed know, the propeller optimisation was done varying the P/D; on the contrary, when the electric motor was involved, the propeller optimisation was made on both P/D and speed (as reported in Section 3.5.7); see Section 5.6.4 for a more in-depth explanation on the selection of the propeller optimum working point.

- Common to all the cases mentioned from Section 3.5.1 to 3.5.9 is the fuel consumption, fuel cost and efficiency evaluation.

  Fuel consumption of the main DF engine and diesel generators are calculated based on the manufacturer project guide.

  The overall energy conversion efficiency was calculated as per Equation 3.1 and 3.2.

$$\eta_{LS} = \eta_{HS} = \frac{P_{ME} + P_{hel}}{\dot{m}_{ME} H_{ME} + \dot{m}_{DG} H_{DG}} \tag{3.1}$$

$$\eta_{NN} = \frac{P_{ME} + P_{rec}}{\dot{m}_{ME} H_{ME}} \tag{3.2}$$

where η_{LS}, η_{HS} and η_{NN} are the energy conversion efficiency of the LS, HS and NN configuration plant respectively; P_{ME} is the mechanical power of the main engines; P_{hel} is the ship hotel electrical power and P_{rec} is the electric power of the possible energy recovery system; $\dot{m}_{ME}$ is the mass flow rate of LNG (or HFO) in the main engines and H_{ME} is its lower heat value; $\dot{m}_{DG}$ is the fuel mass flow rate for diesel generators and H_{DG} is its lower heat value; the different engine performance in gas or diesel mode [5] is taken into account, due to the pertinent value of H_{ME} to be used.

3.5.1   HS with no recovery systems

The simplest case considered, the benchmark, was of course the conventional configuration (named HS in Section 3.3.1): the two dual fuel engine running for the propulsion, the diesel generators for the hotel electric load and no recovery systems at all.

Since the diesel generators are used for the hotel load, the entire main engines power is sent to propulsion.

Knowing the engine power as input, the maximum ship speed achievable at that engine load was simply determined with interpolation between the different propeller required P_B at the different ship speeds. After that, optimum P/D and propeller speed were found.

3.5.2   Emergency: only shaft electric motors

The extreme situation of emergency where the two main engines are not in function and the entire propulsion is carried out by the shaft electric motors. Diesel generators were considered to be running to provide power to the shaft EM which have priority over the others electric loads.

As above, knowing the EM power, ship emergency speed and propeller P/D were determined through interpolation.

3.5.3   Booster

The DF engines provide power for propulsion together with the 2 shaft motors that give extra power to further increase ship speed.

The shaft motor power comes from DGs, which are also running for hotel load.

3.5.4   NN with no recovery

The DF engines are used for both propulsion and power generation through the shaft electric generators.

If the hotel electric load is smaller than the total maximum electric power of the two shaft EG, to determine the actual power for propulsion, half the power needed

for hotel load must be subtracted from each DF engine power (considering the shaft EG and other efficiencies).

If the hotel engine load were greater than the shaft EG power, of course, only the maximum EG power would have been subtracted from DF power and the remaining part would have been taken from the diesel generators.

In this case, the calculation has to be made for every hotel electric load considered.

3.5.5 NN with recovery systems

Also in this case everything has to be repeated for each hotel electric load.

This is the case, as above, where the main engine are used for propulsion but also for shaft generators but, this time, the recovery systems are also running to provide electric power; thus this situation was a bit more complicated to numerically represent. Depending on the recovery system and electric load considered 3 alternatives may occur and each of them is covered in the simulator:

- if the electric load is smaller than the recovered power: DG are off; after subtracting the recovered power to cover the hotel load, the extra recovered power is sent to the shaft electric motors to boost propulsion;
- if the electric load is bigger than the recovered power: the recovered power is entirely used for hotel load; the missing power is taken from the main DF engine tanks to the shaft generators;
- if the electric load is bigger than the recovered power and shaft generators combined: the DGs provide the missing portion.

The described configuration was tested for 5 combinations of recovery systems, simultaneously:

- Hybrid turbocharger (HTC),
- waste heat recovery system with steam turbine (WHRS-ST) single pressure,
- WHRS-ST double pressure,
- WHRS-ST single pressure + HTC,
- WHRS-ST double pressure + HTC.

The outputs of the simulation, for each combination of recovery system and hotel load (5x4=20 in the case study considered), are: ship speed, propeller working point, value of extra or missing power and indication on the number of DGs of each type required and about their working load in respect to their MCR value.

3.5.6 Booster with recovery systems

Diesel generators are only for hotel load.

The DF engines provide power for propulsion together with the 2 shaft motors that give extra power to further increase ship speed.

The power to shaft motors is given by the recovery systems and the motors run only thanks to this recovered power: if it is less than the maximum achievable by

the EM, they set for it. On the other hand, if the recovered power is greater than the maximum power of the shaft motor, the excess is used for hotel electric load and the remaining part (if present) is provided by DGs.

As for previous cases, this simulation is automatically repeated for all the hotel loads and recovery systems combinations to find all the ship speeds and propeller optimum working points and, as above, indication on the number of DGs of each type required and about their working load in respect to their MCR value.

3.5.7   LS

In this case only one DF engine is running to give power to both its propeller and its shaft generator. The power obtained from the latter is sent to the opposite shaft EM and, thus, propeller.

In this scenario, the evaluation of ship speed is more tricky. The procedure is the following.

1. Calculation of propeller thrust for the shaft with DF running: DF engine power and speed were, as always, known. Using this power minus the power absorbed by the shaft generator, the K_Q provided was determined (the gear ratio was previously calculated in a more traditional configuration and, therefore, known). Entering with this value in the (numerical) openwater diagram (Figure 3.6), all the corresponding K_Q provided by the propeller were matched, one for each value of P/D, each corresponding to a value of J and K_T; from J, V_{Ship} was calculated and from K_T the corresponding thrust; for the propeller moved by the DF engine, the curve V_{Ship}-Thrust, where each point is at a different P/D but fixed propeller speed, is obtained. An example is reported in Figure 3.7.
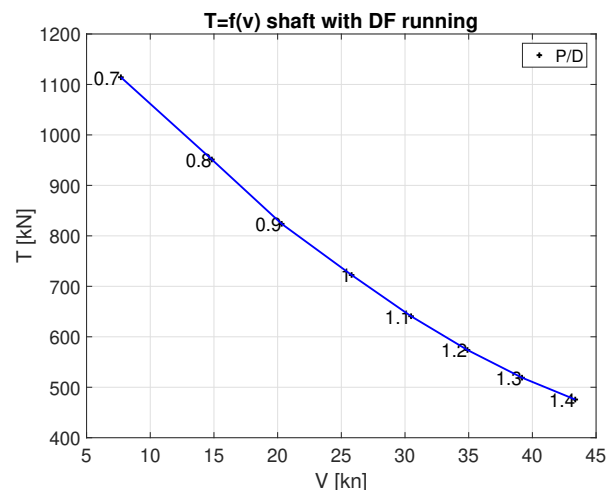
FIGURE 3.7: Example of propeller Thrust of the shaft with DF engine running.

2. Calculation of propeller thrust for the shaft with EM running: power is, again, known, since it is the shaft electric motor (EM) power considering efficiencies, but propeller speed is not; thus the auxiliary variable of K_Q/J^3 was calculated to

enter the openwater diagram and find the J of equilibrium and, thus, similarly as before, the curve of thrust over ship speed was found (Figure 3.8); in this case, each point of the curve corresponds to a different value of P/D and of propeller rotational speed: for each ship speed the optimum propeller speed and P/D were calculated.
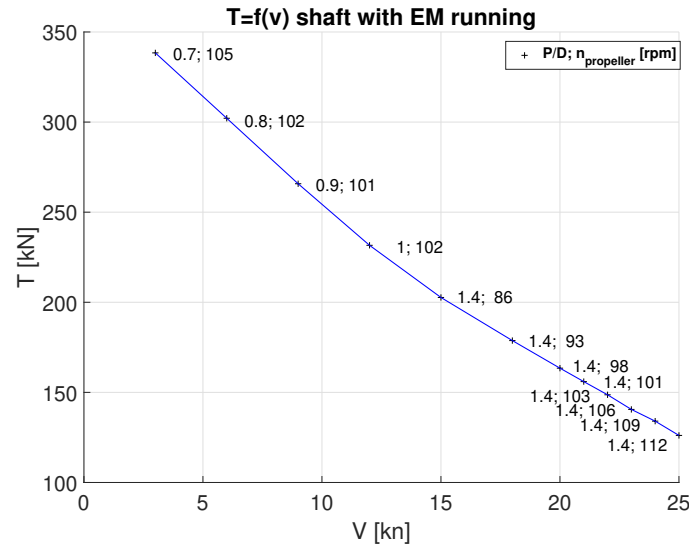
FIGURE 3.8: Example of propeller Thrust of the shaft with EM running.

3. Thrusts equilibrium point (see Figure 3.9 for reference): it was found where the curve of the thrust provided by the propeller on the DF engine running shaft (blue line) intersects the curve of ship resistance diminished by the curve of thrust provided by the EM running shaft (dashed red line).
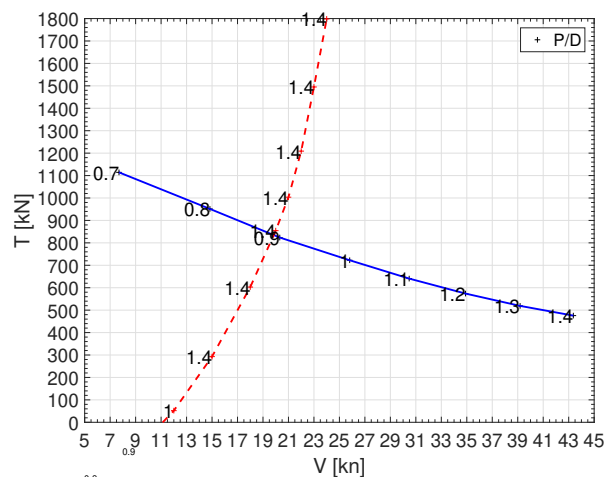
FIGURE 3.9: Example of thrusts equilibrium.

The ship speed reached in this configuration is the one found in the thrusts equilibrium point.

The presence or not of any recovery system can be appreciated in the DGs power demand, since the recovered power is used only for hotel electric load.

3.5.8   1 shaft blocked

If only one propeller is running and the opposite shaft is blocked, the ship speed was simply evaluated as if the ship had been equipped with just one shaft.

3.5.9   1 shaft trailing

If only one propeller is running and the opposite shaft is left free to spin driven by the water (windmilling propeller), the ship speed was evaluated following the procedure of Section 3.5.7 but some clarification is needed: the windmilling propeller, left free to spin with the water, reaches a certain speed and thus J. To find them, K_Q can be used, in fact Q is known ad it is equal to 0 (in the ideal case; in reality it is very small and negative but unknown). For each K_Q=0 of the openwater diagram, K_T and J are found and thus the curve of the trailing thrust in respect to ship speed. This $T_{trailing}$ represent an increase in ship resistance; therefore it is added to the ship resistance curve and the intersection between the new total resistance considering trailing and the thrust of the effectively operating shaft represent the equilibrium and the ship speed is found.

3.6   Case study

As already said, the ship considered as a case study is an existing ro-ro ferry, in particular the GNV Excelsior (Figure 3.10a), whose characteristics are reported in Table 3.1 and Figure 3.10b.
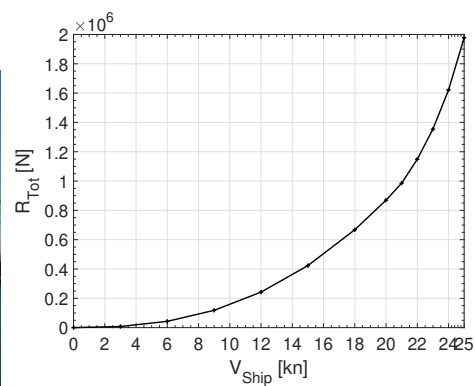
| (A) GNV Excelsior. | (B) GNV Excelsior resistance-speed curve. |

FIGURE 3.10: Case study ship.

GNV has also provided the ship routes and speed profiles in which they were interested most:

- Genova - Palermo medium V_{ship}=23 knots;
- Napoli - Palermo medium V_{ship}=17 knots;
- Genova - Barcellona medium V_{ship}=20 knots;
- Tangeri - Barcellona medium V_{ship}=16 knots.

In respect to these information, the three operational profiles introduced in Section 3.3.1 are specified for the case study in the following way:

LOA	202 m
LPP	176 m
B	27 m
T	7.45 m
GT	40200 t
DWT	7300 t
Passengers	2200
Cars	1000
Propellers CPP	2 x 4 blades, D=4.6 m, A_e/A_o=0.682, P/D= [0.4:0.1:1.4]
Main engines	4 x 7.2 MW Sulzer-Wärtsilä 8L46A
Diesel generators	3 x 2.3 MW Wärtsilä-Vasa 6R32LNE
Electric load winter day	2.2 MW
Electric load summer day	4 MW

TABLE 3.1: GNV Excelsior characteristics.

- HS configuration: V_{ship}=23-25 knots;
- NN configuration: V_{ship}=17-23 knots;
- LS configuration: V_{ship}=up to 14 knots.

These are the ships speed that, using the developed numerical simulator, have to be verified to be achievable in the respective propulsive configuration with 5 combinations of recovery systems:

- Hybrid turbocharger (HTC),
- waste heat recovery system with steam turbine (WHRS-ST) single pressure,
- WHRS-ST double pressure,
- WHRS-ST single pressure + HTC,
- WHRS-ST double pressure + HTC.

3.6.1 Ship re-powering

The four main engines of the existing ship have been replaced by two dual fuel engines 4T DF MAN 51/60 18 cylinders, whose Maximum Continuous Rating (MCR) power is 18 MW at 514 rpm.

The 3 diesel generators have been replaced by two of 2.34 MW each plus a small one DG MAN L16/24 of 0.63 MW.

A shaft electric motor-generator of 2.2 MW has been added at each shaft. They are synchronous motors with permanent magnets, smaller and lighter then asynchronous ones.

Table 3.2 reports the re-powering details of the case study.

Main engines	2 x 18 MW DF MAN 51/60
Diesel generators	1 x 0.63 MW + 2 x 2.34 MW
Shaft electric M/G	2 x 2.2 MW

TABLE 3.2: Case study re-powering

The main engines (DF MAN 51/60) data are available from the engine project guide [79], in five working conditions at given power conditions (100, 85, 75, 50, 25% MCR) and rotational speeds (514, 514, 501, 462, 402 rpm).

The fuel consumption map provided by MAN for L16/24 in [78] was used for representation of diesel generators.

It can be noted that the total main engines power is higher than before; this is due to the request of GNV of increasing the ship speed. Moreover, the original propulsive configuration had four main engines and the new one has only two. This aspect required further investigation.

Firstly the dimensions and weights were considered and, after a specific analysis, the shipping company confirmed the compatibility of the new engines with the spaces available in the engine room.

Then, a comparison between a 2 engines (B) or a 4 engines (A) configuration, as reported in Figure 3.11, was studied to assess that the choice made was not detrimental in terms of fuel consumption.
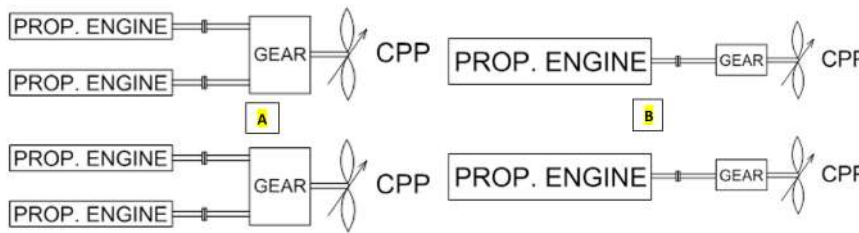
FIGURE 3.11: Configurations of the main engines.

The same engine type, the MAN 51/60 DF, was applied to both cases: the 9 cylinders version for the four engines plant (A) and the 18 cylinder one for the two engines plant (B). The project guide is available for both versions.

By the analysis of the fuel consumption of one shaft line it is possible to understand whether the choice made is acceptable or not.

The results are reported in Figure for both cases of diesel (on the right) and gas mode (on the left).
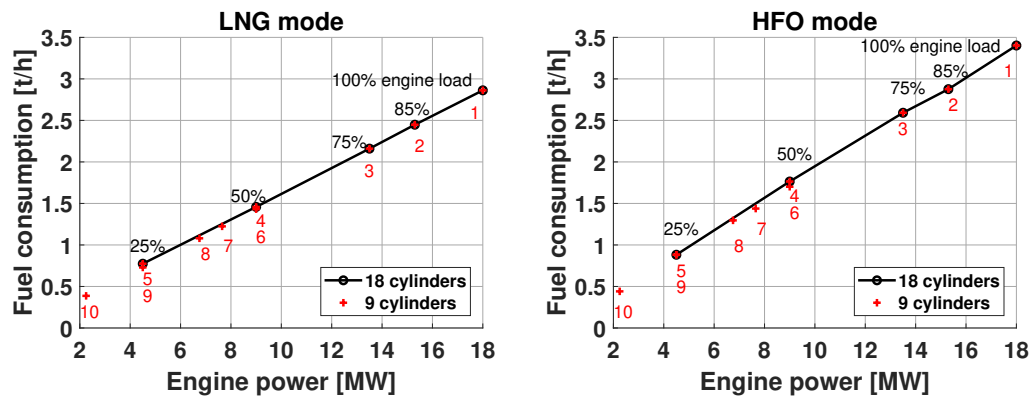
FIGURE 3.12: Comparison between propulsive configuration with one 18 cylinders or two 9 cylinders engines per shaft line.

In Figure 3.12, the black line shows the fuel consumption of the single 18 cylinder engine per shaft line working in the configuration represented in Figure 3.11B. Each black dot is a specific engine working condition as reported in the graph (100, 85, 75, 50 and 25% of MCR power).

The red dots of Figure 3.12 represents the working points of the 9 cylinders engines configuration, the four engines one (Figure 3.11A); red dots from number 1 to 5 are for when both 9 cyl. engines per shaft line are in function, while red numbers from 6 to 10 are for when only one among the two 9 cyl. engine per shaft line is on.
More clearly, 1: 2 9 cyl. ON at 100%, 2: 2 9 cyl. engines ON at 85%, 3: 2 9 cyl. engines ON at 75%, 4: 2 9 cyl. engines ON at 50%, 5: 2 9 cyl. engines ON at 25%, 6: 1 9 cyl. engine OFF and 1 ON at 100%, 7: 1 9 cyl. engine OFF and 1 ON at 85%, 8: 1 9 cyl. engine OFF and 1 ON at 75%, 9: 1 9 cyl. engine OFF and 1 ON at 50%, 10: 1 9 cyl. engine OFF and 1 ON at at 25%.

From Figure 3.12, it can be deduced that the fuel consumption is almost the same for the two considered alternatives, with the exception of red point 6 and 7, where the fuel consumption is slightly lower than the black line. Here, the two 9 cylinders option seems the best choice but in reality, these are operating condition hardly ever reached: point 6 is for one engine is on at 100% of the MCR and the other one off.

On the other hand, installing only one engine per shaft line instead of two is beneficial in terms of CAPEX and OPEX of the propulsion systems and also from both the space and weight point of view.

Therefore, the choice of installing only one engine per shaft line is acceptable.

3.6.2 Case study recovered powers

In [93], the extensive calculations done to obtain the recovered power from the various recovery systems are reported. In that numerical simulation each recovery system was modelled in details (for example, also considering the quantity of steam to subtract to the WHRS because of the ship thermal utilities). For the full detailed explanation please refer to [93].

In this work, since the focus is on the matching between recovery systems and ship, only the results of the recovery systems simulation ares reported in Table 3.3, where the recovered powers for the different engine working points can be found.

Recovery system	25%	50%	75%	85%	100%
WHRS-ST single pressure	1015	1539	1919	2026	2115
WHRS-ST double pressure	1350	1935	2436	2576	2659
HTC	718	1779	1763	1698	1535
WHRS-ST 1 + HTC	1733	3318	3682	3725	3650
WHRS-ST 2 + HTC	2068	3714	4199	4275	4194

TABLE 3.3: P_{rec} [Kw] in summer day navigation with LNG.
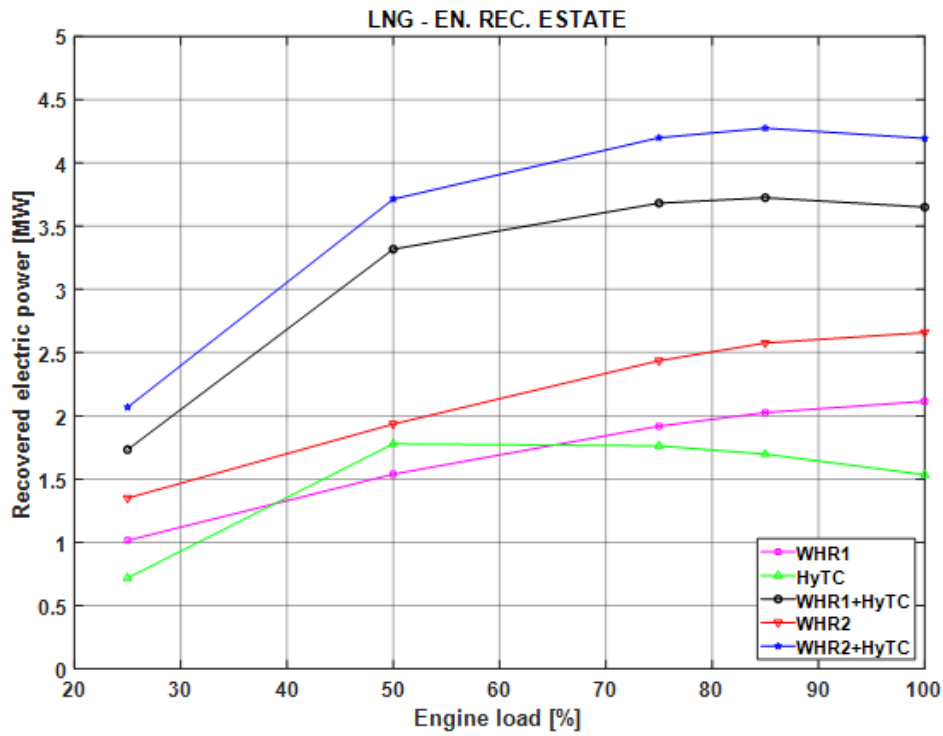
(A) P_{rec} LNG mode summer day.
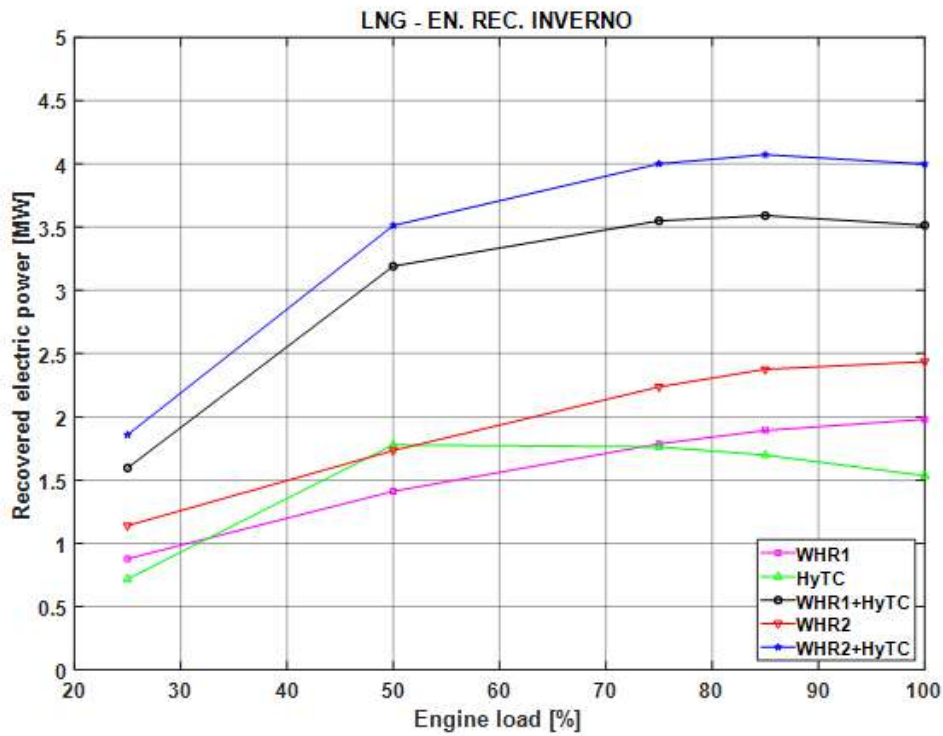
(B) P_{rec} LNG mode winter day.

FIGURE 3.13: P_{rec} in LNG mode.
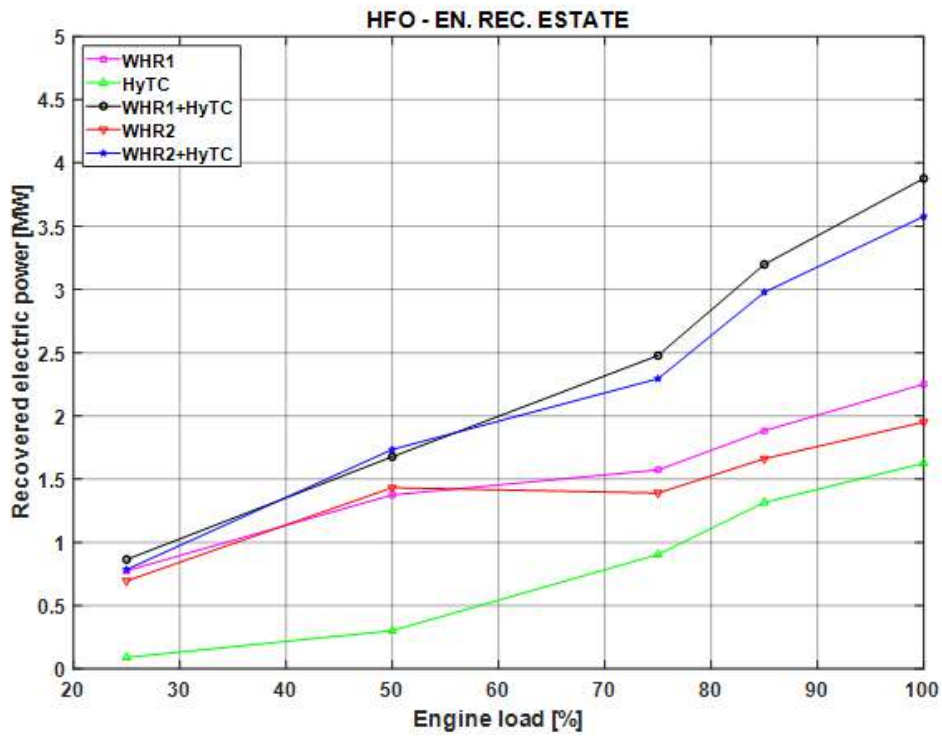
(A) P_{rec} HFO mode summer day.
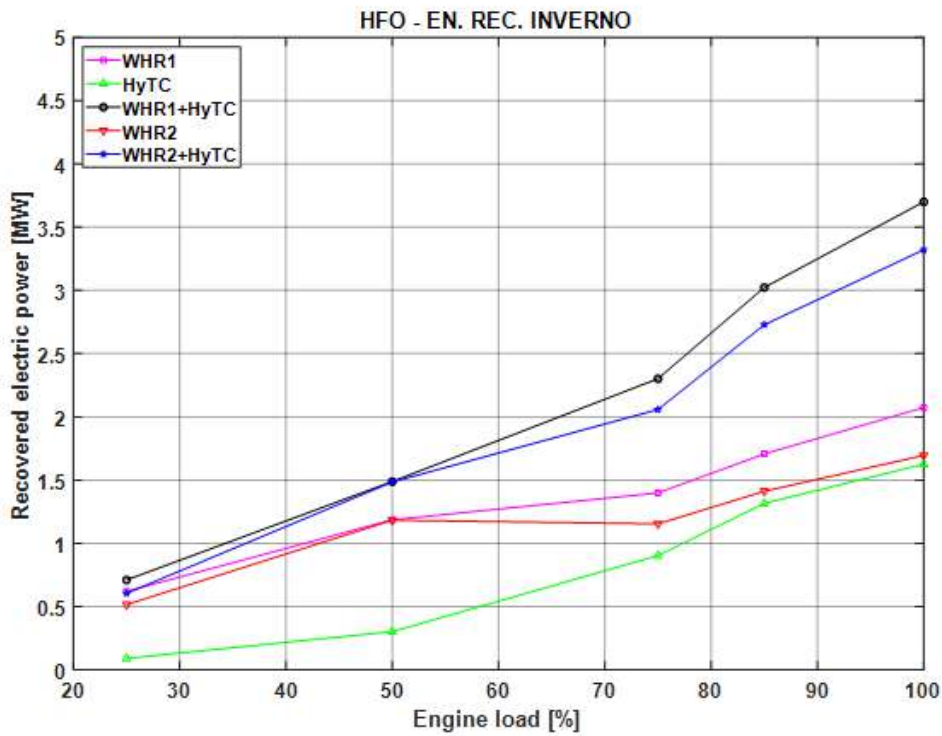
(B) P_{rec} HFO mode winter day.
FIGURE 3.14: P_{rec} in HFO mode.

In Table 3.3 the recovered electric powers (P_{rec}) expressed in [Kw] for the summer day navigation in LNG mode with both engines running are reported, one for each engines working point. For a more immediate representation, Figure 3.13a was made. The same was made for both fuels (LNG and HFO) and for summer and winter day navigation. The results are reported in Figures 3.13 and 3.14.

From the Figures 3.13 and 3.14 it is possible to notice that the behaviour of the HTC is influenced only by the type of fuel and not by summer or winter condition as it acts directly outside the engine before the spilling of heat for the onboard steam load.

On the contrary, WHRS 1 and 2 are heavily influenced by both since the steam turbine behaviour is subjected to the quantity of steam subtracted to it to be used for the other onboard steam users.

Moreover, fore some condition, e.g. LNG winter (Fig. 3.13b), the electrical power recovered is more that the hotel load; the surplus, represented in Figure 3.15, can be sent to the shaft motor to boost the propulsion, as explained in Section 3.5.5.
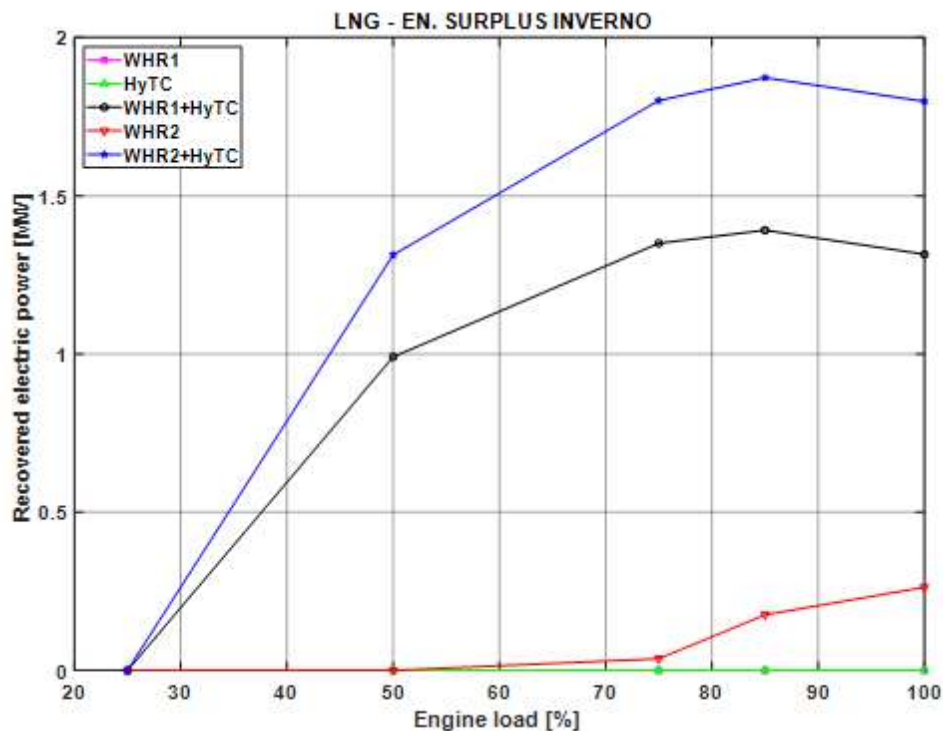
FIGURE 3.15: P_{rec} surplus, LNG mode, winter navigation.

3.6.3 Fuel consumption, fuel cost and efficiency evaluation

Fuel consumption of the main DF engine were calculated based on the manufacturer project guide [79].

Fuel consumption of the two diesel generators Wärtsilä-Vasa 6R32LNE was known in every load condition [95].

Fuel consumption of the small diesel generator MAN 6L16/24 660kW, which works at the low electric loads of when recovery systems supply the majority of the request, was obtained from the manufacturers project guide [78].

For more details see Appendix B, where also the low heating values of the fuels (H_{ME} and H_{DG}) necessary to calculate efficiency, are reported.

For the fuel costs, the prices reported in Table 3.4 were assumed [21].

LNG	398 €/ton
HFO	380 €/ton
MDO	575 €/ton

TABLE 3.4: Fuel prices

3.7 Results

The comparison between the various operational configurations (HS, NN, LS), combinations of recovery technologies and fuel modes were studied.

The aim of this work was to give to the shipping company guidelines about what is the best solution in terms of cost and efficiency to reach a certain ship speed.

Some of the numerous results are presented in this section by means of 2 types of Figures:

- graphs of the overall energy conversion efficiency of the power plant depending on the working load of the main DF engines, as calculated in Equations 3.1 and 3.2;
- graphs of the cost of the navigation per nautical mile [€/nm] expressed as a function of the ship speed [kn]. This cost included the fuel cost for main engine main fuel and pilot fuel and diesel generator's fuel.

The simulations were made in all the possible combinations described (summer-winter, day-night, LNG-HFO) but, for simplicity, since all cases are very similar, the results shown are referred to the summer day navigation, with main engines running in LNG mode, unless otherwise specified.

3.7.1 No recovery systems

Figure 3.16 reports the performances of the power plant without any recovery system, in summer day LNG configuration.

Fig. 3.16a shows NN condition as the most efficient plant configuration from the 40% up to the full load of the engine. On the contrary, the energy conversion efficiency is better for LS condition at 25% of the engine load. This is because, at low engine loads, the main engines have a low efficiency, while diesel generators at full load have an higher efficiency and, thus, they increase the overall efficiency when they are in use (case HS and LS) in respect to when they are off (NN).

On the other hand, Figure 3.16b shows the lowest fuel cost for NN configuration in all the ship speeds. From an economic point of view, NN configuration is always

(A) Efficiency

(B) Cost
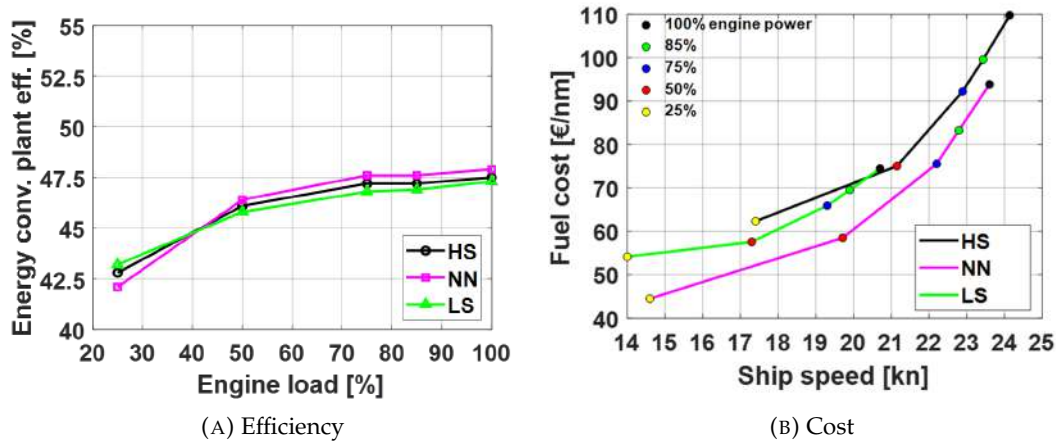
FIGURE 3.16: Performances without any recovery system in LNG mode

cheaper. The reason is the difference in the cost of the two fuel types, as the LNG
(burned by the DF engines in NN mode) is less expensive than fuel oil (used by DGs
in LS and HS mode).

In this regard, it was tested a fictional situation where the dual fuel engines burned
diesel oil as the DGs and the cost differences per nautical mile were almost negligible
[9].

From these considerations it emerges that the main benefit of the LS configuration,
compared to the NN configuration, if no recovery systems are involved, does not con-
cern significantly higher energy efficiency, but rather the possibility of using a single
main motor, with evident advantages in terms of lower vibrations and noise, together
to a reduction of maintenance costs.

From Figure 3.16b the maximum ship speed achievable in each configuration are
show: in LS the top speed is 20.5 kn, while in HS a 24 kn of speed is reached. The
wider range of speed is obtained in NN mode from 14.5 to 23.5 kn.

3.7.2   With recovery systems

Figure 3.17 reports the performances of the power plant with hybrid turbocharger;
Figure 3.18 with single pressure waste heat recovery systems with steam turbine; Fig-
ure 3.19 with double pressure waste heat recovery systems with steam turbine; Figure
3.20 with single pressure waste heat recovery systems with steam turbine and hybrid
turbocharger together; Figure 3.21 with double pressure waste heat recovery systems
with steam turbine and hybrid turbocharger together. They were all made for summer
day navigation in LNG mode.

In each case illustrated from Figure 3.17 to 3.21, it is possible to recognise the same
main result: NN is the optimum configuration among the three considered propul-
sion modes, in terms of efficiency and fuel consumption. This is possible thanks to
the energy recovery systems, which allow the diesel generators to be off and the shaft
generators to absorb less power.
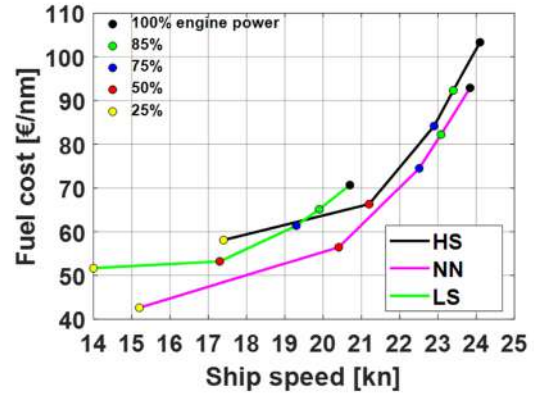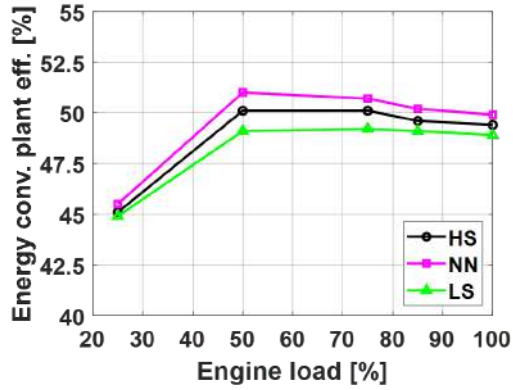
(A) Efficiency   (B) Cost

FIGURE 3.17: Performances with HTC in LNG mode
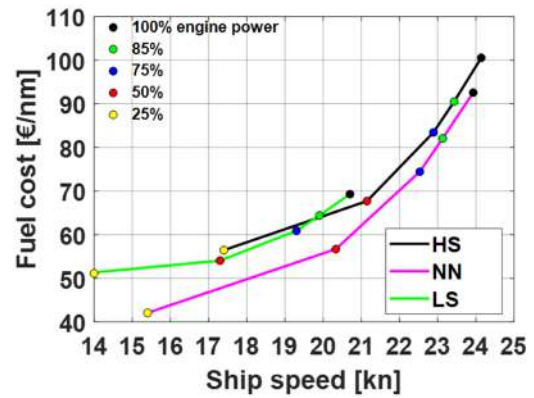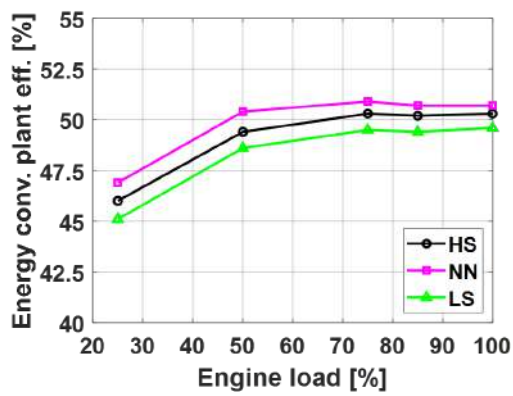
(A) Efficiency   (B) Cost

FIGURE 3.18: Performances with WHR-ST 1p in LNG mode
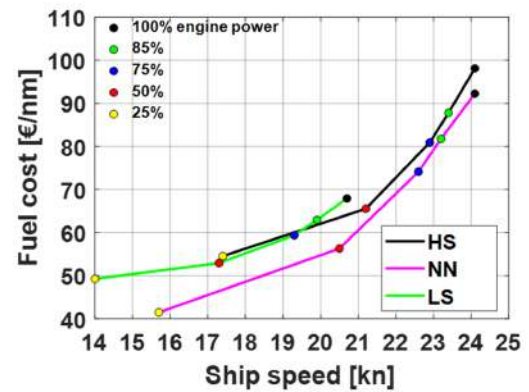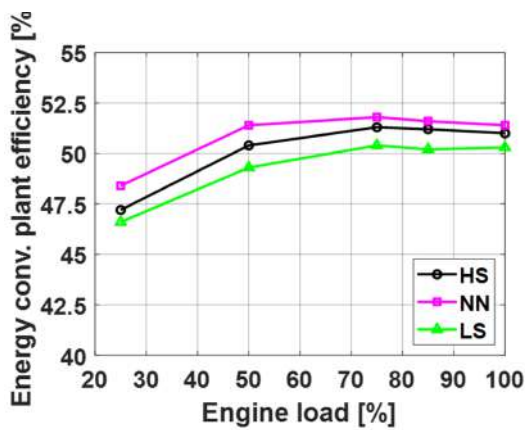
(A) Efficiency   (B) Cost

FIGURE 3.19: Performances with WHR-ST 2p in LNG mode

(A) Efficiency

(B) Cost
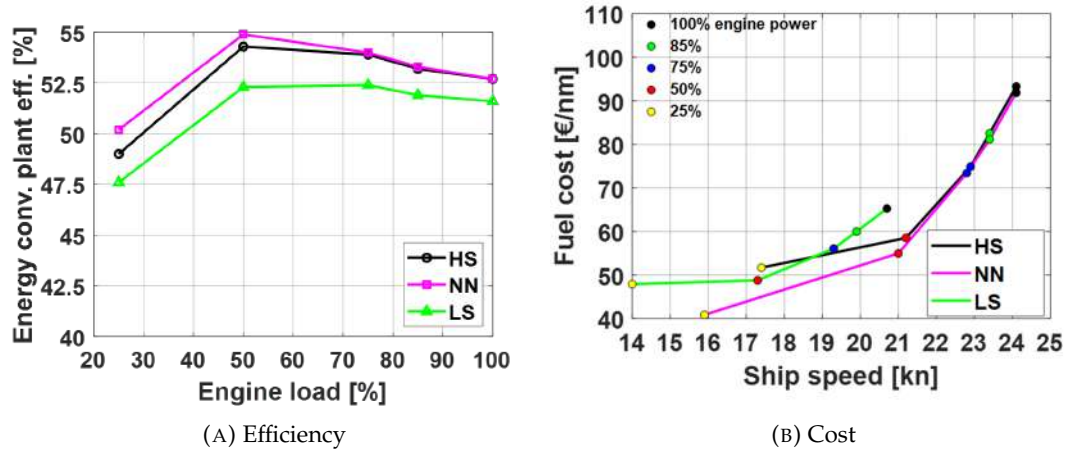
FIGURE 3.20: Performances with WHRS-ST 1p + HTC in LNG mode

(A) Efficiency

(B) Cost
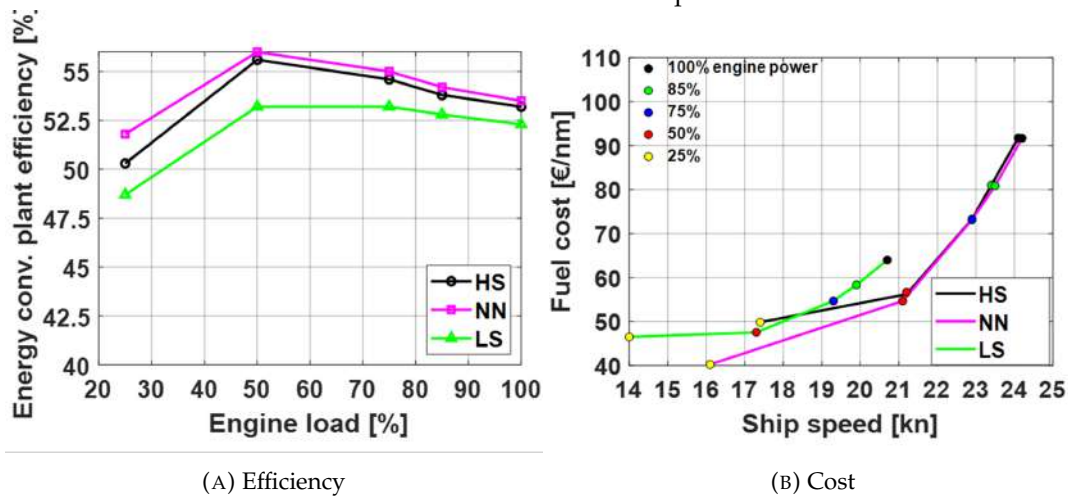
FIGURE 3.21: Performances with WHRS-ST 2p + HTC in LNG mode

Regarding the single technologies, the comparison of Figure 3.17a, 3.18a and 3.19a shows that HTC technology is the least advantageous at 25% of the engine load, while at other loads, the three of them are comparable.

As expected, the best plant efficiency is achieved with 2 recovery systems working together: Figure 3.20a and 3.21a, with a maximum efficiency of over 55%, at around 50% of the engine load (due to a better HTC performance in the same working range) for both cases.

To sum up, the system is more efficient in the propulsive configuration of normal navigation, corresponding to the nominal speed of the ship, achieved with the two main engines working (energy conversion efficiency around 47.5% at 85% of the main engine load). However, the flexibility of the examined power system in using only a single main engine at low speed, is still important because it reduces vibrations and noise, as well as maintenance costs. The additional power contribution due to the adoption of particular energy recovery solutions, such as the simultaneous use of the WHR system and hybrid turbochargers of the main engines, can improve efficiency up to more than 55% for the nominal speed of the vessel.

3.8 EEDI evaluation

To assess the expected improvement in the ship energy efficiency, the IMO energy efficiency design index (EEDI) was calculated.

The attained EEDI, as introduced in Section 1.5, represents the total amount of carbon emissions of the ship in respect to the work done (expressed in terms of capacity multiplied by speed), as reported in Equation 1.1.

This value must be under a certain threshold, the Required EEDI, specific for the ship type considered.

Firstly the Attained EEDI was calculated following the IMO formulation reported in Equation 3.3:

$$
\begin{aligned}
EEDI = &\frac{\left(\prod_{j=1}^{M} f_j\right)\left(\sum_{i=1}^{nME} P_{MEi} \cdot C_{FMEi} \cdot SFC_{MEi}\right) + \left(P_{AE} \cdot C_{FAE} \cdot SFC_{AE} *\right) +}{f_i \cdot f_c \cdot f_w \cdot Capacity \cdot v_{ref}} \\
&+ \frac{\left(\left(\prod_{j=1}^{M} f_j \cdot \sum_{i=1}^{nPTI} P_{PTI(i)} - \sum_{i=1}^{neff} f_{eff(i)} \cdot P_{AEeff(i)}\right) \cdot C_{FAE} \cdot SFC_{AE}\right) +}{f_i \cdot f_c \cdot f_w \cdot Capacity \cdot v_{ref}} \\
&\frac{- \sum_{i=1}^{neff} f_{eff(i)} \cdot P_{eff(i)} \cdot C_{FME} \cdot SFC_{ME}}{f_i \cdot f_c \cdot f_w \cdot Capacity \cdot v_{ref}}
\end{aligned}
\tag{3.3}
$$

To apply the EEDI formulation the following assumptions were made:
- there are no innovative technologies for the propulsion onboard and so P_{eff}=0;
- $f_i = f_w = f_{eff} = 1$ for the ship and power plant considered and f_j and f_c were calculated following the IMO guidelines [64];
- P_{PTI} =0 since the shaft EM-Gs are considered only as generators; for this reason, their power at 75% was subtracted from MCR power of the main DF engines; the obtained value was the one considered as the "new MCR" for the main engines and the 75% of that value is P_{ME};
- the emission of the main engines (SFC_{ME}) have been evaluated considering both the main fuel (LNG) and the pilot fuel (MDO), each with its own correction factor C_F;
- the recovery contributions and hotel electric load assumed are the one for the summer day navigation

Then the IMO procedure was applied and the Attained EEDI calculated. This value, as said, must be smaller than the required EEDI, calculated as per Equation 3.4.

$$
Required\ EEDI = (1 - X/100) \cdot a \cdot b^{-c}
\tag{3.4}
$$

Where b for ro-ro ferries is the deadweight tonnage (DWT), a and c are coefficients depending on the type of ship and year of construction and X is a correction factor, increasingly severe for the various IMO EEDI Phases.

The procedure was repeated for every recovery technology combination and also for both LNG and HFO, but the real EEDI for a ship with dual fuel engine is only the one evaluated with LNG, the HFO value was calculated just for comparison.

The results are reported in Figures 3.22 and 3.23, where the usual abbreviation are used (E is for the scenario with no recovery systems, only the engine).
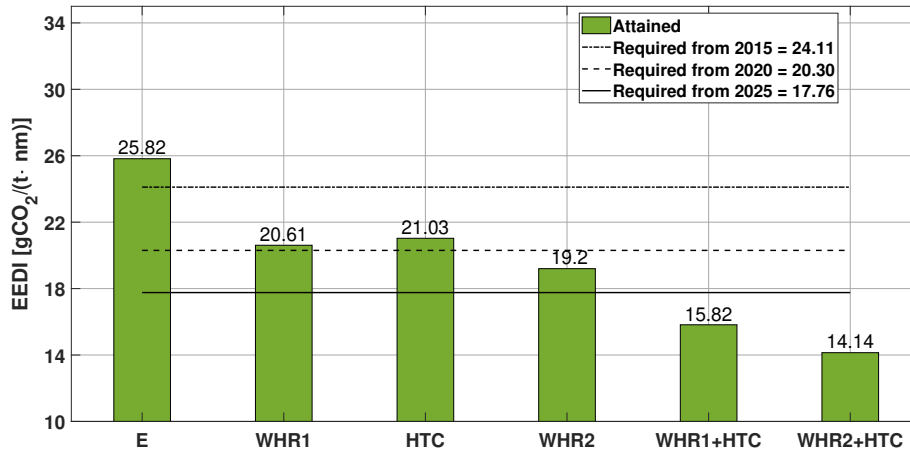
FIGURE 3.22: EEDI LNG mode
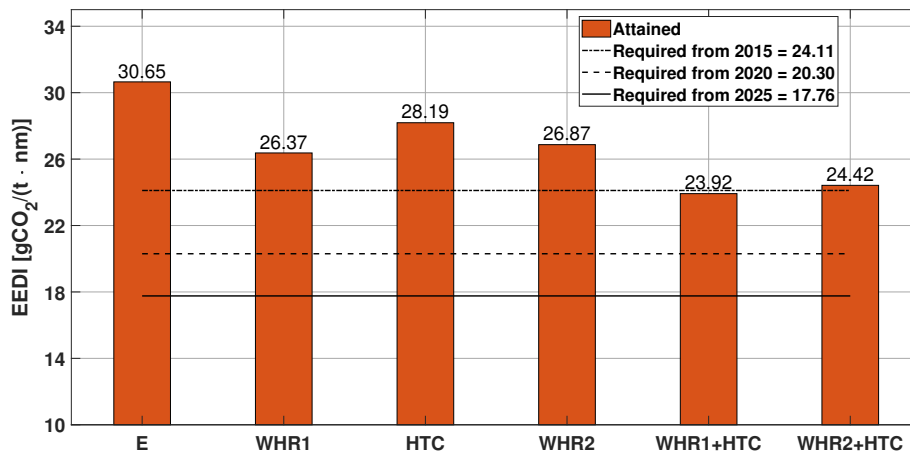
FIGURE 3.23: EEDI HFO mode

The merely academic HFO EEDI of Figure 3.23 shows that none of the alternatives would comply with IMO regulation.

For the real EEDI, evaluated in LNG mode and represented in Figure 3.22, the situation is better: if the two cases of single pressure WHRS-ST and hybrid turbocharger alone are not sufficient to comply with the rules since 2020, when the two technologies are combined the ship is compliant also for the stricter required EEDI of 2025. The double pressure WHRS-ST alone is sufficient for now, but from 2025 the combination of WHRS-ST 2 and HTC will be necessary.

3.9 Economic analysis

An evaluation of the possible fuel cost saving was attempted, considering the typical ship routes.

Here the results regarding the Genova-Palermo route (427 nm) are reported. For a more complete set of results please refer to [93].

The calculation was made considering an entire year of operation in LNG mode, made of 192 summer days and 112 winter days, as requested by GNV. The ship speed requested from the shipping company for this route was 23 knots, achievable with both the NN and HS configurations.

The fuel cost was calculated considering the LNG fuel consumption for the main DF engines and the MDO fuel consumption for both the diesel generators and the pilot fuel of the DF main engines. The results are reported in Tables 3.5 and 3.6.

| Plant | HS | | NN | |
	Annual fuel cost [M€]	Savings [M€]	Annual fuel cost [M€]	Savings [M€]
No recovery	11.7	-	10.9	-
HTC	10.7	-1.0	10.3	-0.6
WHRS-ST 1	10.6	-1.1	10.2	-0.7
WHRS-ST 2	10.3	-1.4	10.1	-0.7
WHRS-ST 1 + HTC	9.8	-1.9	9.6	-1.3
WHRS-ST 2 + HTC	9.7	-2	9.5	-1.4

TABLE 3.5: Annual fuel costs and savings with respect to no recovery configuration

Plant	Savings NN respect to HS [M€]
No recovery	-0.81
HTC	-0.35
WHRS-ST 1	-0.38
WHRS-ST 2	-0.17
WHRS-ST 1 + HTC	-0.21
WHRS-ST 2 + HTC	-0.23

TABLE 3.6: Annual savings of the NN configuration in respect to HS configuration.

Form Table 3.5 it can be noted that, in HS configuration, for every recovery system combination studied a certain amount of fuel cost saving is achieved, thanks to the possibility of using the recovered power for the hotel electric loads and reduce the load of the diesel generators. In NN configuration this effect is even larger because, if the recovered power is not enough for the ship electric load, the shaft generator is used in place of the diesel generators that remain off.

The larger savings possible in NN configuration with respect to HS is confirmed by the values reported in Table 3.6.

The installation onboard of one or more recovery systems allows considerable savings in both HS and NN configurations, against a moderate CAPEX increase. In the end the annual total cost of the plants with recovery systems (considering both CAPEX and OPEX) is inferior to the cost of the no-recovery condition [93].

In particular, the hybrid turbocharger is the more interesting: the initial investment is way smaller than the one for a WHRS-ST and the annual savings are comparable.

3.10   Final remarks

In this research an innovative propulsion and power plant has been studied. The plant was developed to accommodate the requests of the shipping company GNV in terms of high efficiency in a wide cruise speed range to reduce fuel consumption and thus operating costs.

At the same time, this plant is required to comply with the MARPOL regulations for the reduction of pollutant emissions.

For all the reasons listed above, flexibility, cost saving, emission reduction, the proposed plant combined dual fuel engines (in LNG or HFO mode) with shaft electric motor-generators and with different possible recovery systems, in particular hybrid turbocharger, single and double pressure waste heat recovery system with steam turbine and the HTC used simultaneously to the WHRS-STs.

Three main operational configuration were studied: high speed (HS), the more traditional one, normal navigation (NN), where the shaft electric generator is in charge of the hotel electric load, and low speed (LS), where only one main engine is running to move both propellers.

A numerical simulator was implemented in MATLAB® environment.

With the developed code it was possible to obtain information about powers, fuel consumption, efficiency and ship speed achievable at each main engine load for every propulsion and recovery plant configuration.

The inputs to provide to the simulator are: propeller characteristics, ship resistance, main engines and DG project guides, shaft EM-G power, recovered powers from HTC and/or WHRS-ST, hotel electric loads. The results obtained are: ship speed, powers involved, propeller optimum P/D, plant efficiency and total fuel consumption for each operational and recovery plan configuration.

The results found show that the Normal Navigation (NN) operational configuration is the one associated with the lowest fuel costs and highest plant efficiency in the

entire ship speed range considered, for all the possible recovery systems configurations, in both LNG and HFO mode.

Moreover, as expected, the WHRS-ST + HTC are the more beneficial, being the double pressure plant better than the single pressure one.

With that results it was then possible to analyze EEDI and cost savings of the various recovery plant configuration alternatives in respect to the no-recovery baseline.

In this case, it was found that the installation onboard of one or more recovery systems allows considerable savings, against a moderate CAPEX increase and, in particular, the hybrid turbocharger is the more interesting since the very low initial investment is paid off by considerable annual savings.

4 Wind assisted ship propulsion

The use of wind for marine propulsion is nothing new. The first documented examples date back to the Egyptians in 3100 B.C. [30]. During the nineteenth and twentieth centuries, the need for increasing ship speed control has led to a gradual abandonment of the volubility of the wind to address the much more reliable and flexible mechanical propeller-engine propulsion.

Interest in wind potential has grown in recent years. It is, nowadays, seen no longer as the sole propulsive force of the ship but as an aid to the engine propulsion to achieve the 2050 emission targets. The wind aid allows, if properly exploited, to meet the design speed by reducing power, fuel consumption and therefore emissions of the ship.

Although real existing operating wind assisted ships are limited, there are numerous studies and many alternatives to choose from: traditional sails, wing sail, Flettner rotors, wind turbines and kites.

All of these solutions use wind power to directly generate thrust for the ship, except for wind turbines that generate electricity.

In this chapter a short overview of the available technologies is presented. Benefits and drawbacks have been reported from the few available sources. In the next chapter the Flettner rotor technology is exploited through numerical simulation.

4.1 Wind turbines

As previously mentioned, wind generators convert wind energy into electric energy. The most common ones are those with horizontal axis, even if there are also some examples with vertical axis.

Due to the low power generated-dimensions ratio, they are not very widespread and they are only commonly seen on recreational craft, especially sailing yachts, where the energy demand is very limited [30].

4.2 Sails

Well-known solution supported by an highly specialized industry. However it fails to break through in the merchant ships sector because, despite the low initial investment, the maintenance costs are high. Moreover, some space onboard is not available for the payload [31].

FIGURE 4.1:
Small
wind
tur-
bine.

FIGURE 4.2: Oceanco Black Pearl
rigged with DynaRig.[91]

This, however, is not the case for mega-yachts that are, for now, the main recipients: an example is shown in Figure 4.2.
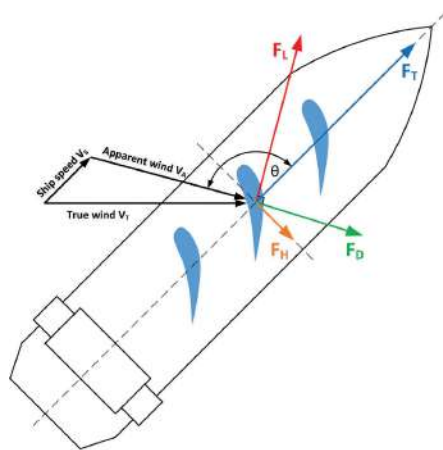
(A) Wing sail, forces.[[94]]

(B) Orcelle wind, RoRo ship; concept by Wallenius
Wilhelmsen with Oceanbird. [119]

FIGURE 4.3: Wing sails

4.3   Wing sails

Wing sails are wing profiles that can be oriented to produce lift; an example is the VentiFoil®, produced by the Dutch company eConowind [38].

In Figure 4.3a the operating principle is illustrated: θ is the angle of direction of incoming apparent wind relative to the ship's bow; the apparent wind, which is the vector composition of the true atmospheric wind and the ship speed, acting on the sail, generates lift (F_L, perpendicular to the apparent wind) and drag (F_D, parallel to the wind). Composing these two forces along the forward direction of the ship gives the thrust provided by the profile (F_T) and, perpendicularly to it, a drift force (F_H).

To maximize F_T, the profile, that can rotate 360°, is suitably oriented with respect to the wind, changing the angle of attack [94].

These profiles have a high coefficient of lift, compared to sails. They can be made in the shape and size best suited to the specific case, using light but resistant materials. The substantial initial investment is outweighed by limited operating costs. However, the space occupied is quite large [31].

(A) Kite, forces [94].

(B) MS Beluga SkySails, container ship. Fuel savings up to 30% [108]
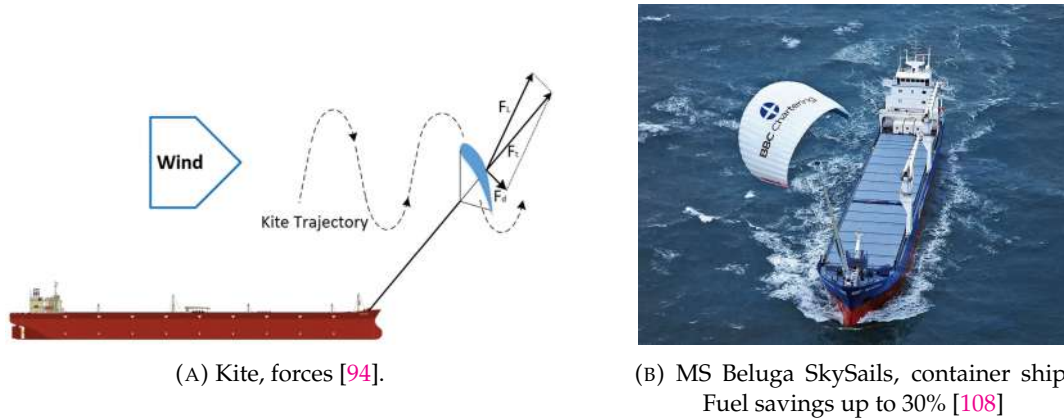
FIGURE 4.4: Kite

4.4 Kites

Kites generate propulsive thrust, as illustrated in Figure 4.4a, taking advantage of high-altitude winds; for this reason they must be maintained between 100 and 300m of altitude [94].

The swinging performances, the complexity and the delicacy of the system of launch and withdrawal of the sail and of its control techniques are the main disadvantages of this technology. On the other hand, it has a very small size and low costs.

(A) Flettner rotor, forces.

(B) SC Connector, Sea-cargo; 2 Rotor Sail Norsepower installed onboard January 2021. Emission reduction -25% [88]
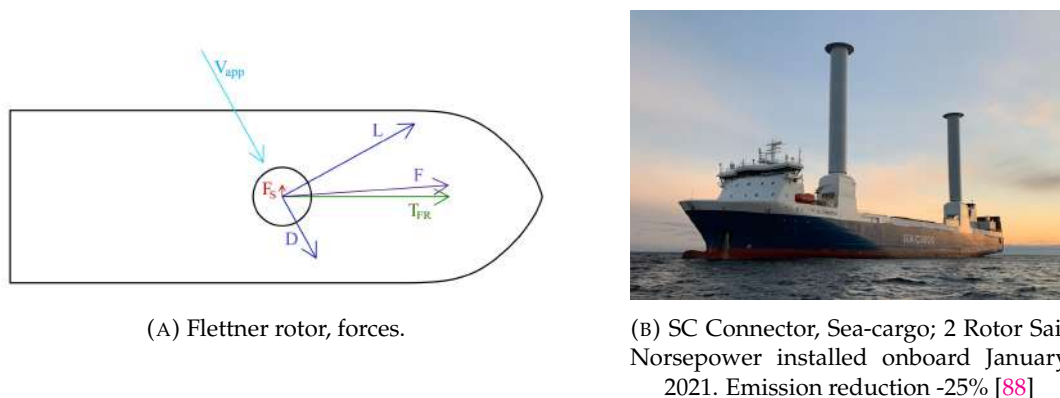
FIGURE 4.5: Flettner rotor

4.5 Flettner Rotors

Named after inventor Anton Flettner, these rotating cylinders generate aerodynamic lift and drag thanks to the Magnus effect. They must be installed on the upper deck

and rotated by means of an electric motor. Rotation in an airflow, which is the apparent wind V_{app} in Figure 4.5a, generates drag (D) in the wind direction and lift (L) perpendicularly to it; their resultant (F) projected on the ship's advance direction is the propulsive thrust T_{FR}.

They are very compact and lightweight being empty inside and often made of aluminum. They use simple technology, do not require trained crew and involve low initial and maintenance costs. The overall fuel savings must consider the energy for propulsion and the energy required by the electric motor to spin the rotor [31].

Although the results in terms of emission savings seem promising, there are still few examples of ships equipped with wind assisted propulsion technologies. This is probably due to a limited availability of experimental data and systematic studies in this field. The uncertainties in estimating the possible reduction in fuel consumption are still considerable and therefore it is difficult to assess the effectiveness of the investment.

5 Flettner rotor: modelling from wind to power

Energy efficiency and Carbon Intensity indexes are evaluated in terms of ratio between the ship CO_2 emissions with respect to the performance output (i.e. transport work). Because CO_2 is proportional to fuel consumption, a way to improve the ship efficiency is to adopt propulsion technologies able to reduce the installed engine power and lower the fuel consumption for the same transport work. This way of thinking is also economically beneficial because it has the advantage to lower ship running costs with moderate CAPEX increase.

As already stated, for a new ship design, multiple technologies can be considered to achieve this goal. On the contrary, for existing ships the range of possibilities is reduced and the fuel consumption reduction has to be achieved by a proper integration between the existing plant with the new technologies. Among others, one of the best solutions for retrofitting, as well as for new ships, is the installation onboard of some kind of renewable energy source and, in this study, the wind assisted propulsion has been addressed.

Wind assisted ship propulsion (WASP), as reported in Chapter 4, embraces a number of technologies that use the wind force to produce thrust for the ship propulsion; the wind energy is harnessed and directly used for propulsion, and not converted into electric energy, as in wind farms. This is, certainly, not a new idea, since sails are known to humankind since thousands of years.
Multiple WASP technologies are proposed for ships such as traditional sails and wing sails, kite and Flettner rotors.

The latter is the one chosen in this study because it is considered simple to install onboard and cost effective, it's light weigh, compact and easy to operate. Flettner rotors are rotating cylinders (usually spin by an electric motor) that generate aerodynamic lift and drag when immersed in a fluid stream; the working principle belongs to the so called Magnus effect [105].

5.1 Aim of the study

The aim of this study is to propose a generalised procedure able to address the rotor propulsive thrust and its influence on the engine-propeller working point in order to evaluate the ship fuel consumption and the possible fuel savings.

The innovation is the numerical simulation that enables to optimise the integration of the wind power, renewable but unreliable, with more "controllable" and reliable propulsion systems such as diesel engines with screw propellers. The optimised integration aims to provide tangible benefits such as downsizing of the diesel Maximum Continuous Rating (MCR), propeller optimization for different working points (in case of new buildings), and above all, the least possible fuel consumption.

This Chapter reports the first part of the aforementioned study, in particular the methodology for the evaluation of the rotor thrust, the related shift of the propeller working point and the brake power requirement, the evaluation of the power to spin the rotor and a parametric study to asses the influence of the rotor dimensions and wind on ship resistance. In Chapter 6 the evaluation of engine working points and fuel consumption is reported.

The described methodology is implemented in Matlab® environment to perform numerical simulations.

5.2   Flettner rotors performance: state of the art

5.2.1   Literature review

In the following the most recent literature on the rotor physics is analysed.
In [37] the rotor aerodynamics has been analyzed by means of numerical simulations to create a tool for the preliminary design. Some parameters, such as spin ratio, aspect ratio and rotor dimensions, have been systematically varied to evaluate their impact on the lift and drag coefficients and these data were validated. The simulation results were used for the development of a model of lift and drag coefficients useful for the preliminary design of Flettner rotor.

In [18] a series of experiments were conducted to better understand the influence of Reynolds number on rotors; the large amount of data collected showed that Reynolds number does not influence the power consumption of the rotor and allowed to derive an analytical function for its calculation; the authors also suggest to take into proper consideration the rotor mechanical systems when computing the actual power consumption. The rotor's power consumption is also analysed in [71] alongside power developed.

The rotor impact on ship stability is addressed in [117], the outcome of the study shows a moderate or insignificant impact. In [34] the relationship between rotor and ship's roll motion is addressed. The rotor thrust force is observed to decrease in roll motion because of the reduction of the rotor projected area with increasing heel angles. Furthermore, it has been observed that the maximum heel angle is increased in roll motion of non-rotor ship case.

Several studies exist on the analysis of the system performance onboard. According to [30] there are 6 Kite, 2 Suction wing, 3 Rigid sails and 9 Flettner rotor installations, onboard different ship types. Articles and press releases [48] report important benefits. Some of the more recent studies show a significant fuel consumption reduction with the use of the rotor as an auxiliary propulsion device; in particular [30] reports a list of measured fuel saving values in the range 1-50%, [104] report up to 22% savings of the annual ship fuel consumption, with a pay-back time of six years. Similar results of up to 20% savings are reported by [113] and by [115] where both a rotor and a kite are investigated.

In [76] different wind assisted technologies (rotor, wingsail and DynaRig) are compared and the most significant fuel savings have been provided by the Flettner rotor, with an average value of 9%. On the contrary, [102] shows quite low benefits of under 1% of using the rotor on a DWT 4000 ton container ship.

Despite the focus of the studies is the same: the environmental benefit, the metrics used to compare the solutions are different. Comparisons in terms of propulsion power, fuel consumption, power, costs, are proposed by using very few or any technical/scientific marine engineering ground.

In conclusion, the literature review shows a lack of studies about the methodology on how to compute the contribution of the rotor on thrust, power and consumption of the ship, in particular about the onboard integration of the rotor and its implementation as an auxiliary technology for ship propulsion.
This is precisely what will be addressed in this research.

5.2.2 Rotors off the shelf

Flettner rotors are a technology solution already available for shipowners. There are two companies offering rotors: Norsepower and Anemoi.

Norsepower is a Finnish company. Its "Rotor sails" have been installed, as a retrofit, onboard of the tanker Timberwolf (ex Maersk Pelican) in 2018 and underwent testing and data analysis at sea until the end of 2019. Lloyd's Register independents measurements confirmed savings of 8.2% during the first year of operation [86]. Other examples are 2 passenger ships (Scandlines M/V Copenhagen and Viking Grace), the bulk carrier VLOC Sea Zhoushan and the ro-ro vessel SC Connector owned by Sea-Cargo.

Anemoi is a Rotor sails UK company, partner of Wärtsilä. The 2 bulk carrier M/V Afros M/V Axios are equipped with Anemoi rotor sails and claim about 12% of fuel savings [13].

5.3   Ship propulsion modelling

5.3.1   Methodology

The aim of this study is to evaluate the ship fuel consumption with a wind assisted propulsion technology in a comfortable way for a naval architect/marine engineer. The proposed methodology make use of the well-known engine-propeller matching procedure [110] and try to integrate the Flettner rotor into this procedure.
The following data are supposed to be known:

- ship dimensions and hull resistance at different speeds;

- propeller characteristics, in terms of dimensionless thrust an torque by means of coefficient K_T and K_Q;

- Flettner rotor geometric dimensions;

- engines load diagram in terms of Power - engine speed and specific fuel consumption curves;

- efficiencies (shaft line, gear box, etc.) and hydrodynamic coefficients;

- ship electric load balance;

- wind conditions.

The methodology can be summarised by the following steps:

1. Analysis of the environmental conditions: wind speed and direction.

2. Evaluation of the rotor forces and their influence on the ship forward motion.

3. Evaluation of the effective net resistance ($\underline{R}_N$) that the propeller has to balance with the thrust, taking into account the presence of rotor and wind.

4. Evaluation of the propeller working point by imposing the equilibrium between the propeller thrust and the ship net resistance ($\underline{T}_P = \underline{R}_N$) at a specific ship speed. The propeller speed n_p is calculated by solving the forward equilibrium equation written in terms of the auxiliary variable K_T/J^2:

$$\frac{K_T}{J^2} = \frac{R_N}{n_{prop} \cdot \rho \cdot V_A^2 \cdot (1-t) \cdot D_p^2} \tag{5.1}$$

   where J is the advance coefficient $V_A/(n_p \cdot D_p)$; n_{prop} is the number of propellers; ρ is the water density; the advance velocity V_A is = $V_{ship} \cdot (1-w)$; V_{ship} is the ship speed, w the wake coefficient, t the thrust deduction factor, and D_p the propeller diameter.
   Where the values of K_T/J^2 requested are equal to the K_T/J^2 provided by the propeller, the J of equilibrium are found and thus the corresponding n_p. K_Q is

calculated from J and the propeller torque from K_Q.

The required engine power to achieve the ship speed is then evaluated as:

$$P_B = \frac{P_O}{\eta_r \eta_s \eta_g} = \frac{2\pi\rho}{\eta_r \eta_s \eta_g} \cdot K_Q \cdot D^5 \cdot n_p^3 \qquad [W] \qquad (5.2)$$

where P_O is the openwater propeller power, η_r is the relative rotative efficiency, η_s the shaft line efficiency and η_g the gear efficiency. Further details and applications can be found in [81].

5. Matching between the identified propeller working point and the engine working point by using the engine load diagram map. The propeller required engine power P_B and the corresponding engine speed n_e (= n_p · gear ratio), are positioned in the engine load diagram, by means of the transformation imposed by the gear ratio.

6. Evaluation of the engine fuel consumption by using the SFOC (Specific fuel oil consumption) in the engine working point

7. Estimate of exhaust emissions based on engine data.

This Chapter is dedicated to the first four points of the previous list, presenting the modelling of the rotor related phenomena on the ship propulsion. Thrust produced and power required are presented. The integration of these quantities with a CPP-diesel propulsion and overall ship fuel consumption quantification (points from 5 to 7) are examined is Chapter 6.

The evaluation of the ship net resistance is addressed in Section 5.3.5 while the evaluation of the rotor forces is addressed in Section 5.3.7.

5.3.2 Numerical simulation

The described methodology was applied and all these steps were followed in the writing of the numerical simulator.

The developed code was implemented in MATLAB® environment.
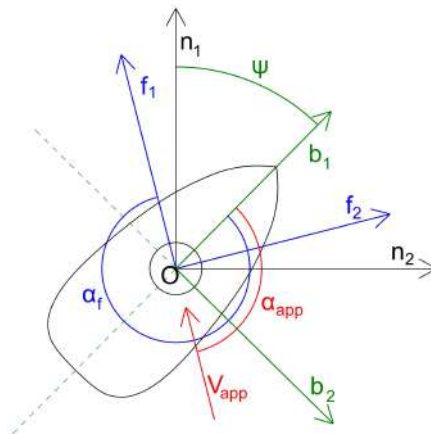
FIGURE 5.1: Reference frames.

5.3.3 Reference frames

Since forces and vectors are extensively discussed, it is useful to define the reference frames used, in accordance with the ones defined by [45].

Firstly, the inertial $\underline{n}_i$ frame ($\mathcal{O}_n$, $\underline{n}_1$, $\underline{n}_2$, $\underline{n}_3$) is the geographical reference system fixed to the Earth, where $\underline{n}_1$ points towards the North, $\underline{n}_2$ to the East and $\underline{n}_3$ towards the center of the Earth.

For the purposes of this study the body-fixed base is more convenient: $\underline{b}_i$ (Ω_b, $\underline{b}_1$, $\underline{b}_2$, $\underline{b}_3$) is fixed to the hull with $\underline{b}_1$ pointing forward, $\underline{b}_2$ towards starboard and $\underline{b}_3$ downwards; the frame origin Ω_b is chosen to coincide with the center of the base of the rotor as reported in Figure 5.1.

The transformations between the bases $\underline{n}_i$ and $\underline{b}_i$ are described by the following equations:

$$\begin{cases} \underline{b}_1 = \cos\left(\Psi\right)\underline{n}_1 + \sin\left(\Psi\right)\underline{n}_2 \\ \underline{b}_2 = -\sin\left(\Psi\right)\underline{n}_1 + \cos\left(\Psi\right)\underline{n}_2 \\ \underline{b}_3 = \underline{n}_3 \end{cases}$$

where Ψ [rad] is the Yaw angle and, for the purpose of this study, it is assumed equal to 0.

To more easily describe the wind related vectors, the $\underline{f}_i$ base is introduced ($\mathcal{O}_f$, $\underline{f}_1$, $\underline{f}_2$, $\underline{f}_3$): $\mathcal{O}_f \equiv \Omega_b$, $\underline{f}_1$ is parallel to the apparent wind, as defined in section 5.3.4, and it has the same direction, $\underline{f}_2$ is perpendicular to the apparent wind and $\underline{f}_3$ is pointing downwards, as it can be seen in Figure 5.1.

If α_f is the angle between $\underline{b}_1$ and $\underline{f}_1$, the transformations between the bases $\underline{b}_i$ and $\underline{f}_i$ are described by the following equations:

$$\begin{cases} \underline{f}_1 = \cos\left(\alpha_f\right)\underline{b}_1 + \sin\left(\alpha_f\right)\underline{b}_2 \\ \underline{f}_2 = -\sin\left(\alpha_f\right)\underline{b}_1 + \cos\left(\alpha_f\right)\underline{b}_2 \\ \underline{f}_3 = \underline{b}_3 \end{cases}$$

For practical reasons these transformations can be expressed as a function of α_{app}, the angle between $\underline{b}_1$ and the direction of the incoming apparent wind:

$$\begin{cases} \underline{f}_1 = -\cos\left(\alpha_{app}\right)\underline{b}_1 - \sin\left(\alpha_{app}\right)\underline{b}_2 \\ \underline{f}_2 = \sin\left(\alpha_{app}\right)\underline{b}_1 - \cos\left(\alpha_{app}\right)\underline{b}_2 \\ \underline{f}_3 = \underline{b}_3 \end{cases}$$

5.3.4 True wind and apparent wind

Some considerations about wind are required, since wind is an essential component of the propulsion system and many equations of the presented model contain wind characteristics, in terms of speed and direction.

The true wind represents the wind characteristics over a sea area, the wind speed V_{True} and the wind direction of origin α_{True} are generally provided with respect to the $\underline{n}_i$ frame. The true wind is assumed to be an input of the procedure. The forces developed by the rotor can be more easily formulated in the $\underline{f}_i$ frame.

The apparent wind ($\underline{V}_{app}$) is defined by vector composition of true wind ($\underline{V}_{True}$) and ship speed ($\underline{V}_{ship}$) as per Equation 5.3.

$$\underline{V}_{app} = -\underline{V}_{ship} + \underline{V}_{True} \tag{5.3}$$

Its magnitude and angle of origin are found using the cosine formula reported in Equation 5.4:

$$
\begin{aligned}
V_{app} &= \sqrt{V_{True}^2 + V_{ship}^2 + 2 \cdot V_{True} \cdot V_{ship} \cdot \cos(\alpha_{True})} \\
\alpha_{app} &= \arccos\left(\frac{V_{True}^2 - V_{app}^2 - V_{ship}^2}{-2 \cdot V_{app} \cdot V_{ship}} \right)
\end{aligned}
\tag{5.4}
$$

In Figure 5.2 the influence of the ship speed on apparent wind composition is shown: for the same true wind speed (blue dotted line) an increase in ship speed (red dashed line) corresponds to a progressive shift of the apparent wind direction towards the bow (black solid line).
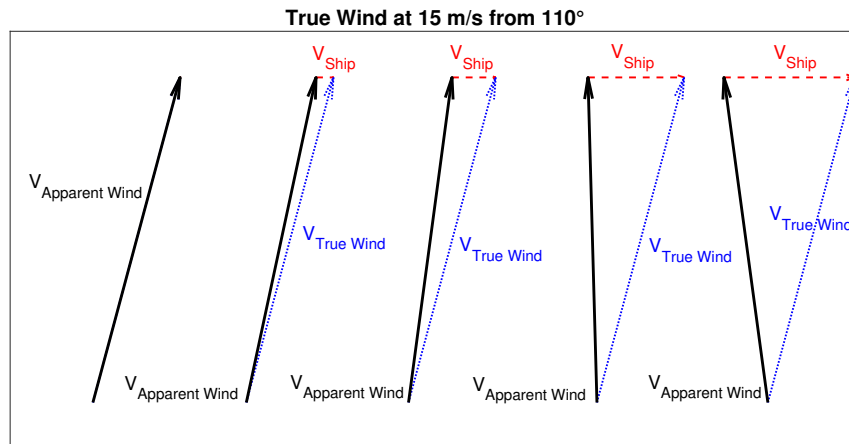
FIGURE 5.2: Ship speed effect on apparent Wind composition.

5.3.5 Net resistance

At the equilibrium, it is well known that the total ship resistance ($\underline{R}_T$) must be counterbalanced by the total ship thrust ($\underline{T}_T$), as reported in Equation 5.5, which represents the propulsion equilibrium condition along the ship longitudinal axis ($\underline{b}_1$).

$$\underline{R}_T = -\underline{T}_T \tag{5.5}$$

When a wind added resistance is present, $\underline{R}_T$ is calculated as per Equation 5.6, where $\underline{R}_H$ is the hull resistance in calm condition (no air, no wind, no waves), $\underline{R}_W$ is the added resistance due to air friction on the whole ship (ship superstructure and rotor).

$$\underline{R}_T = \underline{R}_H + \underline{R}_W \tag{5.6}$$

If a thrust generator device as the rotor is introduced, the total ship thrust ($\underline{T}_T$) is given by the sum between the thrust generated by the propeller ($\underline{T}_P$) and the thrust given by the Flettner rotor ($\underline{T}_F R$) (Equation 5.7).

$$\underline{T}_T = \underline{T}_P + \underline{T}_{FR} \tag{5.7}$$

By the substitution of Equation 5.6 and 5.7 in Equation 5.5, Equation 5.8 is found.

$$\underline{R}_H + \underline{R}_W = -(\underline{T}_P + \underline{T}_{FR}) \tag{5.8}$$

If a thrust generator device, as the rotor, is introduced, the main problem is to compute the effective net resistance for the propeller.

In this work the ship net resistance will be defined as the part of the ship resistance that is not overcome by the rotor forward force and has to be counterbalanced solely by the propeller thrust $\underline{T}_P$, as per Equation 5.9.

$$\underline{R}_N = -\underline{T}_P \tag{5.9}$$

This resistance will be addressed as "Net Resistance $\underline{R}_N$" and can be evaluated as follows, considering that the main interest, regarding the ship propulsion system, is the direction of advance and, therefore, from now on, the equations will be expressed in terms of $\underline{b}_1$ components.

$$\begin{aligned}
-T_P \underline{b}_1 &= R_H \underline{b}_1 + R_W \underline{b}_1 + T_{FR} \underline{b}_1 \\
R_N \underline{b}_1 &= R_H \underline{b}_1 + R_W \underline{b}_1 + T_{FR} \underline{b}_1
\end{aligned} \tag{5.10}$$

Due to hypotheses in Section 5.3.1 the force $R_H \underline{b}_1$ is known, only forces $R_W \underline{b}_1$ and $T_{FR} \underline{b}_1$ need to be evaluated.

The net resistance evaluation is an essential step to determine the propeller working point when the rotor is active.

5.3.6   Air and wind added resistance

The air and wind added resistance includes the effect of the air friction and of the wind on the ship's superstructures. When the rotor is switched-off it is considered as an additional superstructure.

$R_W \underline{b}_1$ is determined, as reported in Equation (5.11), as the effect of the wind on the transverse (S_T) ship projected area above waterline [19] [70].

$$R_W \underline{b}_1 = -0.5 \cdot CX \cdot \rho_{air} \cdot V_{app}^2 \cdot S_T \tag{5.11}$$

In Equation (5.11) CX is a drag factor assumed equal to $0.6 \cdot \cos \alpha_{app}$ [19], ρ_{air} is the density of air ($1.225 \ kg/m^3$), V_{app} is apparent wind velocity and α_{app} is direction of incoming apparent wind. The effects of the Reynolds number were considered negligible, as previously done and stated by the source of the formula [19].

If the rotor is installed onboard but switched off, a further term to R_W must be added; this term considers the wind added resistance of the rotor as an additional superstructure:

$$R_{W_{rotorOFF}}\underline{b}_1 = -0.5 \cdot K \cdot \rho_{air} \cdot V_{app}^2 \cdot S_{rotor} \cdot \cos \alpha_{app} \qquad (5.12)$$

where the drag factor K is a function of the rotor aspect ratio (AR) and it was assumed equal to 0.8 [17]. The effects of the Reynolds number were not considered since [70] proved that the rotor aerodynamic coefficients are almost constant for $Re = 1.0 \cdot 10^6$ or greater. The area S_{rotor} is the product between the height and diameter of the rotor.

On the contrary, when the rotor is working, there is no need for Equation(5.12) since the wind added resistance of the rotor will be incorporated in the subsequent aerodynamic considerations leading to the evaluation of $T_{FR}\underline{b}_1$.

5.3.7 Rotor thrust force

In Figure 5.3a the forces generated by the rotor are represented, while in Figure 5.3b the main dimensions of the rotor are drawn.

(A) Rotor forces.
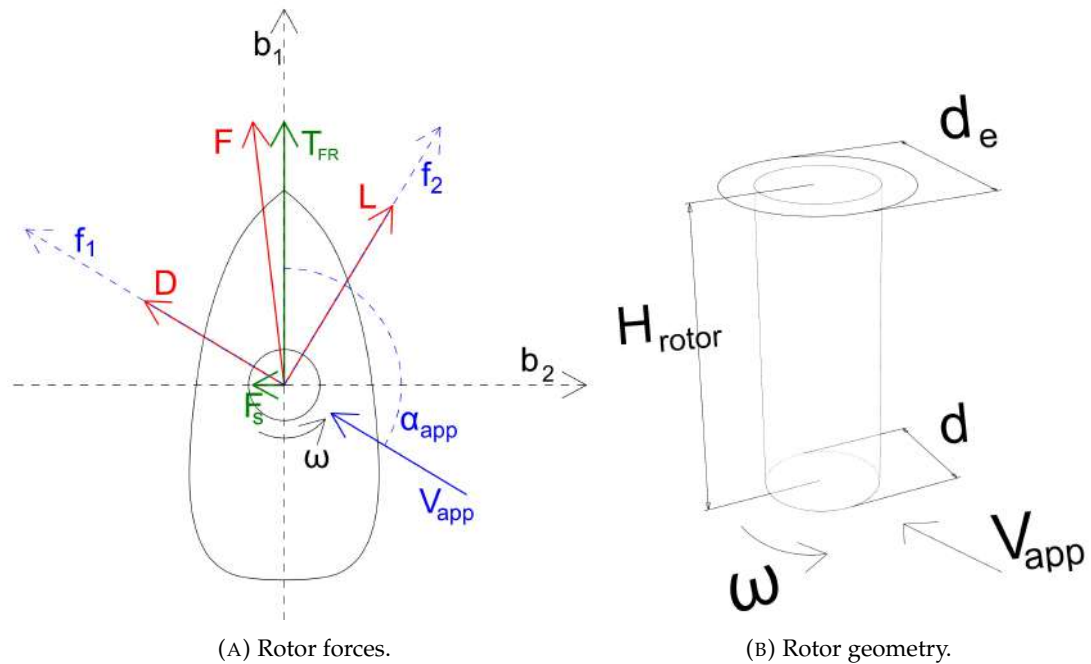
(B) Rotor geometry.

FIGURE 5.3: Rotor forces and geometry.

$\underline{T}_{FR}$ is the effective thrust produced by the rotor along the ship direction, and it is simply obtained as the projection along the ship longitudinal axis of the total force generated by the rotor ($\underline{F}$). $\underline{F}_S$ is the sway force, the projection of total force $\underline{F}$ on the transverse axis .

$\underline{F}_S$ should be counteracted by a force generated by a given rudder angle; this phenomenon would generate an increase in ship resistance that was not considered in this study.

The total force developed by the rotor $\underline{F}$ is the composition of rotor's aerodynamic lift ($\underline{L}$) and drag ($\underline{D}$): $\underline{F} = L\underline{f}_2 + D\underline{f}_1$, as shown in Figure 5.3a.

So, basically, to find the rotor force $\underline{T}_{FR}$ it is necessary to calculate the rotor lift and drag.

They can be computed using the following Equations:

$$L = 0.5 \cdot C_L \cdot \rho_{air} \cdot V_{app}^2 \cdot S_{rotor}$$
$$D = 0.5 \cdot C_D \cdot \rho_{air} \cdot V_{app}^2 \cdot S_{rotor} \tag{5.13}$$

where C_L and C_D are the coefficient of lift and drag of the rotor as calculated in [37] and reported in Equations 5.14, where coefficients a_{ijk} and b_{ijk} are, again, evaluated in [37], SR is the rotor spin ratio ($\frac{\omega \cdot d}{2 \cdot V_{app}}$), AR is the rotor aspect ratio (H_{rotor}/d), H_{rotor} is the rotor height, d its diameter and d_e is the end plate diameter. The effects of the Reynolds number (Re) were not considered, in accordance with what was done by the source of the formula [37]; furthermore, [70] showed that the aerodynamic coefficients of the rotor are almost constant with the Reynolds number for $Re = 1.0 \cdot 10^6$ or greater.

$$C_L = \sum_{i=1}^{4} \sum_{j=1}^{4} \sum_{k=1}^{3} a_{ijk} \cdot SR^i \cdot AR^j \cdot \left(\frac{d_e}{d}\right)^k$$
$$C_D = \sum_{i=1}^{4} \sum_{j=1}^{4} \sum_{k=1}^{3} b_{ijk} \cdot SR^i \cdot AR^j \cdot \left(\frac{d_e}{d}\right)^k \tag{5.14}$$

Remembering that the rotor force can be conveniently expressed in both reference frames as follows: $L\underline{f}_2 + D\underline{f}_1 = \underline{F} = T_{FR}\underline{b}_1 + F_s\underline{b}_2$, the rotor's trust ($T_{FR}$) and sway force ($F_S$) can be computed as:

$$\begin{cases} T_{FR}\underline{b}_1 & = L\underline{b}_1 + D\underline{b}_1 \\ F_S\underline{b}_2 & = L\underline{b}_2 + D\underline{b}_2 \end{cases} \implies \begin{cases} T_{FR} & = L \cdot \sin\alpha_{app} - D \cdot \cos\alpha_{app} \\ F_S & = -L \cdot \cos\alpha_{app} - D \cdot \sin\alpha_{app} \end{cases} \tag{5.15}$$

$\underline{T}_{FR}$ is positive when it's pointing forward and $\underline{F}_S$ when it's pointing to starboard, since they are on $\underline{b}_1$ and $\underline{b}_2$.

Finally, net resistance is found using Equation 5.10.

To sum up, by knowing some simple geometrical parameter of the rotor, wind condition and ship resistance-speed curve it is possible to determine all the forces involved in the phenomenon and obtain $\underline{R}_N$.

5.3.8   Propeller power and rotor power

With the newly calculated net resistance $\underline{R}_N$ it is an easy task to determine all the propeller working points, by using Equations 5.1 and 5.2, for any speed.

In case of fixed pitch propeller (FPP), by repeating the process for each ship speed, the propeller curve of P_B - V_{ship} is obtained.

The described methodology assumes knowledge of the propeller pitch value and, in case of controllable pitch propeller (CPP), in addition to for each speed, it should be repeated for each P/D and the result is the propeller surface; from that surface, the

curve of P_B - V_{ship} can be drawn by considering, for each ship speed, only the engine power required by the propeller at the optimum P/D (which means the minimum power to achieve a defined speed).

The first key parameter indicator (KPI), the Saved $P_{B_{propeller}}$, can be defined as the difference between the propeller power required when the rotor is off with respect to the case when the rotor is on, as per Equation 5.16:

$$Saved\ P_{B_{propeller}} = P_{B_{Propeller@FRoff}} - P_{B_{Propeller@FRon}} \tag{5.16}$$

But this information is not sufficient to state whether the rotor is beneficial for the total power consumption of the ship or not; in fact the power required to spin the rotor is yet to determine.

Another important power to be considered in the system design is the power absorbed to spin the rotor. As reported in [18] the mechanical power absorbed to spin the Flettner rotor can be evaluated as:

$$P_{absspin} = 1/2 \cdot C_f \cdot rho_{air} \cdot U_{tan}^3 \cdot Area_S \tag{5.17}$$

given that C_f is a coefficient of friction = 0.007, $U_{tan} = SR \cdot V_{app}$ is the flow tangential velocity and $Area_S = S_{rotor} \cdot \pi$ is the lateral surface of the rotor

In order to have an homogeneous quantity with P_B (i.e. engine mechanical power at shaft flange), $P_{absspin}$ is converted in $P_{B_{rotor}}$ the effective power required to spin the rotor considering a rotor transmission efficiency η_{mr}, as per Equation (5.18)

$$P_{B_{rotor}} = \frac{P_{absspin}}{\eta_{mr}} \tag{5.18}$$

5.3.9 Total ship propulsive power

The total ship propulsive power P_{TOT} has been defined as per Equation (5.19):

$$P_{TOT} = \begin{cases} P_{TOT_{RotorOFF}} = n_{prop} \cdot P_{B_{Propeller@FRoff}} & \text{if Rotor is off} \\ P_{TOT_{RotorON}} = n_{prop} \cdot P_{B_{Propeller@FRon}} + n_{rotor} \cdot P_{B_{rotor}} & \text{if Rofor is on} \end{cases} \tag{5.19}$$

This quantity is given by the sum of the engine mechanical power required for the ship propulsion and the mechanical power to spin the rotor.

In particular, when the rotor is switched off the power P_{TOT} is simply the engine power P_B calculated for this configuration (with the resistance increased by $\underline{R}_W$), multiplied by the number of propellers (n_{prop}); on the other hand, if the rotor is in use, the total propulsive power is the sum of P_B, calculated with the new diminished resistance $\underline{R}_N$, multiplied by the number of propellers and the power required to spin the rotor $P_{B_{rotor}}$, obtained in the previous paragraph, by the number of rotors (n_{rotor}).

Now all the elements to calculate the power savings are available and the KPI chosen is the percentage in savings according to the following formulation:

$$\text{Power savings gained using the rotor} = \frac{P_{TOT_{RotorOFF}} - P_{TOT_{RotorON}}}{P_{TOT_{RotorOFF}}} \cdot 100 \qquad (5.20)$$

This KPI expresses the percentage of power savings achieved when the rotor is in use versus when it is not and its value is positive if the total propulsive power required with the rotor in use is less than that required without it, otherwise it is negative; in other words, if the KPI is positive, the effect of the rotor is beneficial for the propulsion, if it is negative it requires more energy than the contribution it gives, so it's better to turn it off.

5.3.10   Model validation

The model validation was carried out following different approaches for the rotor itself, the propulsive model and the ship-rotor interaction.

- Rotor: the model of the forces generated by the isolated rotor has been validated by comparing the obtained numerical results with values of rotor's lift and drag available in literature, in particular those reported in [37], obtained from unsteady Reynolds averaged Navier-Stokes simulations.
- Propulsion: the ship propulsion model, designed to find the equilibrium condition between propeller thrust and ship resistance, has been validated by comparison with recorded data from sea trials. Some examples of these validations can be found in [81], [82], [4] and [23].
- Ship-rotor interaction: the complete model of the rotor installed onboard has not been validated since no references have been found in literature, further it was not possible performing sea-trials.

5.4   Case study

The 3000 tons Ro-ro ferry with 2 CPP represented in Figure 5.4a has been chosen as a case study to be tested using the numerical simulator written and developed in MATLAB® environment.

The ship is normally engaged in coastal services linking islands and mainland in Italy. For this case study, the ship speed variation and wind conditions are suitable for the specific trade.

The ship's hull resistance curve is reported in Figure 5.5 and the main case study parameters are reported in Tables 5.1 and 5.3.

Ship					
LOA	B	T	V_{cruise}	Power	A_T
133 m	21 m	4m	14 kn	2x3 MW	72 m^2

TABLE 5.1: Main ship characteristics.

(A) Elio

(B) Propulsion plant schematizing
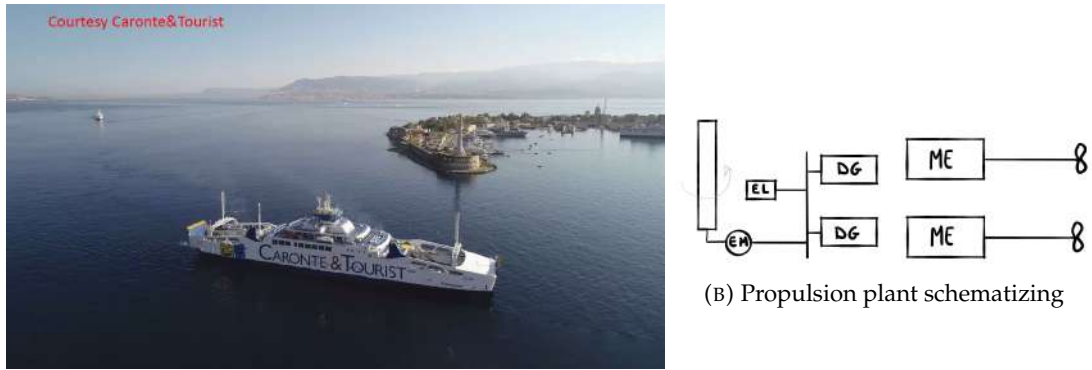
FIGURE 5.4: Case study ship
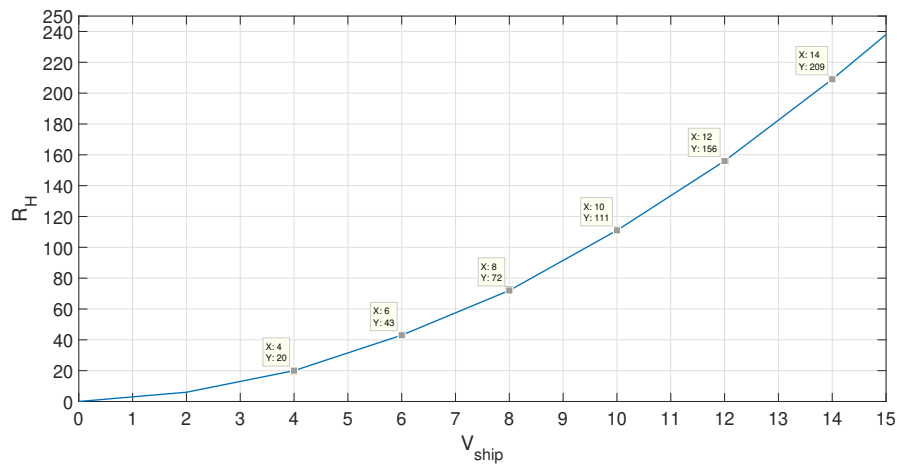
FIGURE 5.5: Ship hull resistance curve.

Propeller

n_{prop}	Blades	Diameter	A_e/A_o	P/D
2	5	2.8 m	0.682	[0.4;1.4]

TABLE 5.2: Propeller characteristics.

The ship has been virtually equipped, as schematically represented in Figure 5.4b, with 1 Flettner rotor of variable geometric dimensions and tested at different wind conditions. Only one rotor was considered in this study to keep it simple but the developed model can be used for multiple rotors installation without any problem, as long as they are all of the same size and do not interfere with each other.

The rotor position considered in the calculations is located in the fore part of the ship, close to the fore mast, to maximize the wind effect. However, other aspects related to the rotor position such as structural aspects, visibility from the bridge, cargo operations in the fore part, etc. were not considered in this study.

The rotor characteristics are reported in Table 5.2, together with the corresponding calculated values of C_L and C_D.

The values reported in Table 5.3 are chosen according to the market availability and to already rotor-equipped existing vessels similar to the case study. [14] [87].

Rotor						
n_{rotor}	H_{rotor}	d	d_e	SR	C_L	C_D
1	18 m	3 m	4.5m	3	8.07	3.82

TABLE 5.3: Chosen values of rotor dimensions.

5.5   Assessment of the weather scenario

A brief evaluation of the weather on the main route of the case study ship was performed, in order to assess if a rotor could be profitably installed onboard.

Currently, the ship is involved in coastal service in the Messina strait.

In Figure 5.6 the averages of the values and directions of the wind of the last years are represented.
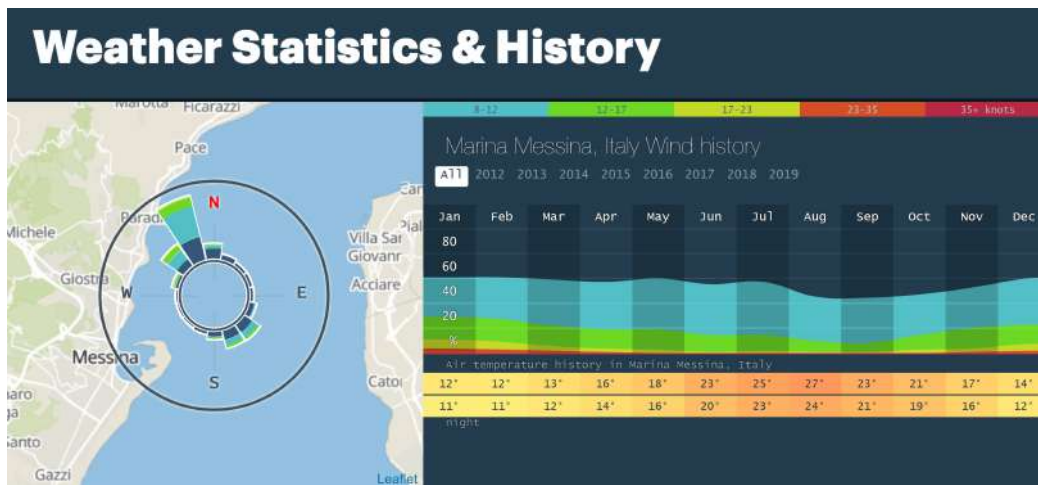
FIGURE 5.6: Messina strait wind statistics. Source: [123]

The numerical values are clearly underestimated because the recording station is near the coast, but the directions are reliable. It can be noted that the prevailing direction of incoming wind is almost perpendicular to the ship route or around that value; almost no wind is coming directly from the bow or stern of the ship.

This is an ideal situation, since in literature was clearly stated that a wind slightly from the aft is the perfect scenario.

5.6   Parametric investigations

5.6.1   Rotor geometry

Before choosing the values reported in Table 5.3, the influence of rotor geometric dimensions on rotor forces $\underline{R}_T$ and $\underline{T}_{FR}$ was investigated.

The geometrical value for the parametric analysis were chosen from literature, more specifically from [37] to, simultaneously, validate the obtained results by comparison with the numbers reported there.

Figures 5.7 and 5.8 show the influence of rotor geometric dimensions for all the operational ship speeds, reported on the x-axis.
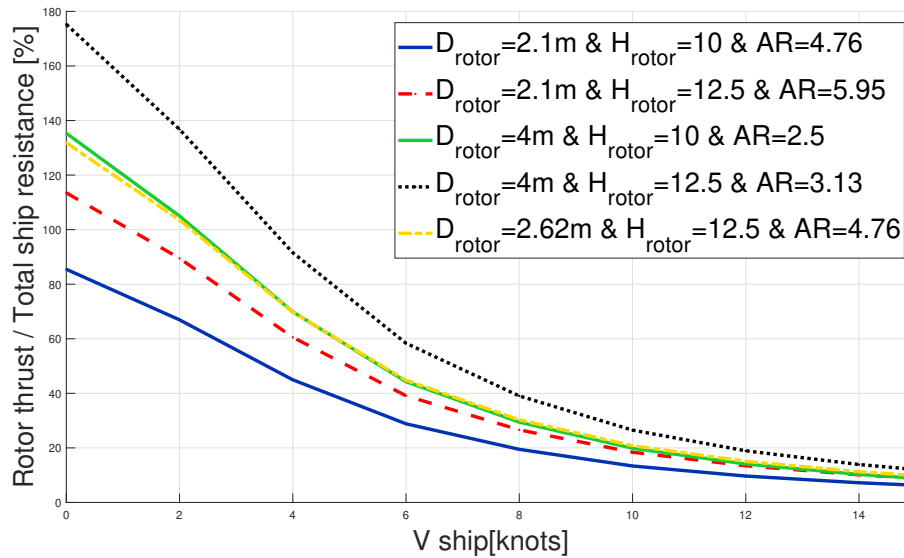
FIGURE 5.7: Influence of rotor's geometric dimensions on rotor thrust-ship resistance ratio $\frac{T_{FR}}{R_T}$

In Figures 5.7, on the y-axis, the results are expressed in terms of rotor thrust over total ship resistance ratio ($\frac{T_{FR}}{R_H + R_W}$).

The objective of this analysis wasn't maximizing the rotor thrust but the minimisation of the total hourly fuel consumption of the ship; for this reason, the results are expressed in terms of the ratio between rotor thrust and total ship resistance. The wind condition is kept constant at 15 m/s and 110° direction, in order to vary the ship speed. It can be noted that the distance between the curves tapers off as the ship speed increases and that the effect of the rotor is progressively reducing; this is because of the wind composition: at high speeds the apparent wind comes more and more from the bow, a less advantageous configuration, and thus the thrust generated decreases while the resistance increases. At 10 knots of ship speed, promising values of thrust generated by the rotor between 10 and 20% of the total ship resistance are found. Another result is that forces increase with rotor size, in particular, enlarging the diameter is more effective than increasing its height (black dotted line).

This results are confirmed by Figure 5.8 where the value of total ship resistance (R_T) and rotor thrust are reported separately (T_{FR}). Thanks to this representation it is clear how the dimensions of the rotor have a great impact on the rotor thrust but a negligible effect on the total ship resistance: the bold lines, representing R_T are all overlayed and indiscernible one from the other; on the contrary, the dashed lines of T_{FR} are well separated and clearly indicates that the bigger is the rotor, the stronger is the thrust generated.

After the discovery that the bigger, the better, we choose to adopt a commercially available rotor, bigger than the previously tested values but still suitable for the vessel type. The chosen one, whose characteristics are reported in Table 5.3, provides the best compromise between performance and easy installation onboard and integration with the shipboard systems.
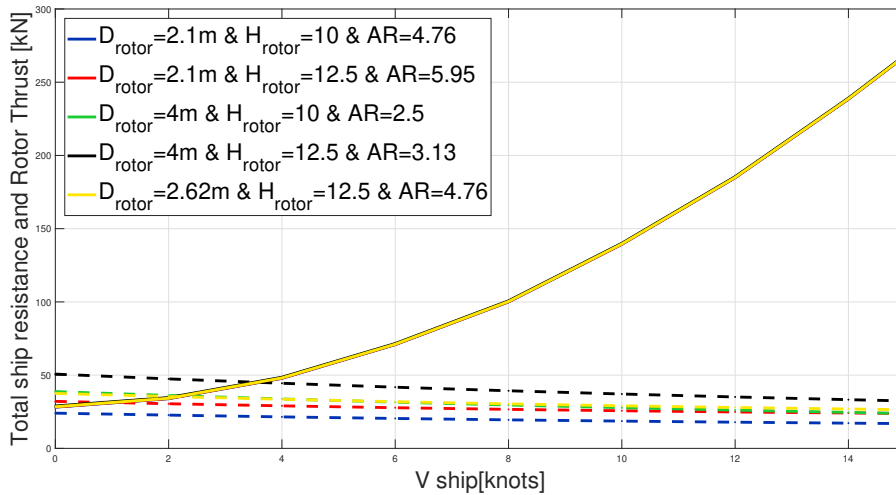
FIGURE 5.8: Influence of rotor's geometric dimensions on rotor thrust
and total ship resistance

5.6.2   Ship speed and wind interaction.

The next step was the analysis of the effects of wind speed and direction combined with different ship speeds on the forces involved. All the graphs reported, refers to the $\underline{b}_i$ reference frame described in Section 5.3.3 and, thus, all the negative forces are resistances and the positive ones are thrusts.

First of all, the added wind resistance (R_W) has been studied and in Figure 5.9 R_W is represented.
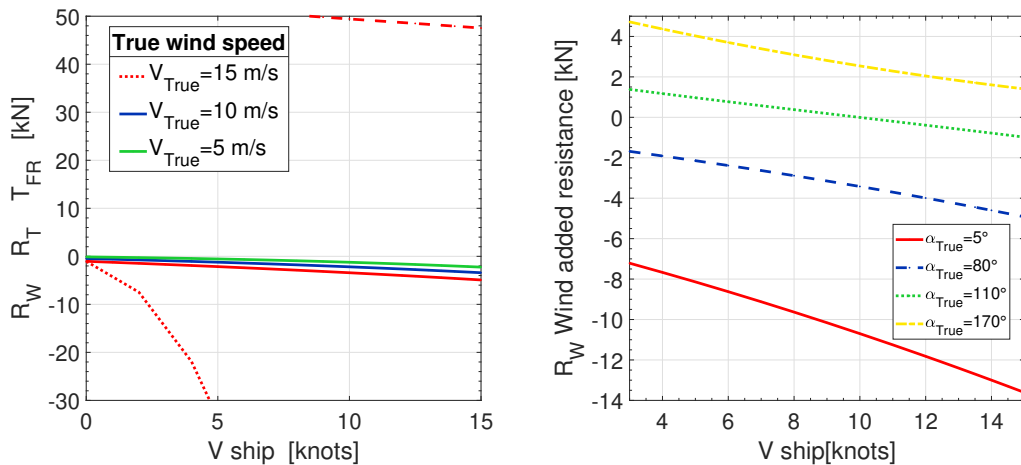
(A) Influence of true wind speed on R_W
at fixed $\alpha_{True} = 80°$

(B) Influence of true wind direction on R_W
at fixed $V_{True} = 15$ m/s

FIGURE 5.9: Influence of true wind on wind added resistance.

Figure 5.9a shows, for a given true wind angle ($\alpha_{True} = 80°$), R_W, the slightly negative bold lines, one curve for each true wind speed reported in the legend. For V_{True}=15 m/s also total ship resistance (R_T: red dotted line) and rotor thrust (T_{FR} positive red dashed line) are represented, to show how small R_W really is, compared to these other two forces. Clearly, R_W increases with the ship speed and also with the wind speed.

In Figure 5.9b the influence of true wind direction and ship speed is reported for a fixed true wind speed of 15 m/s. Again, for every true wind angle, as the ship speed increases, so does R_W. Moreover, the smaller the angle, the larger the wind added resistance, which means that R_W is stronger for bow winds and minimum for stern winds. A peculiar condition occurs for 170°, the top yellow curve: in this condition the wind added resistance is always positive regardless of the ship speed, which means that winds coming from the stern contribute to the ship thrust, having a beneficial effect. This is partially true also when $\alpha_{True} = 110°$, but in this case, the beneficial influence is lost after a certain ship speed (10 knots) because the resulting apparent wind is coming from the bow.

As seen in Figure 5.9a, R_W is really small, almost negligible, if compared to R_T and T_{FR}; thus the latter were studied more in depth and the following Figures refer to some results found in this regard.

(A) Influence of α_{True} on T_{FR} and R_T

(B) Influence of α_{True} on $\frac{T_{FR}}{R_T}$
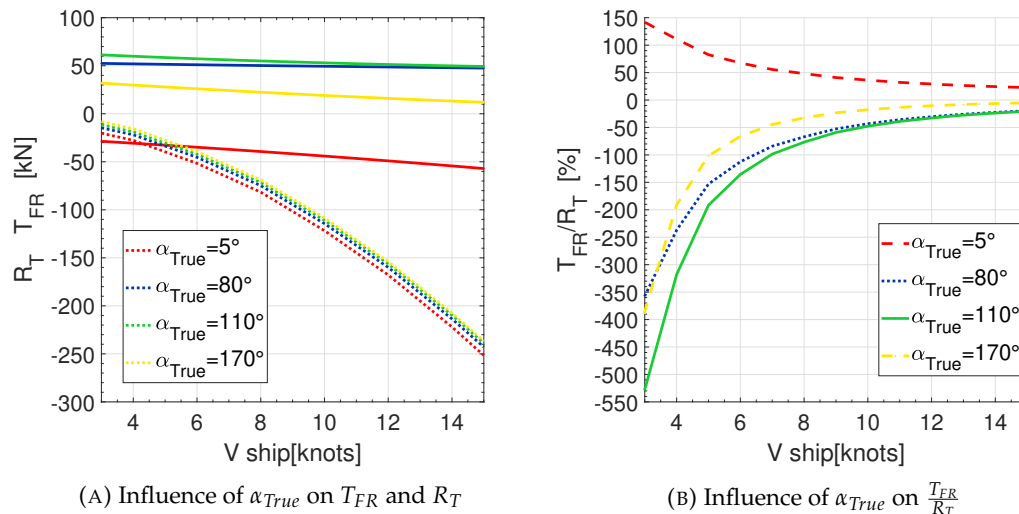
FIGURE 5.10: Influence of true wind direction on rotor thrust, ship resistance and their ratio, for V_{True}=15 m/s.

In Figure 5.10, the influence of true wind direction combined with ship speed on total ship resistance and rotor thrust is shown. True wind speed is kept constant at 15m/s to emphasize differences. Firstly, in Figure 5.10a can be noted that the dotted curves of R_T are only slightly dependent on the angle, being rationally bigger the more the wind is coming from the bow; since, as seen previously, R_W is so small, R_T is, as expected, almost independent from the wind. On the contrary, rotor thrust is strongly dependent on the direction of incoming wind because, together with the ship speed, it effects the intensity and angle of the apparent wind, the real responsible of the rotor forces. From the graph is clear that a wind coming slightly from aft (110°) is the optimal solution to maximize rotor thrust generation. The worst scenario is wind from the bow: the negative bold red line means ad added resistance rather than a thrust. This can be deduced also from Figure 5.10b where the ratio $\frac{T_{FR}}{R_T}$ is represented. The red line, corresponding to bow wind, is the only positive one, meaning that both numerator and denominator are negative and, thus, resistances. For all the other cases,

it can be noted that the best performance is given by the slightly from the stern wind and that the ratio decreases with ship speed; this because of two combined effects: at higher ship speeds, the total ship resistance is stronger and the apparent wind comes more and more towards the bow becoming less advantageous.

The next step is to keep constant the true wind angle to investigate the effect of true wind speed and ship speed on the same parameters.

(A) Influence of α_{True} on T_{FR} and R_T

(B) Influence of α_{True} on $\frac{T_{FR}}{R_T}$
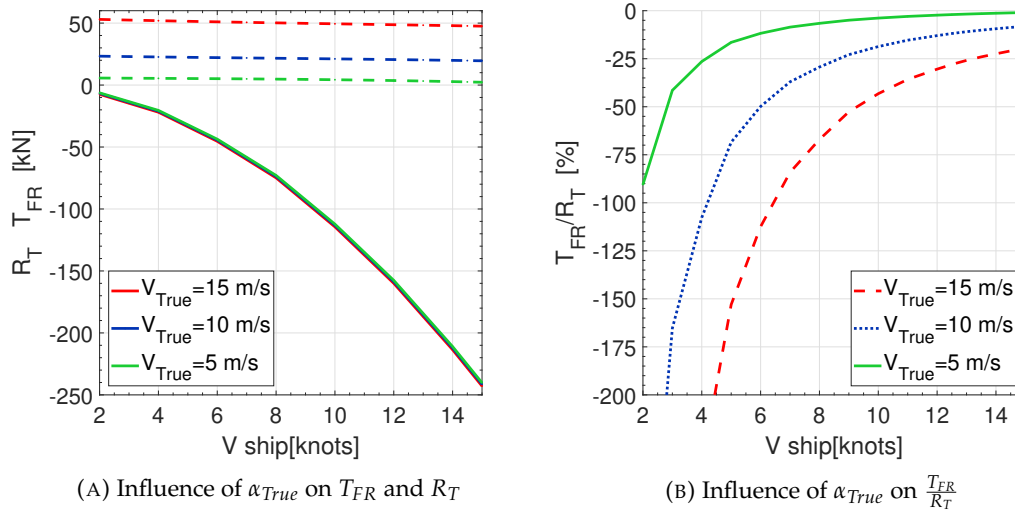
FIGURE 5.11: Influence of true wind speed on rotor thrust, ship resistance and their ratio, for α_{True}=80°.

(A) Influence of α_{True} on T_{FR} and R_T

(B) Influence of α_{True} on $\frac{T_{FR}}{R_T}$
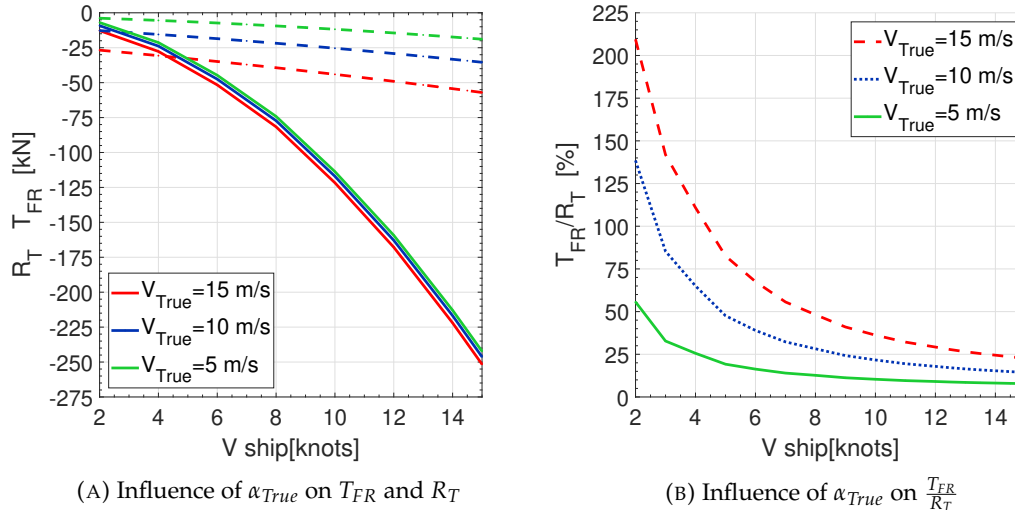
FIGURE 5.12: Influence of true wind speed on rotor thrust, ship resistance and their ratio, for α_{True}=5°.

The best (Figure 5.11) and worst (Figure 5.12) cases of α_{True} are chosen to be kept constant.

In Figure 5.11a the influence of true wind speed and ship speed on R_T and T_{FR} is reported for the best case of true wind angle α_{True}=80°. The rotor thrust decreases slightly with the increase of ship speed and it can be noted that a stronger wind is overall beneficial. This may seem an obvious result but it is not, in fact, a stronger wind increases rotor thrust but also ship resistance and this graph, but especially Figure 5.11b where the ratio between rotor thrust and ship resistance is shown, clearly shows

that the effect on rotor thrust is prevailing. Unfortunately, this is referred only to a true wind coming from 80° (lateral wind). In fact, when the wind is coming from the bow, from 5°, the results are similar and very different at the same time, as shown in Figure 5.12a: it is still true that a stronger wind produces a stronger thrust but, this time, it is negative and thus it is no more a thrust but an added resistance. This is visible also in Figure 5.12b where all the curves are above zero, meaning a ratio between resistances.

A more complete analysis of the wind direction and speed influence on forces generated and on ship resistance is discussed in section 5.6.3.

5.6.3 Wind speeds and directions.

To better understand the effects of wind, some polar diagrams were made keeping constant the ship speed at the design value of 14 knots.

In Figure 5.13, 5.14, 5.15 and 5.16 the influence of true wind speed and direction is reported.

The polar plots are made around the angles of direction of the incoming wind with respect to the bow: 0° is the fore wind, 180° is the aft wind, 90° is wind from the starboard and 270° from port side.

True wind speed is a parameter: each line on the graphs is made keeping constant the true wind speed, choosing from one of the three values tested between 5 (represented in red), 10 (in green) and 15 m/s (in blue).

(A) Rotor Lift and Drag. (B) Rotor Thrust and Sway force.
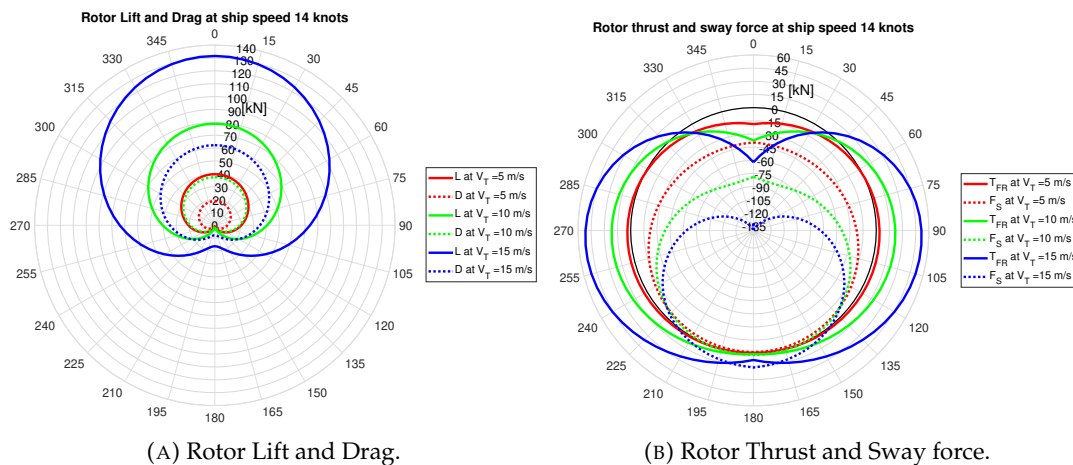
FIGURE 5.13: True wind speed and direction influence on rotor forces.

In Figure 5.13 the rotor forces are represented, expressed in [kN]. In more detail, in Figure 5.13a rotor Lift (L, solid lines) and Drag (D, dashed lines) (see Figure 5.3 for reference) are represented: as expected, the magnitude increases with wind speed. A maybe surprising result, at first sight, is that L and D are dependent on true wind angle. Being the rotor a cylinder, lift and drag should not be dependent on the direction of the incoming fluid stream, but, since the stream really responsible of generation of L and D is the apparent wind, the angle on which L and D are not dependent on is α_{app} and not α_{True}. L and D changes with α_{True} because changing the true wind direction

means, after the composition with ship speed, changing apparent wind speed and angle, the real cause of rotor forces generation. To confirm this, L and D are bigger when true wind comes more towards the bow because there it is where the apparent wind is the strongest.

Rotor thrust (T_{FR}, bold lines) and sway force (F_S, dotted lines) are shown in Figure 5.13b: in this case some negative values are visible. The sign is meaningful since it represents the direction of the force: a negative thrust is pointing aft and a negative sway force to the port side, in accordance to the definition of the $\underline{b}_i$ base. However, while a negative sway force has the same effect of a positive one of the same magnitude on the ship efficiency, a negative thrust is detrimental as it means an increase in ship resistance. The figure points out that the rotor must be switched off in head wind conditions. In fact, from this figure it can be deduced that, for this ship speed (14 knots), a true wind is beneficial when it comes from about 40° to 320° and the intensity is about equal or greater than 5 m/s. On the other hand, a true head wind (from 320° to 40°) results in an increase of ship resistance.

To better understand when it's convenient to turn the rotor on, Figure 5.14 can be useful, where both rotor and propeller thrust are analyzed.
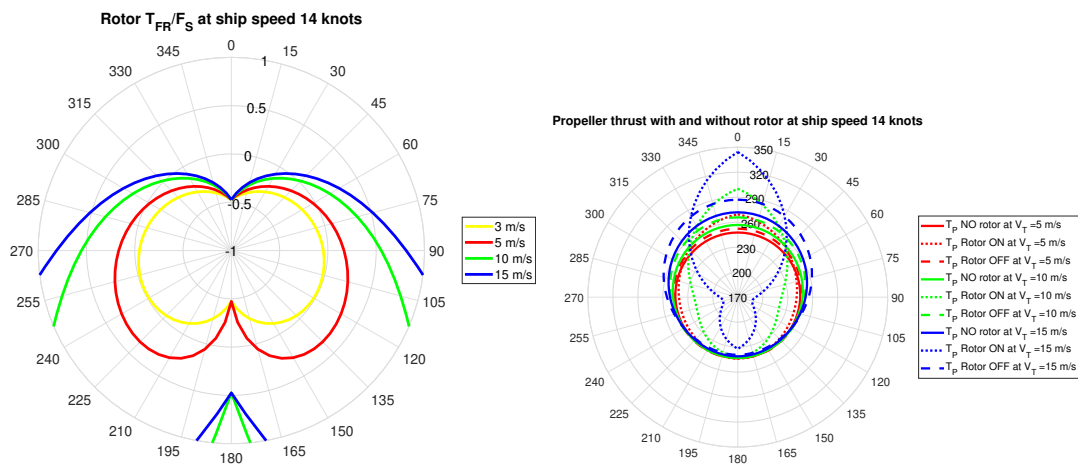
(A) Ratio between rotor thrust and sway force for different True winds.

(B) Propeller thrust with and without rotor for different True winds.

FIGURE 5.14: Influence of true wind speed and direction on thrust.

In Figure 5.14a the ratio between the rotor thrust and sway force ($\frac{T_{FR}}{|F_S|}$) is represented. The denominator has the absolute value of the sway force since it's not important here if it's towards starboard or port side. The graph radius limits are [-1;1]: a ratio <-1 indicates a remarkably strong thrust towards the aft (equal to an increase in resistance); the ratio in the interval [-1;0] occurs when the sway force is larger than the thrust and also the latter is pointing backwards; in (0;1) thrust starts pointing forward (which is the desired situation) but F_S is still stronger than it; finally when $\frac{T_{FR}}{|F_S|}$ >1 there are optimal solutions, where thrust is forward and it's also stronger than the sway force. In this optimal range the figure shows only the two strongest (10 and 15 m/s) winds coming from side to aft (from about 100° to 170°); in this range the 5 m/s wind is generating thrust but smaller than the sway force. An even smaller wind of 3 m/s is reported to show the minimum value of wind to turn on the rotor: under this

limit of 3 m/s of true wind, the rotor kept functioning generates additional resistance, as it does for all the other wind speeds if the true wind is coming from the bow: the values of the ratio between about 320° and 40° are negatives and thus the rotor should be switched off.

Figure 5.14b provides another useful point of view: it's a comparison of the propeller thrust in three different scenarios. The solid lines represent the scenario where no rotor is installed onboard (existing ship); the dashed lines are for the rotor installed onboard but switched off; the dotted lines are for the rotor installed onboard and switched on. First of all, the difference between no rotor at all and rotor off is almost negligible for stern and cross wind where the presence of the rotor induces only a small increase in ship wind added resistance; for head wind, the increase in resistance is clearly visible, especially for the strongest wind. Secondly, the use of the rotor is beneficial from the efficiency point of view when the thrust required by the propeller becomes smaller when the rotor is in function in respect to when it is off; this occurance is visually represented in the graph by the intersection between the dashed line (rotor off) and the dotted one (rotor on) at an angle dependent on wind speed: in the most favourable case of 15 m/s of wind, the angle of intersection is approximately 40°, while in the case of 10 m/s it is about 45°; on the contrary, a wind from the bow with rotor on causes, as expected, a sharp rise in the propeller thrust. The use of the rotor in these conditions causes a large reduction in ship efficiency and it is strongly discouraged.

A more intuitive representation of whether the rotor should be turned on or not is made using the KPI introduced in Section 5.3.8 and 5.3.9 and represented in Figure 5.15.

(A) Rotor absorbed power and respective propeller power savings, V_{ship}=14 kn.

(B) Total propulsive power with and without the rotor in use.
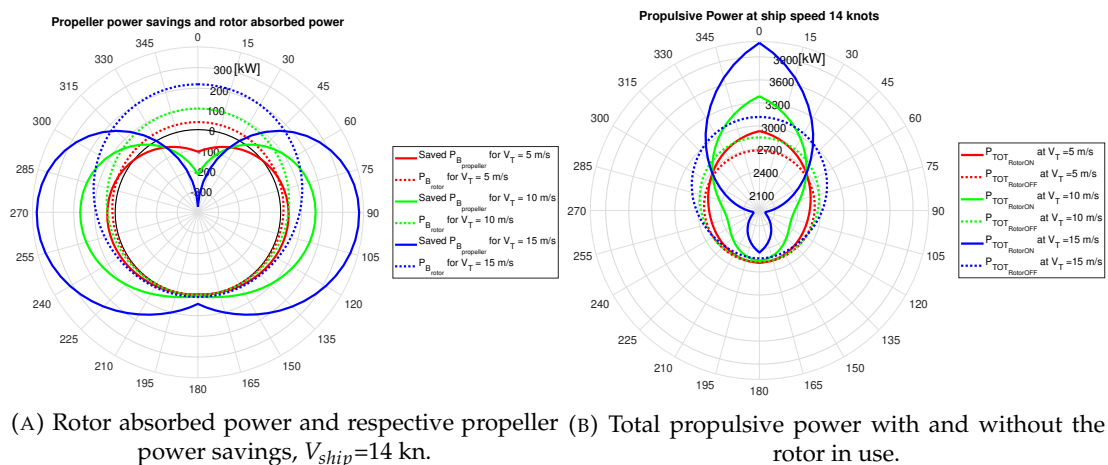
FIGURE 5.15: Influence of true wind on powers.

Figure 5.15a reports $P_{B_{rotor}}$ in dashed lines and the Saved $P_{B_{propeller}}$ in solid lines. $P_{B_{rotor}}$ is the one evaluated with Equation 5.18 and the Saved $P_{B_{propeller}}$ is calculated using Equation 5.16, with reference to section 5.3.9.

A rise in $P_{B_{rotor}}$ can be observed in head wind, only due to the apparent wind increase. This effect, combined with an higher resistance and opposite thrust, results in negative

saved $P_{B_{propeller}}$, which means larger propeller power required when the rotor is on with respect to the rotor off; that is the rotor has a negative effect on the propulsion inhead wind, as already stated.

The same conclusion can be drawn from Figure 5.15b, where $P_{TOT_{RotorON}}$ and $P_{TOT_{RotorOFF}}$ as calculated with Equation 5.19 are shown; here it's clearly visible, in head wind cases, an higher total propulsive power when the rotor is in use (solid lines), compared to without rotor (dashed lines). On the contrary, for wind coming from about 40° and over there's an actual saving in power; this angle decrease progressively as the wind speed increases: the stronger the wind, the more advantageous condition there are. For the strongest cross wind it is possible to save up to 380 kW of propeller power.
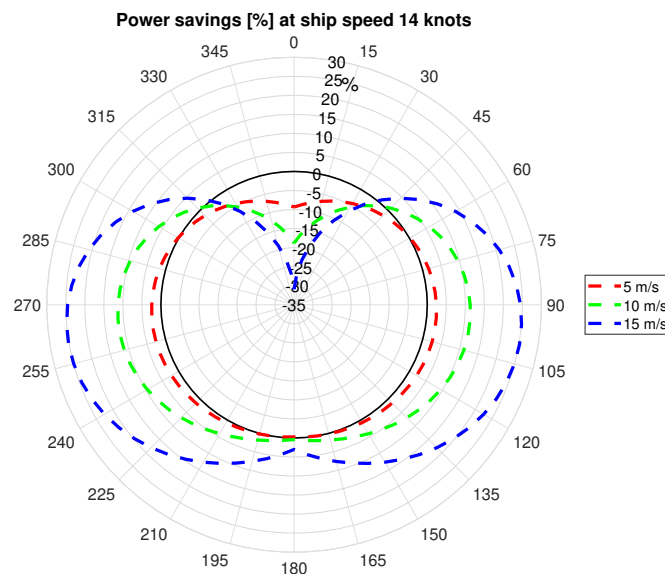
FIGURE 5.16: Power savings percentage when Rotor is on compared to when it is off.

To sum up all these data, Figure 5.16 shows the percentage of savings in terms of propulsive power as calculated in Equation 5.20.

It is clear that, for a ship speed of 14 knots, at any wind speed below 3 m/s the rotor should stay off, otherwise it would lead to an additional power demand. In terms of direction of incoming wind, the best conditions are cross and quarter winds and, the stronger the wind, the wider the range of suitable winds. For example, for a wind of 15 m/s from 100°, a power saving of more than 25% can be achieved.

5.6.4 Ship speed.

In this section the influence of different ship speeds alone has been analysed, keeping the true wind constant at the just discovered best power savings condition of 15 m/s from 100°; obviously the true wind is kept constant but the apparent wind will automatically vary with the ship speed.

In Figure 5.17 the required propeller power P_B is represented.

In Figure 5.17a, the propeller speed [rpm] is presented on the x-axis and the $P_{B_{propeller}}$ [MW] on the y-axis. This graph is obtained computing Equation 5.1 and 5.2 for all the ship speeds and propeller P/D; it shows the controllable pitch propeller working
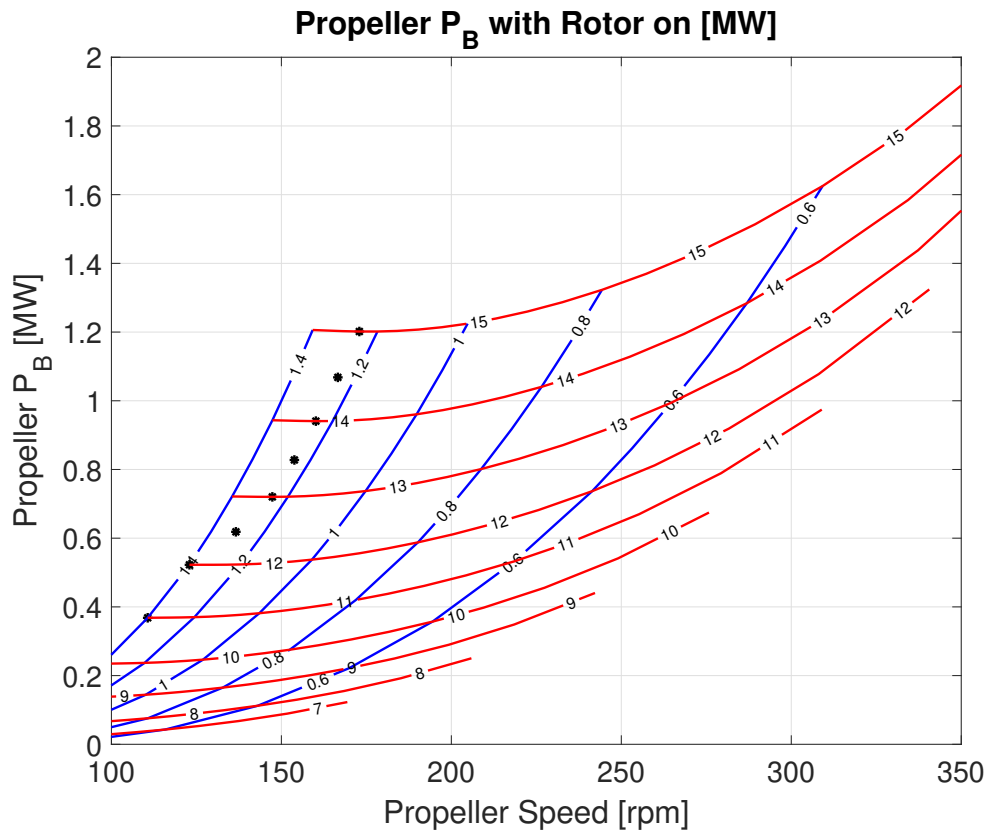
(A) CPP working points.
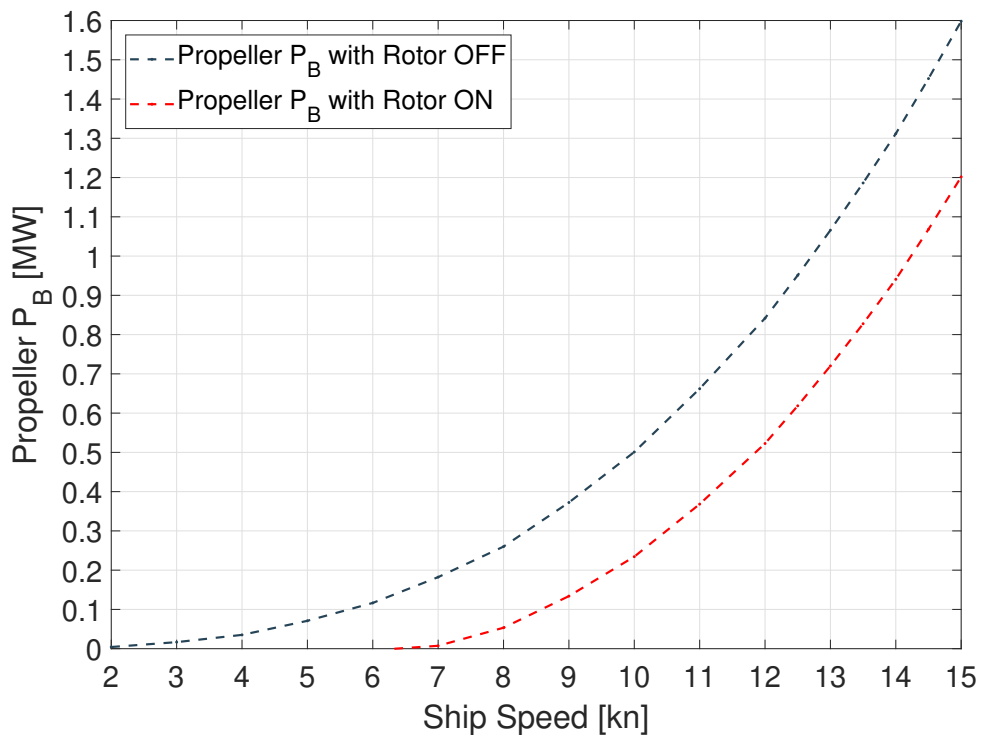
(B) Propeller required power P_B with and without rotor.

FIGURE 5.17: Propeller P_B in different conditions.

points when the rotor is in use in said wind condition. Each red line represents the propeller brake power P_B at constant ship speed and variable P/D; each blue line represents P_B at constant P/D and increasing ship speed. It is possible to identify the minimum power required for achieving each ship speed: the black dots represent, for each ship speed (each red line), the optimum P/D; the couples (P/D; n_p) identifying each optimum point, 1 for each ship speed, all together generate the propeller curve.

Considering only the optimum points (the black dots) just found, for each ship speed, there is only one minimum propeller P_B; therefore, it is now possible to draw the curve of $P_{B_{propeller}}$-V_{ship}, which is reported in Figure 5.17b. Figure 5.17b represents the propeller P_B (y-axis) for different ship speeds (x-axis). The red line represents the optimum working points of the propeller when the rotor is on (the black dots of Figure 5.17a) while the blue one represents the optimum propeller working points when the rotor is off.

From Figure 5.17b it can be deduced that the use of the rotor significantly lowers the power required from the propeller of about 200 kW and even more at higher speeds. But to understand the rotor impact on the total power consumption of the ship, the power required to spin the rotor must be considered.
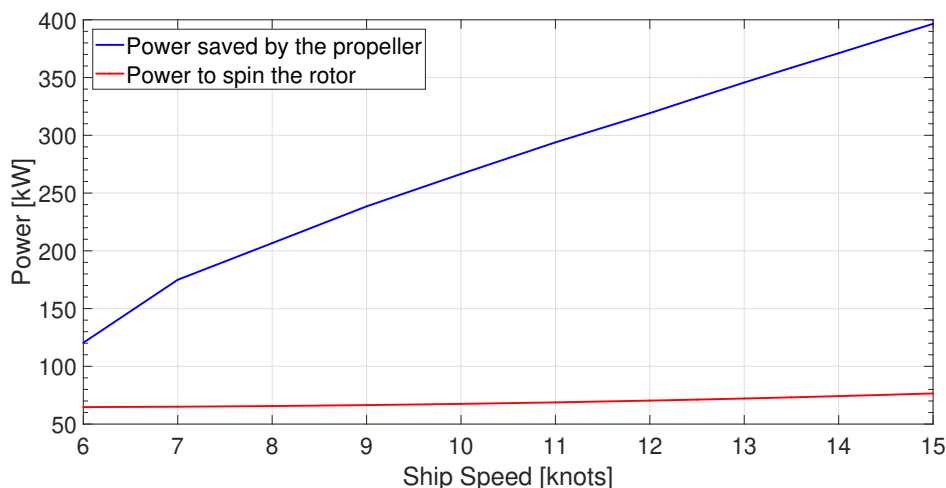
FIGURE 5.18: $P_{B_{rotor}}$ VS Propeller power savings

The power to spin the rotor $P_{B_{rotor}}$ was computed with Equation 5.18 and presented in Figure 5.18 on the y-axis for different ship speed (x-axis) and constant true wind (15 m/s from 100°). $P_{B_{rotor}}$, represented by the red line, is almost constant for each ship speed; this is because it is a function of the apparent wind speed, which, in this case, it is not very much affected by the ship speed. Figure 5.18 also presents, in blue, the propeller power savings, computed as the difference between rotor on and off of Figure 5.17b. From the figure, it seems better, in absolute terms, to sail at higher ship speeds, as savings increase considerably with the ship speed.

To put this result in perspective, it is useful to compute the percentage of savings in relation to the total power demand as per Equation (5.20).
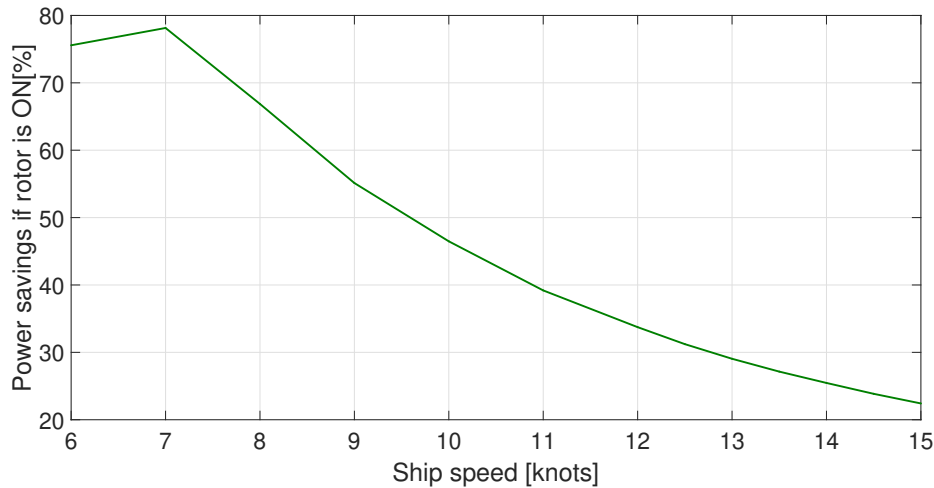
FIGURE 5.19: Total propulsive power savings

The results are shown on y-axis of Figure 5.19 for various ship speed (x-axis). The power savings reported are always positive and greater than 20%, thus, in this wind condition (15 m/s from 100°), the rotor is beneficial for every ship speed considered. In particular, looking at 10 knots of ship speed, the rotor is capable of ensuring more than 45% of power savings. For higher speeds the percentage of savings is smaller, despite the trend of the blue line in Figure 5.18, because the total propulsive power demand increases dramatically with the speed, compared with power savings which increase more modestly.

5.7 Discussion

The aim of this study was to fill the literature gap about the rotor-propeller integration into the ship propulsion plant. The innovation was the integration of two kind of thrust: the traditional one from the screw propellers with the wind thrust given by the rotor.

A generalised model able to evaluate the ship propulsive power due to the use of a rotor as an auxiliary wind propulsion device is proposed. The model is based on the consolidated engine-propeller matching procedure, modified in order to accommodate the rotor effects on the propeller working point. Firstly the reference frame were introduced (Sec. 5.3.3) and true and apparent wind were defined (Sec. 5.3.4); then, the methodology for the evaluation of rotor thrust and other aerodynamic forces, wind added resistance and the related net resistance that the propellers have to counterbalance was explained (Sec. 5.3.5 to 5.3.7); after that, the new propeller working points and its brake power requirement was calculated, together with the evaluation of the power to spin the rotor (Sec. 5.3.8); lastly, an analysis of power savings was carried out (Sec. 5.3.9).

The described methodology was applied and all these steps were followed to write the numerical simulator. The developed code was implemented in MATLAB® environment.

A 3000 tons Ro-Ro/Pax ferry operated in the Mediterranean Sea was chosen as a case study for the newly written simulator and it was virtually equipped with one rotor.

A parametric study to asses the influence of the rotor characteristics on thrust and resistance was performed (Sec. 5.6.1) and the rotor dimensions were chosen.

Some results are reported in Section 5.6.2 to show the consequences of the interaction between ship speed and true wind on rotor thrust and ship resistance .

Then, the effects of ship speed and true wind were studied separately: in Section 5.6.3, the ship speed was kept constant to show the influence of true wind speed and direction on forces and powers; on the other hand, in Section 5.6.4, ship speed variation impact on powers was investigated for a fixed true wind condition.

Some general conclusions can be drawn: a bigger rotor is always a good idea, since the impact on thrust generated is larger than the one on ship resistance; clearly, the stronger the wind, the larger the effects; the best directions of incoming wind are from side to astern but the stronger the wind, the wider the range of suitable angles; for the particular case studied at design speed, if the true wind is below 3 m/s the rotor should stay off or it lead to an additional power demand regardless of the wind angle; in the case studied, at design speed and wind of 15 m/s from 100°, a power saving of 25% is achieved by using the rotor; remarkable power saving are observed in the whole range of ship speeds.

For a more complete analysis of the rotor-propeller integration, not only power but also fuel consumption should be addressed. This is not a trivial task due to the high non-linearity of the engine behaviour, thus the next step of this study was the estimation of the fuel consumption reduction achievable with the rotor.

Moreover, the developed simulator has to be completed with the engine model and fuel consumption evaluation part to be useful, in a design stage, as a tool to select the proper combination of rotor and main engine to be installed onboard, assuming certain wind conditions; in operation, on the contrary, knowing the engine and the rotor, it can be used to select the best wind scenario by means of a weather routing optimisation process. To do so, in the next Chapter, the engine working points evaluation and fuel consumption estimation is presented.

6 Flettner rotor: modelling from power to fuel consumption

In the previous chapter, the definitions of the different power involved in the process has been described. In the following sections a mathematical model for the evaluation and optimisation of the engine fuel consumption is presented.

The use of the proposed methodology is twofold: as a tool to support the selection of the best possible diesel propulsion engine, and as an optimizer of fuel consumption during ship operations.

To compute the fuel consumption, the total propulsive power P_{TOT}, as defined in Equation 5.19, is used, since it represents the power required by the main engines. The marine diesel engine is modelled starting from very few input data and is calibrated using manufacturer data. By this model it is possible to evaluate the fuel consumption in the entire working area of the engine. At design stage the model is useful to determine the best engine option among the alternatives in different working scenarios. In an existing vessel, during operation, the model can be used to compute the fuel consumption of the ship in the actual working condition.

6.1 The optimisation problem

As just said, the model can be used to determine the best option among different engines alternatives. But what does "best" means?

The best solution is an optimised solution and, for an energy system, there are three levels of optimization, as defined in [46]:

- Synthesis optimization: it implies the components that appear in a system and their interconnections.

- Design optimization: it is about the technical characteristics (specifications) of the components and the properties of the substances entering and exiting each component at the 'design' point (nominal load) of the system.

- Operation optimization. For a given system (i.e. one in which the synthesis and design are known) under specified conditions, the optimal operating point is requested, as it is defined by the operating properties of components and substances in the system (speed of revolution, power output, mass flow rates, pressures, temperatures, composition of fluids, etc.).

Having defined the propulsion system to be analyzed in the previous chapters (an hybrid plant composed by 2 CPP, a diesel engine for each shaft line and a Flettner rotor), it is necessary to identify the optimization objective, i.e. the objective function that must be minimized in order to solve the problem posed.

There are several criteria that can be selected as objective functions and the choice, which depends on the application, has a strong effect on the final result (optimal system).

Four macro-categories can be identified:

- technical criteria: minimum weight or volume, maximum efficiency or minimum fuel consumption, maximum net power density, etc.;

- economic criteria: minimum life cycle cost (LCC) or dynamic payback period (DPB), maximum net present value (NPV) or internal rate of return (IRR);

- environmental criteria: minimum CO_2 and other gaseous pollutants emitted, minimum thermal pollution or noise, etc.

- societal criteria: maximum job creation, minimum adverse effects on health, etc.

In order to consider both technical and economic side, the minimisation of the hourly fuel consumption was chosen as objective function. Furthermore it is possible to derive also the environmental aspect by the calculation of the CO_2 emissions from the fuel consumption: since the two are directly linked, minimizing hourly fuel consumption implies minimizing the CO_2 emissions.

To minimize hourly fuel consumption it is necessary to determine the consumption in the entire working range of the engine. Moreover, to optimize the energy system, it is necessary to define its configuration and its characteristics. The above computation requires to set up a model and select which parameters are fixed and which parameters are variable.

To better understand what kind of mathematical model could be the most suitable for the calculation of fuel consumption in the entire working range of the engine, and to define the variables involved to be used to solve the optimization problem, systems previously developed in literature have been taken into consideration.

The model described in [2] is perfect for this problem since it allows to define the fuel consumption map within the engine load diagram.

The authors developed different ship propulsion time-domain simulators, in which each propulsion component is represented by a mathematical model based on algebraic and differential equations. To validate said models of a diesel engine, a marine gas turbine and an electric motor the authors resort to the sea trials data and engine manufactures' data.

The mathematical model describing the consumption map of a four-stroke diesel engine is extrapolated from the aforementioned paper. This approach is suitable for

the present study because it allows to determine the engine entire working area performance by knowing only few inputs.

A similar work to what reported by [2] was described by [1]. The authors present a numerical methodology to derive fuel consumption values in the entire working area of any diesel engine, starting from very few input data and several coefficients. These are obtained through statistical regressions from different fuel consumption maps. Then the method is tuned and tested on high-speed diesel engines load diagrams, provided by manufacturers.

To better understand the optimization process and the most suitable variable parameters, different sources has been studied.

A general method for synthesis, design and operation optimization of energy systems is introduced in [101] where the authors try to answer the question of which combination of a variety of configurations, design specifications and operating states is the best for a complex and integrated system that produces all forms of energy needed onboard (mechanical, electrical and thermal) with as low fuel consumption as technically possible and economically feasible.

More in details, a superconfiguration of the system, which has to provide propulsion, electrical and thermal power which vary with time, is considered and simulated. In the system the main engines are mechanically coupled to the propellers through a gearbox and their waste heat is recovered by heat recovery steam generators (HRSG); the latter produce superheated steam to drive steam turbines in a combined cycle and saturated steam for thermal loads.
The steam turbines are coupled to electric generators on one side but on the other are coupled to the propellers to integrate the propulsion power of the main engines.
In combination with the steam turbine generators or even alone, also Diesel-generator sets are intended to meet electrical loads.
An exhaust gas boiler for thermal loads may operate when exhaust gases are not used by the HRSGs and the auxiliary boilers can supplement with heat, whenever needed.

The optimization is performed, having as the objective function the minimization of the Present Worth Cost of the system for its whole life, using a genetic algorithm and optimizing all the operating modes simultaneously.
The applicability of the method is demonstrated with numerical examples, while its versatility (its adaptability to alternative conditions), by solving the problem with different sets of data, varying some of the parameters.

The solution is found for a nominal set of parameters. Then, the effect on the solution of some of them is investigated.
The first interesting results is that, in case of more than one main engine, they may have different nominal power ratings and/or loading in the optimum configuration; the same is true for the diesel generator sets, their rating and load factor may be different in an optimum solution.
This paper [101] clearly identifies the engine power as a parameter to be optimized,

by keeping in mind that the engine is not characterized by a continuously variable power, but, by a discrete power that varies with engine characteristics such as the number of cylinders etc.

Other sources have been investigated to further understand which are the parameters to consider.
For the authors of [112] and [120], the parameters to vary to solve optimization problems are the speed of the turbocharger, start angle of injection, intake valve timing, amount of injected fuel, boost pressure, compression ratio and the timing of intake valve closing. The performance inside the entire engine working area is defined.

[112] proposes an optimization model of the performance of a four-stroke marine turbocharged diesel engine for different speeds and loads. The study demonstrates that the model allows to minimize the engine fuel consumption, acting on the values of speed of the turbo charger, timing of intake valve opening, start of fuel injection and fuel rate.
Furthermore, the model is good at simulating the performance of a large marine diesel engine for different working conditions, but, at the same time, it remains suitable for a standard computer in terms of computational time consumption. It can be used to verify the exhaust emission limitations by computing CO_2 and NO_X emissions in the entire engine working area; which is an important result since these values are not usually provided by the manufacturers but are fundamentals since the preliminary design stage.
Lastly, said model can be used to simulate the performance of any diesel engine to be a part of a numerical propulsion system for different marine applications.

Similarly, in [120], it's described the NO_X emissions prediction model of a large marine four-stroke dual-fuel engine; the model is built by using AVL-BOOST software and it is calibrated to evaluate the engine performance and emissions. In this study the effects of boost pressure, compression ratio and intake valve closing on marine dual-fuel engine performance and emissions are investigated. Finally, to model, predict, and optimize the emissions and performance the response surface methodology is applied to obtain the engine optimal setting parameters. These optimization results are very close to the simulation ones, which confirms the accuracy of the response surface methodology and its desirability as an optimization method.

These two papers, [112] and [120], are useful to understand how to integrate the engine mathematical model, defined to describe the forecast of consumption within the load diagram, with the propulsion system.
In [101], [112] and [120] energy systems configurations are studied.

The main novelty of this part of the doctorate research activity is the engine mathematical model and its variables: instead of focusing on the engine design, the main focus is the propulsion system as a whole. It is chosen to evaluate the performances

for already existing selected engines, in order to be able to combine existing diesel engines with the chosen innovative propulsion system and evaluate their performances together.

To sum up, the evaluation of the ship fuel consumption takes into account the presence of the Flettner rotor and its influence on the engine working point. The objective function is the fuel consumption of the ship as a whole. The optimisation is focused on the engine: the propeller and the Flettner rotor are fixed while the engine is chosen accordingly. The developed approach uses the results of the ship propulsion, simulate some engine fuel maps, compute the minimum hourly fuel consumption, highlights the best engine. In the following, the method is described in detail and a case study is presented.

6.2 Engine-propulsion system interaction model

The goal of the model is the identification of the engine minimum hourly fuel consumption working point for a given ship speed and wind condition. Different engines can be tested at once, making the simulation code suitable in a design stage to asses the optimum solution given certain parameters, such as ship characteristics, wind condition, propeller and rotor characteristics, engine design characteristics, and so on.
But the model is also suitable in the operational phase: in fact, chosen the engine, it is possible to change the wind conditions and ship speed to find the best configuration possible for the propeller (in terms of P/D) and for the engine (in terms of power and speed).

The proposed methodology is suitable for many different propulsion plant and power generation configurations, consisting of 1 or more CPP or FPP propellers, 1 or more diesel engines and various types of wind assisted propulsion devices. It will be later applied, as a case study, to the propulsion system consisting of 2 CPP, 2 four-stroke main diesel engines and 1 Flettner Rotor.

Having already described the rotor and propeller interaction in Section 5, the remaining component to be analyzed is the diesel engine.

6.2.1 Engine model

The simulation model is built with a numerical methodology to derive fuel consumption values in the entire working area of any diesel engine.

Several coefficients appear in the main mathematical equation, whose numerical values are obtained through statistical regressions of fuel consumption maps of existing diesel engines, as reported by [1].

The model is implemented in Matlab® environment. The output of the previous simulation, about the combined propeller-rotor propulsion system, are now the inputs under specific hypothesis with which the consumption map in the engine load diagram is built and the minimum hourly fuel consumption is calculated.

The required input data are the power and rotational speed at engine MCR and the fuel flow rate at design point (80% MCR).

A mathematical model representing the engine steady state conditions is built, based on the following assumptions:

1. A generic marine diesel engine brake power P_B [kW] is in equilibrium with the power required by the propeller and it can be roughly represented through a cubic law depending on the engine rotational speed n_e and, thus, the torque Q_B is proportional to the square of n_e as per equation 6.1.

$$\begin{aligned} P_B &=\propto n_e^3 \\ Q_B &=\propto n_e^2 \end{aligned} \tag{6.1}$$

Equations 6.1 are generally approximations but they are analytically derivable and strictly true when there is a quadratic resistance curve with ship speed and the propeller has constant propulsive efficiencies.

Considering the relation between engine torque and speed at design conditions (Q_{Bd} and n_{ed}) and their values in a generic working point, the torque equation 6.1 can be rewritten as:

$$\frac{Q_{Bd}}{n_{ed}^2} = \frac{Q_B}{n_e^2} \rightarrow n_{ed} = n_e \cdot \sqrt{\frac{Q_{Bd}}{Q_B}} \tag{6.2}$$

2. Q_B may be considered proportional to the fuel flow m_F [kg/s] in the most of the diesel engine working area if it is working at the fixed speed and with constant engine efficiency; by substituting $Q_B =\propto m_F$ in equation 6.2:

$$n_{ed} = n_e \cdot \sqrt{\frac{m_{Fd}}{m_F}} \tag{6.3}$$

and from equation 6.1 and 6.3:

$$P_{Bd} = P_B \cdot \left(\frac{m_{Fd}}{m_F}\right)^{3/2} \tag{6.4}$$

With these equations it is possible to simulate the entire fuel consumption map: by joining the points (P_B, n_e) at constant fuel rate, it is possible to derive the engine load diagram in terms of power and fuel consumption as a function of the engine speed.

3. The engine power, for a constant fuel rate, can be represented by a third-order polynomial depending on the engine speed, as per the following equation, calculated at the design condition.

$$P_{Bd} = a \cdot n_{ed}^3 + b \cdot n_{ed}^2 + c \cdot n_{ed} \tag{6.5}$$

where the dimensionless a, b, c are calculated by fitting three arbitrary points of the power–speed curve corresponding to the design fuel flow rate, as reported in [2], and can be evaluated as:

$$a = 0.7428 - \frac{2.979}{\frac{P_{B\ MCR}}{n_{e\ MCR}^3}}; \quad b = -2.499 + \frac{2.011}{\frac{P_{B\ MCR}}{n_{e\ MCR}^3}}; \quad c = 2.599 + \frac{0.3588}{\frac{P_{B\ MCR}}{n_{e\ MCR}^3}} \tag{6.6}$$

The power P_B is expressed in watt [W] and the rotational speed n_e in [rps] and they are measured at the engine maximum continuous rating point (MCR). Equation 6.6 allows to estimate the values of a, b, c coefficients for any diesel engine of interest.

Thanks to these 3 assumption, it is possible to obtain, by substitution, equation 6.7.

$$P_B = \left(\frac{m_F}{m_{Fd}}\right)^{3/2} \cdot \left[a \cdot \left(\frac{m_{Fd}}{m_F}\right)^{3/2} \cdot n_e^3 + b \cdot \left(\frac{m_{Fd}}{m_F}\right) \cdot n_e^2 + c \cdot \left(\frac{m_{Fd}}{m_F}\right)^{1/2} \cdot n_e\right] \tag{6.7}$$

To have a more suitable correspondence between equation 6.7 and the power-speed characteristics of a generic marine engine, equation 6.7 is written in the following general form:

$$P_B = \left(\frac{m_F}{m_{Fd}}\right)^{x} \cdot \left[a \cdot \left(\frac{m_{Fd}}{m_F}\right)^{x} \cdot n_e^3 + b \cdot \left(\frac{m_{Fd}}{m_F}\right)^{y} \cdot n_e^2 + c \cdot \left(\frac{m_{Fd}}{m_F}\right)^{z} \cdot n_e\right] \tag{6.8}$$

where the exponents x, y, z shall be adjusted according to the particular marine engine to be represented and their relationship can be found from Equation 6.7 as: $x = \frac{3}{2}y$ and $z = \frac{1}{2}y$. For a typical four-stroke marine diesel engine the following values can be applied [2]: $x = 1.05$; $y = 0.7$; $z = 0.35$.

From the fuel rate results, in order to obtain specific fuel consumption curves, specific fuel consumption ($sfoc$) can be evaluated, as:

$$sfoc = \frac{m_F}{P_B} \qquad \left[\frac{g}{kWh}\right] \tag{6.9}$$

The consumption map and the relative specific fuel consumption surface can be built.

To validate the model, it was applied to two known diesel engines: Wartsila W26XN and Rolls Royce Bergen C25:33.

The coefficients used are reported in Table 6.1.

x	y	z	a	b	c
1.05	0.7	0.35	$2.3156 \cdot 10^{-7}$	$-8,5014 \cdot 10^{-4}$	$-0,8936$

TABLE 6.1: Wartsila W26XN engine model coefficients

To run the model, m_{Fd}, the value of the engine fuel consumption corresponding to 80% MCR, is needed. For the model in exam $m_{Fd} = 0.27 [kg/s]$ and, more generally, $0 < m_F < 0.337 kg/s$ as reported in [2].
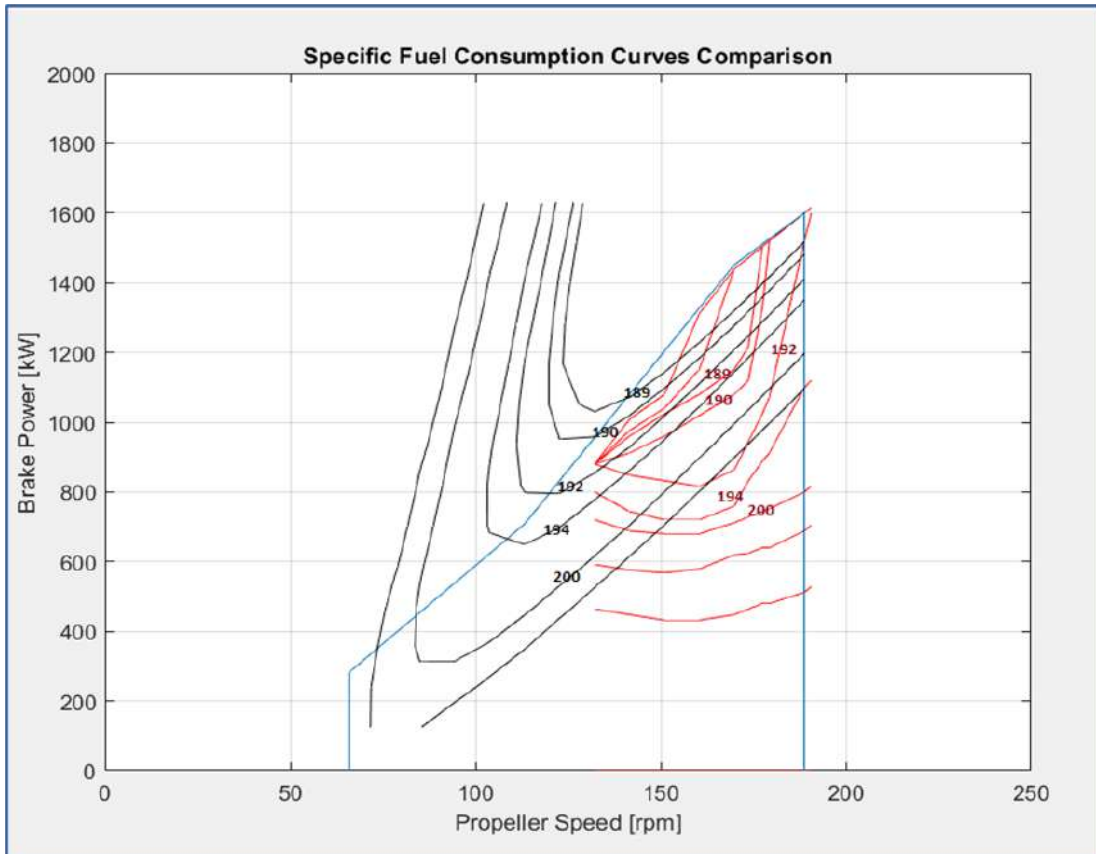
FIGURE 6.1: Mathematically derived fuel consumption curves (in black) and engine manufacturer's curves (in red) comparison.
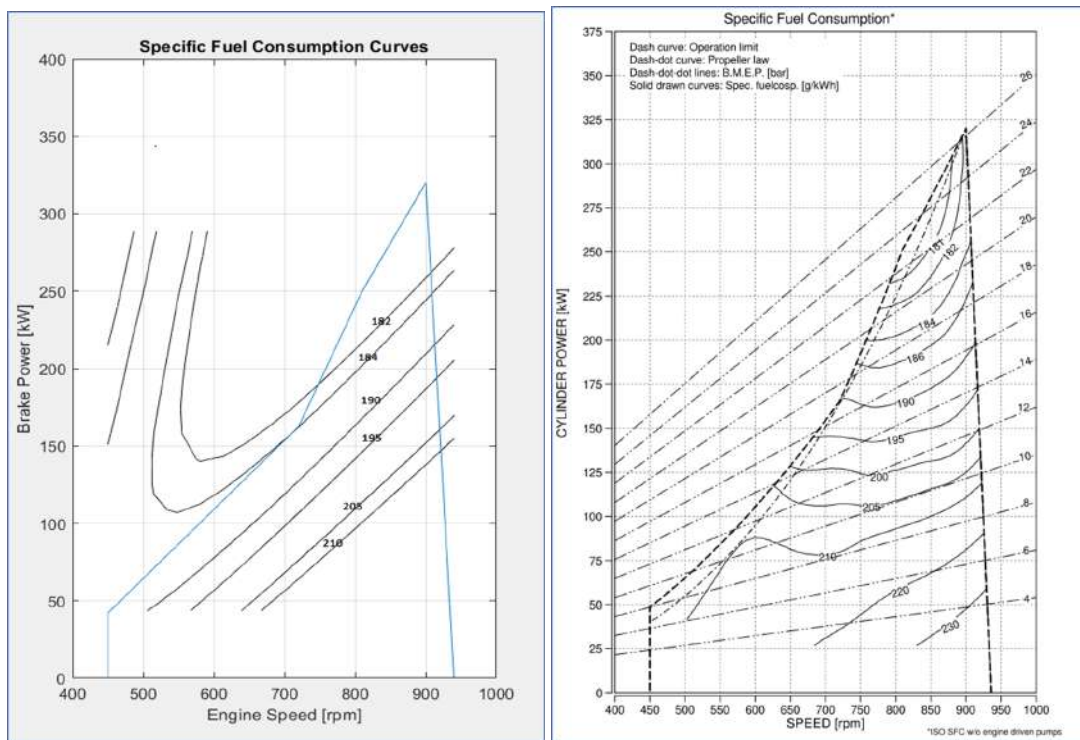
(A) Mathematical values.

(B) Engine manufacturer's curves.

FIGURE 6.2: Model and real fuel consumption curves comparison.

With said values it is possible to build the engine fuel consumption map and to compare it with the one provided by the engine manufacturer. The result of this comparison is reported in Figure 6.1, expressed as [g/kWh]. If the overall values are good, the shape of the curves is different. To better understand if the model is acceptable, another test was made using a second engine, the Rolls Royce Bergen C25:33.

The comparison between calculated values and real ones is reported in Figure 6.2, expressed as [g/kWh] and the model was considered acceptable: its level of approximation is appropriate to its purpose, being the engine only a complementary part of this research work.

6.2.2 Engine - propeller matching

As explained in section 5.3.8, the propeller working points were calculated from the net resistance $\underline{R}_N$, as defined in 5.3.5.

If there was a fixed pitch propeller (FPP), by applying Equations 5.1 and 5.2 (with $\eta_r = 1.01$, $\eta_s = 0.99$ and $\eta_g = 0.98$) for each ship speed, the propeller curve of P_B - V_{ship} would be obtained.

But there is a controllable pitch propeller (CPP) so, in addition to for each speed, the calculation should be repeated also for each P/D and the result is the propeller surface as shown in Figure 6.3.
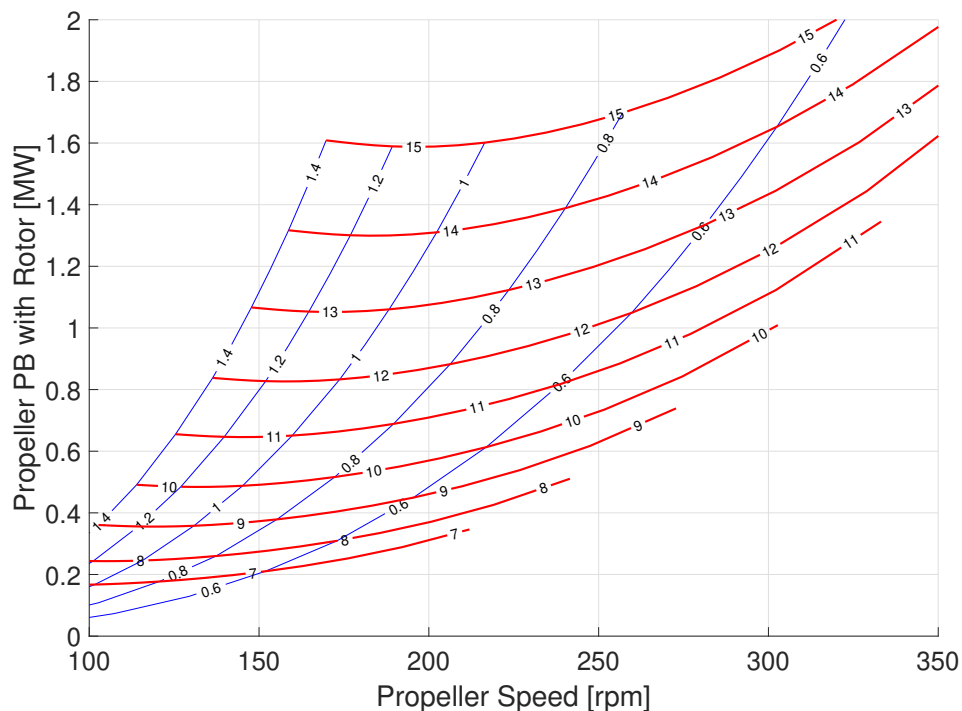
FIGURE 6.3: CPP P_B curves.

The blue thin lines represent the P_B-n_p curves for each P/D and each one of the red thick almost horizontal ones corresponds to a ship speed [kn].

These curves can be superimposed on the engine load diagram to find the engine working points, considering the correct gear ratio which is defined as $i = \frac{n_e}{n_p}$.
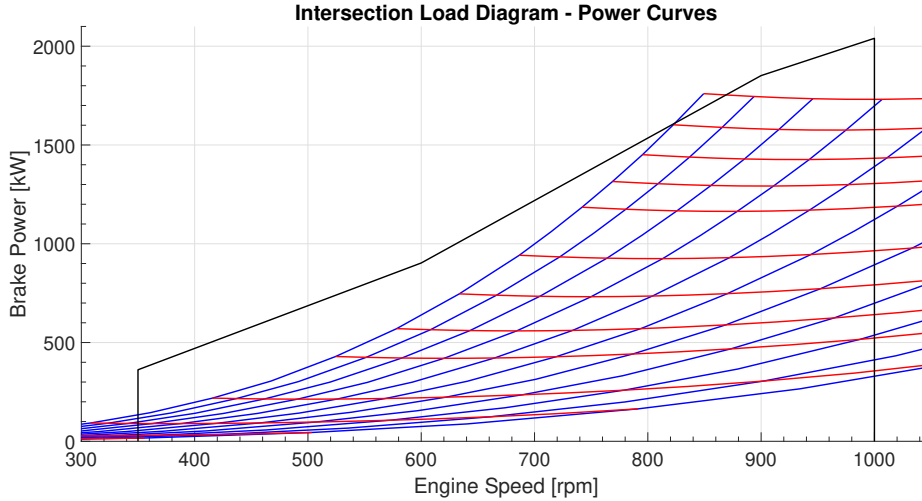
FIGURE 6.4: CPP power curves over engine load diagram (matching).
Red horizontal lines: iso - ship speeds; blue lines: iso - propeller P/D.

To determine i, the ideal gear ratio was calculated as $i_{id} = \frac{n_{e\ MCR}}{n_{p\ V\ des}}$ where $n_{e\ MCR}$ is the engine speed at the MCR and $n_{p\ V\ des}$ is the propeller speed at the design ship speed (if there is a CPP this value must be selected on the P/D of maximum efficiency, that correspond to the condition of the lowest P_B). It is called ideal gear value because it is very unlikely that it would correspond to an off-the shelf solution, thus the most similar available value must be chosen.

At this point it was possible to draw Figure 6.4, multiplying each value of n_p of the curves of Figure 6.3 by i and superimposing them on the engine load diagram.

Then, a typical engine margin ($EM = \frac{P_{B\ MCR}}{P_{B\ CS}}$) between the maximum power ($P_{B\ MCR}$) and the continuous service power ($P_{B\ CS}$) of about 15%-20% should be considered.

Lastly, only the working points within the engine load diagram were considered; all the points outside the engine load diagram limit curves were discarded.

6.2.3 Fuel consumption

For each of the just identified working points, the couple (P_B; n_e) is known, thus Equation 6.7 could be applied to find the fuel flow m_F [g/h] in said point and, then, with Equation 6.9, the specific fuel consumption $sfoc$ [g/kWh].

By joining the point of equal values, it was possible to draw specific fuel consumption curves.

For the sake of simplicity, from now on, the fuel flow will be converted to the hourly fuel consumption q_h expressed in [t/h]. This value is to be minimized.

Since the hourly fuel consumption is a function of the ship speed, the engine speed and P/D, it can be described as a surface, of which each point is characterised by (P_B; n_e; V_{ship}; q_h; P/D); therefore for each ship speed there are several sets of (P_B; n_e; q_h; P/D) but only the one with the minimum value of q_h was considered, after verifying that it is in a acceptable position for engine operation.

Lastly, the CO_2 emissions were evaluated with a simple correlation factor, as stated by the IMO Guidelines to MARPOL Annex VI [57], that, for heavy fuel oil is 3.11, as

per Equation 6.10.

$$CO_2\ [t/h] = q_h\ [t/h] \cdot 3.11 \tag{6.10}$$

6.3 Optimum engine-rotor matching.

The optimisation of the rotor-propeller-engine propulsion plant was written in the form of a parametric investigation. All the components of the system are modelled in a parametric way: the propellers, the rotors, the engines are all parametric. This strategy allows to choose which components, and even more which parameters, are to be considered fixed and which are to be found. Moreover, it allows to systematically vary the value of said fixed parameters in order to derive the others. At the end of the computation, the optimum values are found. Table 6.2 shows the variable parameters of the engine (engine power, speed and fuel consumption at maximum continuous rating), rotor (rotor diameter, height and spin ratio) and propeller (propeller diameter, pitch over diameter ratio and A_e/A_o), together with the value to be minimized, the hourly fuel consumption.

Parameters	Engine	$P_{B_{MCR}}$	$n_{e_{MCR}}$	$m_{F_{MCR}}$
	Rotor	d	H_{rotor}	SR
	Propeller	D_p	P/D	A_e/A_o
Output to be minimized	Hourly fuel consumption q_h			

TABLE 6.2: Model parameters and objective

The parametric model was applied to study a case study, where it was chosen to consider as fixed parameters the rotor dimensions and the propellers characteristics in order to carry out the parametric analysis of different engines alternatives to achieve the minimum fuel consumption.

Different engines were tested to find the best solution for the fixed decided configuration. The variable parameters were the engine power and speed and the propeller P/D as summarized in Table 6.3, where the configuration adopted for the selected case study is shown.

Fixed parameters	Rotor	d	H_{rotor}	SR
	Propeller	D_p	A_e/A_o	
Variable parameters	$P_{B_{MCR}}$	$n_{e_{MCR}}$	$m_{F_{MCR}}$	P/D
Output to be minimized	Hourly fuel consumption q_h			

TABLE 6.3: Model fixed and variable parameters for the case study

6.4 Case study

The methodology described was applied to the wind assisted propulsion system. As said, it was chosen to keep the rotor dimensions as fixed parameters, in order to find

the optimum engine. The engine is described by a parametric model and three alternatives of four-stroke diesel engines were chosen to be compared: Wärtsilä W26XN, Wärtsilä 6L26, Rolls-Royce Bergen C25:33.

The optimisation problem has been solved between these alternatives to choose the most suitable option for the given propulsive system.

Other fixed parameters are: ship characteristics and hull resistance, ship design speed, wind conditions, rotor dimensions, propeller characteristics, efficiencies. All these data are reported in Section 5.4.

6.4.1 Input data and boundary conditions.

Since the engine-fuel consumption model has been integrated with the rotor-propeller model described in Section 5.3, the output of the latter have become the inputs of this new simulation, in addition to engine data.

From the rotor-propeller interaction the propeller delivered power and speed matrices (function of ship speed and P/D) for the given wind condition are considered as inputs.

About the engine, the following coefficients are assumed for the simulation: $x = 1.05$; $y = 0.7$; $z = 0.35$ (see Section 6.2.1 [2]). Three engine are chosen, whose characteristics are reported in Table 6.4.

	Wärtsilä W26XN	Wärtsilä 6L26	Rolls Royce Bergen C25:33
$P_{B_{MCR}}$	2 MW	2.04 MW	1.92 MW
$n_{e_{MCR}}$	1000 rpm	1000 rpm	940 rpm
m_{Fd} (design)	0.0897 kg/s	0.0896 kg/s	0.0894 kg/s
Number of cylinders n_{cyl}	5	6	6
Power per cylinder $P_{B_{cyl}}$	400 kW	340 kW	320 kW
Gear ratio i	5.1	4.9	4.6
Load diagram		from manufacturer's guide	

TABLE 6.4: Three engines input data.

Some considerations about some of the values in the table must be addressed. W26XN: The power required for the case study is much lower than the maximum MCR power provided by the actual 18-cylinders engine. Thus, only 5 cylinders were considered in the calculation but, in a real application, this solution would not be acceptable. 6L26 and C25:33: These 6-cylinders engines are realistically more suitable for the case study.

6.4.2 Results at design speed

From the numerical simulation, the following results are found:

- graphic representation of the superimposition of the engine load diagram with the brake propeller power curves;

- matrix of the engine working points (n_e, P_B, V_{ship}, P/D, q_h);

- curves of the hourly fuel consumption at the design ship speed, one at variables P/D and one at variables n_e, suitable for selecting the value of P/D and n_e corresponding to the minimum fuel consumption;

- the minimum hourly fuel consumption and the relative CO_2 emissions;

- the design ship speed working point: minimum fuel consumption, engine speed, brake power, engine margin, gear ratio, propeller speed, P/D.

Examples of these results can be found in Appendix C and in [32].

To sum up, the goal of the model is the evaluation of the hourly fuel consumption at design ship speed, assuming as constants the hull and rotor characteristics and wind condition.

Three engines results analysis

Table 6.5 reports the comparison between the three engines analysed at the design speed, for a wind of 5 m/s from 170°.

	Wärtsilä W26XN	Wärtsilä 6L26	Bergen C25:33
Gear ratio	4.985	4.787	4.565
$q_{h_{min}}$ [t/h]	0.388	0.383	0.435
n_p [rpm]	182	182	182
n_e [rpm]	928	892	837
P_B [kW]	1287	1287	1287
P/D	1.15	1.15	1.15
CO_2 [t/h]	1.21	1.19	1.35
Engine margin [% P_B]	35	37	32.3

TABLE 6.5: Engines working points for $V_{ship} = 14$ knots

After the calculation of the fuel consumption maps, these working points were identified inside the engine load diagrams as the ones corresponding to the minimum fuel consumption for the given ship speed. From this comparison it is clear that, regarding fuel consumption at the design speed, the best solution is the Wärtsilä 6L26 Diesel Engine.

About the engine margins, it can be seen that they are quite large values; this is because the ship speed tested (design speed) does not correspond to the maximum speed.

A full range of different ship speed and wind conditions were tested and some of the results are reported in the following paragraphs.

The three engines were tested in the full range of possible ship speeds. For simplicity only two cases are reported below: a lower (in Table 6.6) and a higher (see Table

6.7) value of speed in respect to the design condition. They were also tested for a wide range of true winds. The reported results are for the condition of 5 m/s from 170°.

	Wärtsilä W26XN	Wärtsilä 6L26	Bergen C25:33
$q_{h_{min}}$ [t/h]	0.338	0.334	0.379
n_p [rpm]	170	170	170
n_e [rpm]	865	830	780
P_B [kW]	1044	1044	1044

TABLE 6.6: Engines working points for $V_{ship} = 13$ knots

	Wärtsilä W26XN	Wärtsilä 6L26	Bergen C25:33
$q_{h_{min}}$ [t/h]	0.443	0.438	0.497
n_p [rpm]	195	195	195
n_e [rpm]	993	954	896
P_B [kW]	1570	1570	1570

TABLE 6.7: Engines working points for $V_{ship} = 15$ knots

The choice of Wärtsilä 6L26 as the most suitable diesel engine is confirmed also for all the other ship speeds [32].

Since the Wärtsilä 6L26 was found to be the best solution, a summarizing Table (6.8) is reported.

	13 kn	14 kn	15 kn
$q_{h_{min}}$ [t/h]	0.334	0.383	0.438
n_p [rpm]	170	182	195
n_e [rpm]	830	892	954
P_B [kW]	1044	1287	1570
P/D	1.15	1.15	1.15
CO_2 [t/h]	1.07	1.19	1.36
Engine margin [% P_B]	48	37	23

TABLE 6.8: Wärtsilä 6L26 working points in 3 ship speeds.

In Figure 6.5 is reported the engine load diagram and consumption map for the Wärtsilä 6L26. The green "X" represents the engine minimum hourly fuel consumption working point for the ship speed of 14 knots.

As can be seen from Figure 6.5 and in Table 6.8 the engine margin is exaggerated, being over 20% even at the highest speed. This was true also for the other two engine tested.

That being said, it was useful to test them with an inferior number of cylinders, moving from 6 to 5 both the Wärtsilä 6L26 and the Rolls-Royce Bergen C25:33. This was possible because the model is parametric on the cylinder, thus this change was easily applicable. The Wärtsilä W26XN was not recalculated, as it was already been considered a 5 cylinder engine from the beginning, being too powerful. The results are shown in Table 6.9.
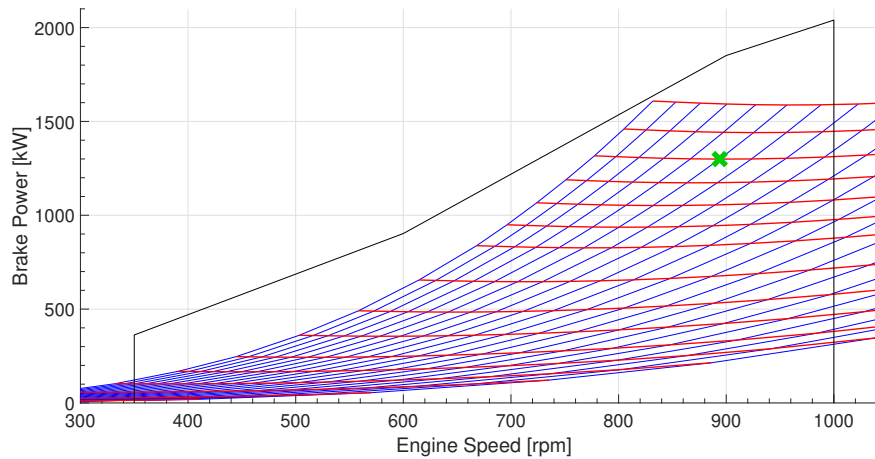
FIGURE 6.5: Engines margin at 14 knots for Wärtsilä 6L26.

	13 kn	14 kn	15 kn
Wärtsilä 6L26 (5 cyl)	31	23	15
RR Bergen C25:33 (5 cyl)	26	18	10

TABLE 6.9: Engine margin [% P_B] for the 5 cylinders 6L26 and C25:33

Regarding Wärtsilä 6L26 (5 cyl) all three values are acceptable, although the last value is at the limit. Unlike speech applies to RR Bergen C25:33 (5 cyl): the engine margin at 15 knots is considered too low and thus not acceptable.

A comparison of the hourly fuel consumption between the real Wärtsilä 6L26 and the 5 cylinder version is reported in Table 6.10.

	13 kn	14 kn	15 kn
Wärtsilä 6L26 (6 cyl) [t/h]	0.334	0.383	0.438
Wärtsilä 6L26 (5 cyl) [t/h]	0.336	0.385	0.441

TABLE 6.10: Hourly fuel consumption for the 6 or 5 cylinders 6L26.

The table shows that the 5 cylinders version consumes about 2 kg/h more that the 6 cylinder in every ship speed. This assessment was, of course, mere speculation since the 5 cylinder version is non existent.

6.4.3   Results for different wind conditions.

All the above considerations were made by having as input a fixed wind state corresponding to 5 m/s of speed, coming from 170°. A study was made changing said condition to evaluate the impact of the wind on the engine working point.

The results obtained from the rotor-propeller interaction were given as input in the form of matrices of propeller speed and delivered power both in function of P/D and ship speed.

A wide variety of wind were tested, keeping constant the ship speed at 14 knots; the most extreme cases are reported here.

1. Firstly, an increase in wind speed was considered: V_{True} =15 m/s but keeping constant the angle at 170°. Table 6.11 shows the results at the design speed for the three engines.

	Wärtsilä W26XN	Wärtsilä 6L26	Bergen C25:33
$q_{h_{min}}$ [t/h]	0.366	0.362	0.411
n_p [rpm]	179	179	179
n_e [rpm]	911	876	821
P_B [kW]	1181	1181	1181
CO_2 [t/h]	1.14	1.13	1.28

TABLE 6.11: Engines working points for $V_{True} = 15$ m/s from 170°

2. For the second wind condition, the most advantageous configuration was chosen: 15 m/s from 100°.

	Wärtsilä W26XN	Wärtsilä 6L26	Bergen C25:33
$q_{h_{min}}$ [t/h]	0.315	0.311	0.353
n_p [rpm]	160	160	160
n_e [rpm]	817	785	737
P_B [kW]	940	940	940
CO_2 [t/h]	0.98	0.97	1.10

TABLE 6.12: Engines working points for $V_{True} = 15$ m/s from 100°

3. Wind condition 3 was $V_{True} = 15$ m/s from 5°, which corresponds to the most disadvantageous among the ones tested. This is confirmed by the higher values of fuel consumption reported in Table 6.13. In this unfavorable wind condition

	Wärtsilä W26XN	Wärtsilä 6L26	Bergen C25:33
$q_{h_{min}}$ [t/h]	0.482	0.476	0.541
n_p [rpm]	196	196	196
n_e [rpm]	999	991	901
P_B [kW]	1783	1783	1783
CO_2 [t/h]	1.50	1.48	1.68
Engine margin [% P_B]	11	13	7

TABLE 6.13: Engines working points for $V_{True} = 15$ m/s from 5°

the engine margins are quite small but sufficient.

To compare results more clearly, the summary Table 6.14 is made reporting only fuel consumption for the already different tested wind condition at design speed plus some more cases.

From the table 6.14, it can be noted that, when the wind is coming from a favorable direction (such as cases 2, 4, 5) a higher wind speed corresponds to a lower fuel consumption.

$q_{h_{min}}$ [t/h] @ V_{True}	Wärtsilä W26XN	Wärtsilä 6L26	Bergen C25:33
0) 5 m/s from 170°	0.388	0.383	0.435
1) 15 m/s from 170°	0.366	0.362	0.411
2) 15 m/s from 100°	0.315	0.311	0.353
3) 15 m/s from 5°	0.482	0.476	0.541
4) 5 m/s from 100°	0.384	0.380	0.430
5) 10 m/s from 100°	0.359	0.354	0.402
6) 10 m/s from 90°	0.360	0.356	0.404
7) 10 m/s from 80°	0.364	0.359	0.408
8) 10 m/s from 45°	0.394	0.390	0.442
9) 10 m/s from 0°	0.451	0.446	0.506
10) 10 m/s from 180°	0.386	0.381	0.433
11) 10 m/s from 225°	0.369	0.364	0.414

TABLE 6.14: Engines working points at $V_{ship} = 14$ kn for different wind conditions.

The opposite is, of course, true when the incoming wind is contrary to the ship direction, as happens looking at cases 3 and 9. As expected the head wind is the worst scenario.

On the contrary, case number 2 seems to be the best of this series of tests: wind from cross to quarter-stern are optimal for fuel consumption reduction maximisation.

Moreover, the direction of the incoming wind is more important than the wind speed. This is due to the similarities in the magnitude of wind speed and ship speed, which results to a stronger importance of the direction in the composition of the apparent wind.

Lastly, the Wärtsilä 6L26 was confirmed to be the best option among the three considered; for every wind scenario studied this engine had the lowest values of fuel consumption.

Thus, the simulation method was firstly used to choose the best diesel engine and secondly to evaluate its minimum hourly fuel consumption working point in term of propeller P/D, engine power and speed for a generic wind condition. Therefore it could be useful both at the design stage and at the operating stage.

6.4.4 Fuel consumption with and without rotor

The last step is the evaluation of fuel consumption reduction achievable using the rotor. To do that, the Wärtsilä 6L26 was chosen as the main engine and kept constant; different wind condition were tested for the the entire range of ship speeds.

Some results are reported in Figures 6.6, 6.7 and 6.8.

An important warning common to all these figures is that, not only the the total propulsion fuel consumption calculated with the rotor in function (green line) varies, but also the one with the rotor turned off (red line) and with no rotor at all installed onboard (blue line) are different in each graph. This is because, even if there is no rotor or if it is turned off, the wind is still acting on the ship resistance and being different in
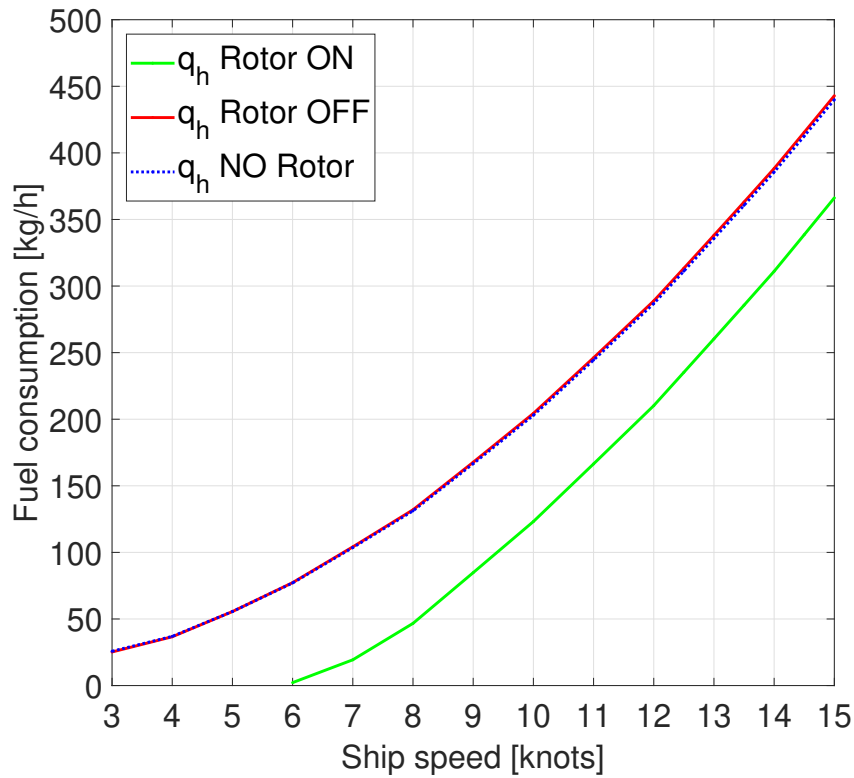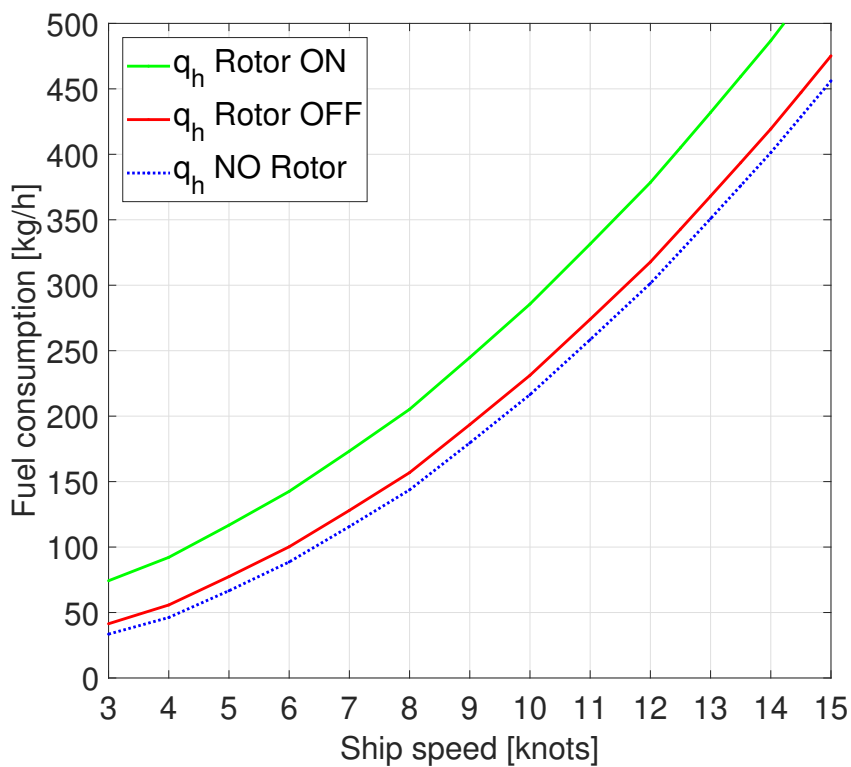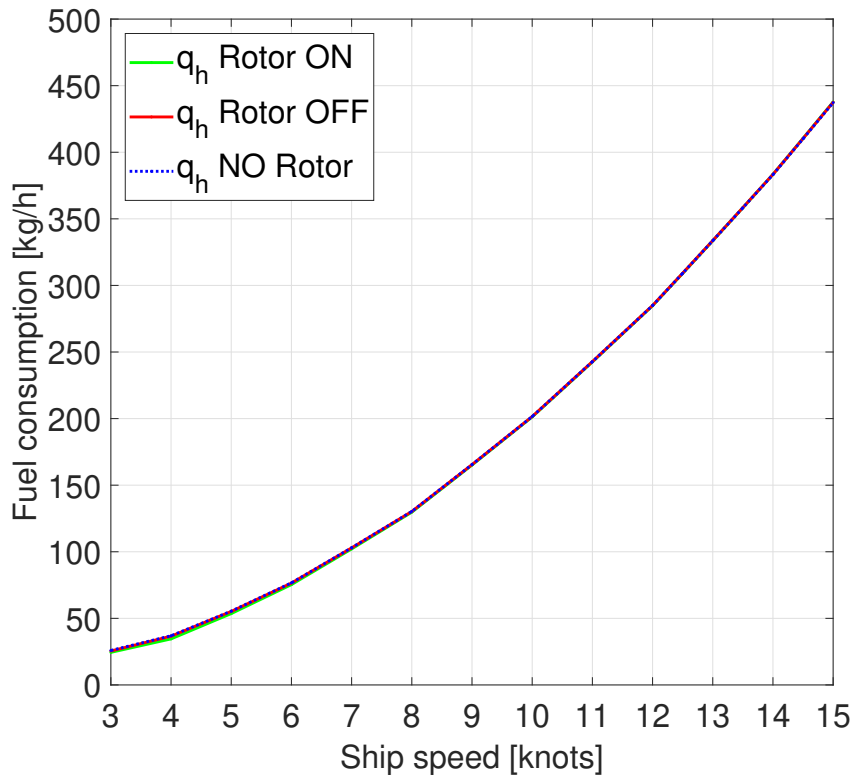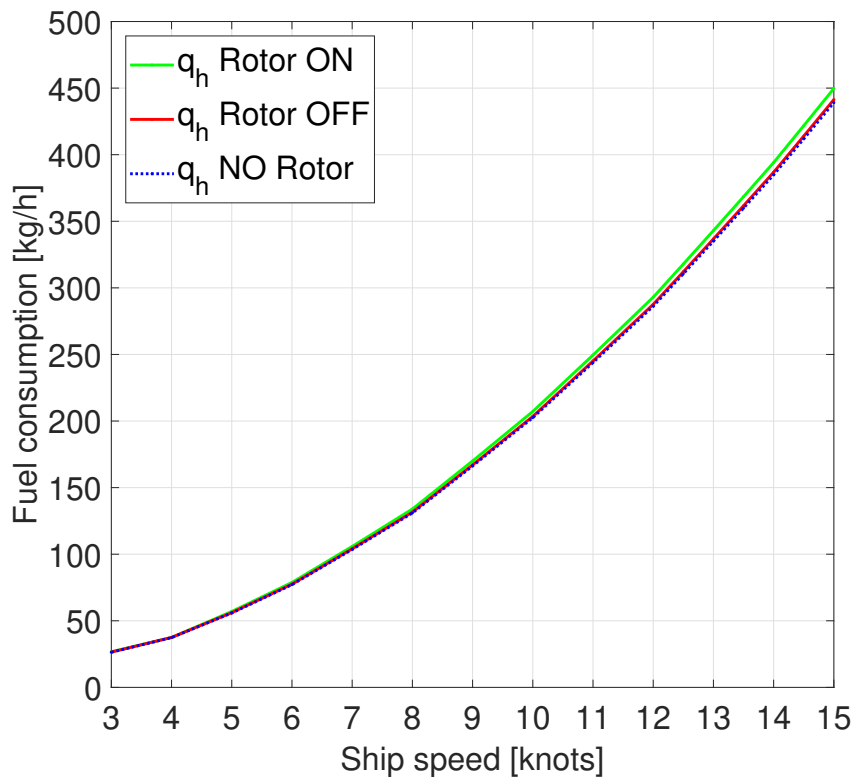
(A) V_{True}=15 m/s 100°.

(B) V_{True}=15 m/s 0°.

FIGURE 6.6: Fuel consumption with and without rotor.

(A) V_{True}=5 m/s 170°.

(B) V_{True}=0 m/s.
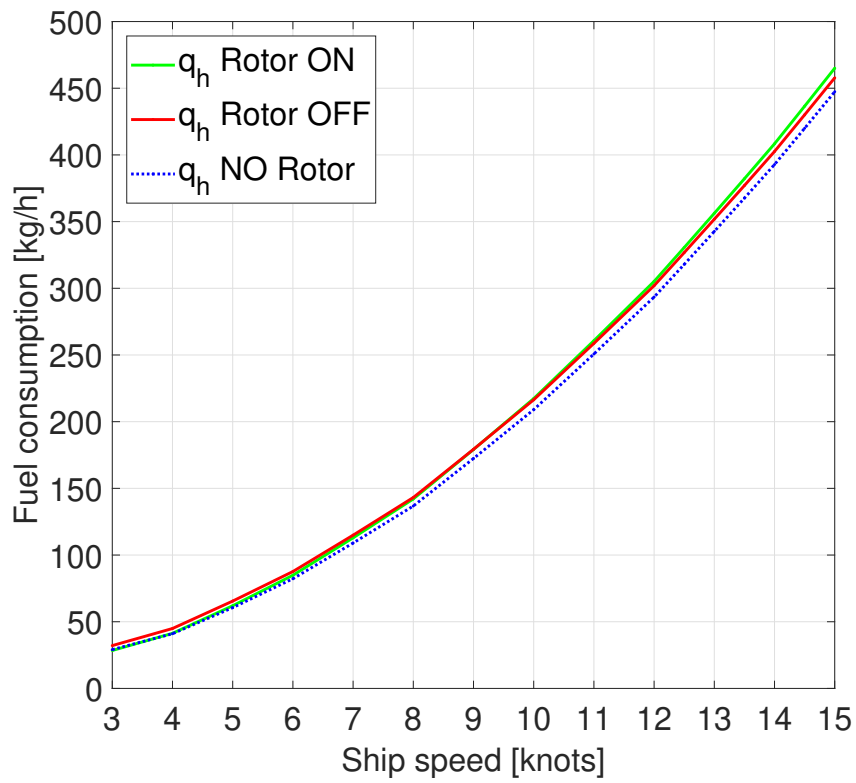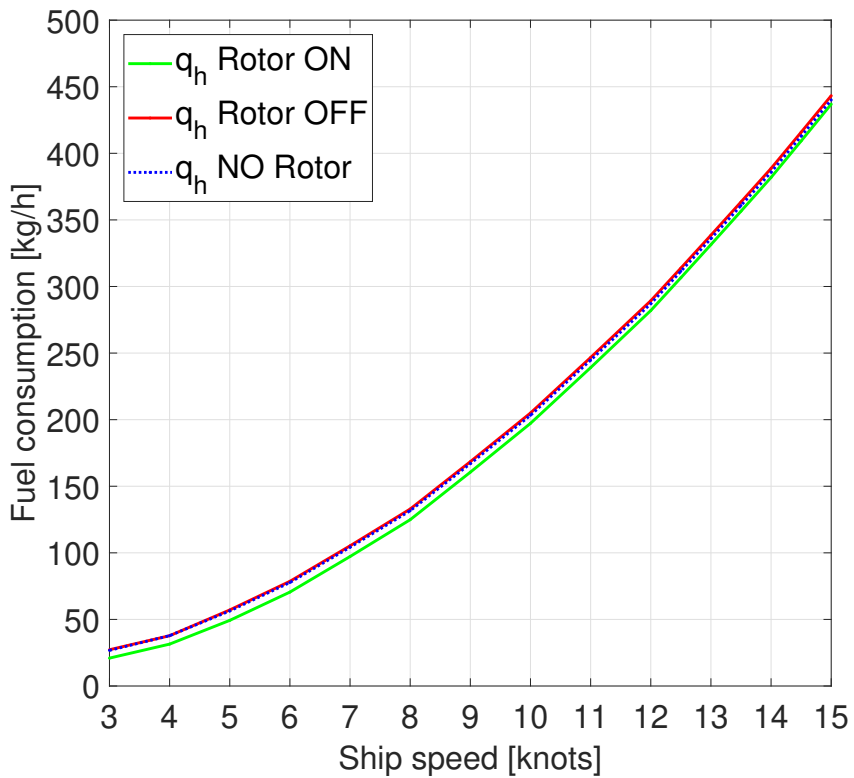
FIGURE 6.7: Fuel consumption with and without rotor.

(A) V_{True}=10 m/s 30°.

(B) V_{True}=5 m/s 80°.

FIGURE 6.8: Fuel consumption with and without rotor.

each case tested, it generates various ship wind added resistance, leading to as many propeller and engine working point.

Figure 6.6 shows the effects of the best (Figure 6.6a) and worst (6.6b) wind possible. It can be noted that the blue and red lines of Figure 6.6a, which represent the fuel consumption when there is no rotor installed onboard and when there is a rotor but it is turned off respectively, overlap; this is due to the fact that, with cross wind, the component of the added resistance provided by the rotor is negligible compared to the large longitudinal area of the ship. As expected, with strong cross wind (15 m/s from 100°) the rotor in function (green line) allows an important fuel consumption reduction: for the ship speed of 14 knots about 20% of savings is achieved and for slower speeds even more. It is important to note that, in this wind condition, the results are accurate only for a ship speed higher than 6 knots; if the ship speed is lower than six knots, the rotor can provide all the thrust by itself, leading to almost no fuel consumption. However, these results are an approximation because the numerical model is not suitable to take into account the case in which the propeller is windmilling and does not provide thrust. The numerical model is valid only when the propeller is providing thrust; it was decided so because the model was written for the higher design speeds, where the rotor is intended to be a simple aid to the propulsion and it is not meant to replace the propeller. A possible future integration of the code will take into account the windmilling propeller, as done in [12].

On the contrary, with strong head wind (15m/s from 0°, Figure 6.6b) and rotor in function a significant increase in consumption of 16%, in respect to the condition with rotor turned off, is visible at design speed. Unsurprisingly, if the ship had not been equipped with a rotor (blue line), a small saving would have been possible in this condition, since the ship transverse area and the rotor projected area are more comparable than the previous case.

Figure 6.7a reports the wind condition applied in Section 6.4.2. From this image it is clear how this particular true wind (5 m/s from 170°), combined with the ship speed, generates an apparent wind that has the effect to neutralize the rotor: if the rotor is kept on or off or is not there at all, there is no difference in fuel consumption.

Figure 6.7b is for the dead calm situation with no true wind at all. From the graph, it can be deduced that the rotor has the negative effect, more visible at higher ship speeds, of slightly increasing consumption, because of the apparent wind generated solely by the ship speed component: at 15 knots the rotor lead to an increase of 2.4% in fuel consumption, in respect to the "no rotor" condition.

In Figure 6.8a a change of trend between the two curves is reported when the wind is 10 m/s from 30°. For slower ship speeds the rotor is beneficial but, for speed higher than 9 knots, it is better to turn the rotor off (or better yet, not having it all). This is because, at slower ship speed, the apparent wind, generated by the composition of true wind and ship speed, is coming from the side, being the true wind component prevailing; but, when the ship speed magnitude overcomes the true wind, the apparent wind starts to move more and more towards the bow, becoming less advantageous.

Lastly, in Figure 6.8b another good condition for the rotor is represented. With true wind of 5 m/s from 80°, the rotor allows a small reduction in fuel consumption, for every ship speed.

6.5   Final remarks

In this chapter the goal of minimizing the hourly fuel consumption of the main diesel engines working together with a Flettner rotor was studied.

A numerical model was implemented in MATLAB ®, based on a parametric model of the diesel engine. The simulator is able to evaluate the fuel consumption of any diesel engine starting from very few inputs such as engine power and speed at MCR and some given parameters.

After the validation (Sec. 6.2.1), the developed parametric model of the engine was then incorporated with the already tested numerical simulator of Chapter 5.

The new complete parametric simulator is able to provide fuel consumption, powers and forces evaluations starting from very few inputs, such as hull resistance-speed curve of the selected ship, propeller(s) (CPP or FPP) geometric characteristics, rotor(s) dimensions, engine(s) MCR, some coefficients and, of course, true wind condition(s). The model is written to be able to handle more than one engine type at a time, more than one wind speed and all the 360° direction simultaneously.

Two different perspectives are applicable to the proposed methodology: at the design stage, the simulator can be used to define the best solution among certain alternatives for the given propulsive plant; in operational mode, it can be used to determine the optimum propeller and engine working point to minimise consumption for each ship speed and wind condition.

To test the simulator, a ro-ro ferry was chose as a case study. Three engines were selected and one rotor was considered. This propulsive configuration was subjected to several wind conditions to determine the respective propulsive powers and fuel consumption and to select the best option among the three engines.

For the selected case study the Wärtsilä 6L26 turned out to be the best alternative, in all the ship speed range and at different wind conditions, even changing the engines number of cylinders.

Moreover, it was confirmed what found in Chapter 5, that the most favourable wind is the stronger one coming from the side or slightly aft and that the worst case scenario is with head wind. Moreover it was found that the angle of the wind has a greater effect that its speed on the fuel consumption.

As just said, the model can be also used to optimise fuel consumption during ship operation, thus an analysis on fuel consumption in different wind condition and ship speed with the selected engine was reported. In each scenario the model is able to determine the propeller and engine working points that correspond to the minimum engine fuel consumption and to evaluate fuel savings achievable thanks to the rotor in respect to the "no-rotor" condition.

With the optimized propulsion plant, for the design ship speed and the optimal wind condition, 20% of fuel saving is reached.

7 Conclusions

This research aimed to study emerging innovative solutions to improve the energy efficiency of the ship power and propulsion plants.

Three main innovative solutions, having in common the possibility to improve the energy use onboard, were studied: onboard sludge recycling, a flexible hybrid propulsion plant with waste heat recovery and wind assisted propulsion with Flettner rotors.

For each of these possibilities, a numerical simulator was written, to evaluate the fuel consumption reductions and energy efficiency improvements.

For the sludge recycling onboard plant, the study focused on the possible advantages for the ship system in term of fuel consumption and EEOI reduction.

A feasibility study for the installation of the plant was carried out: the results showed an easy integration of the system inside the incinerator, also able to provide the heat needed for the chemical reaction.

The study showed that the integration onboard of a sludge recycling plant leads to the reduction of time and costs thanks to the elimination of the process of proper disposal of sludge at the port facilities; moreover, a small fuel saving of about 0.17% of the yearly fuel consumption was obtained.

Unfortunately, the environmental benefits are not adequately represented in the energy efficiency index. In fact, the EEOI formula is not yet tailored for innovative waste recycling technologies, as the one investigated in this thesis, and the attempt made to calculate it was unsatisfactory.

The very small gain in the efficiency index, combined with small economic savings, do not encourage the adoption of this solution, despite its environmental advantages.

The second investigated solution to further improve the ship efficiency was a flexible propulsion and power system with heat recovery. This innovative plant was studied in collaboration with a shipping company to obtain a high impact on the ship energy efficiency in respect to the existing configuration.

The proposed plant is made of dual fuel engines, shaft electric motor-generators and combinations of recovery systems, such as hybrid turbocharger and single and double pressure waste heat recovery.

Three main operational configuration were studied: high speed, normal navigation with shaft generators and low speed, with only one main engine to drive both

propellers.

A numerical simulator was implemented in MATLAB® environment to obtain information about power, fuel consumption, plant efficiency and ship speed for every operational and recovery plan configuration.

The results showed that the Normal Navigation scenario is the one associated with the lowest fuel costs and highest plant efficiency, for all considered recovery systems. Moreover, they all allow considerable cost savings. In particular, the hybrid turbocharger is the more interesting because the low initial investment is paid off by considerable annual savings. On the other hand, heat recovery with steam turbines are more effective to improve EEDI.

Lastly, a more risky and cutting edge solution was analysed: wind assisted ship propulsion. Among the possible alternatives, the Flettner rotor was chosen because of its simplicity, low costs and compactness.

A hybrid propulsion plant, made of propellers and Flettner rotors was studied, with the final goal of minimizing the ship fuel consumption.

A literature gap about the rotor-propeller integration into the ship propulsion plant was found. To fill it, a parametric model based on the consolidated engine-propeller matching procedure, modified in order to accommodate the rotor effects on the propeller working point, was proposed and implemented in MATLAB® environment. This simulator was intended to be an useful tool, in a design stage, to select the best combination of rotors and main engines (among certain alternatives). In operational mode, it can be used to determine the optimum propeller and engine working point to minimise consumption for each ship speed and wind condition.

The parametric simulator is able to provide information about forces, power and fuel consumption, starting from very few input, such as hull resistance-speed curve, propellers characteristics, rotors dimensions, engines MCR and true wind conditions. The numerical model can handle more than one engine type at a time, more than one wind speed and all the 360° wind directions simultaneously. For each scenario the simulator can identify the propeller and engine working points that correspond to the minimum engine fuel consumption.

A Ro-Ro/Pax ferry equipped with one rotor and three different main engines was chosen as a case study. The results showed that a bigger rotor is always beneficial. As expected, the best directions of incoming wind are from side to astern; the stronger the wind, the wider the range of suitable angles. The worst case is head wind; the wind angle has a greater influence on the fuel consumption than the wind speed.

With the optimized propulsion plant, remarkable double digit power savings are observed in the whole range of ship speeds, while a 20% of fuel saving was achieved at the design ship speed.

The three developed numerical models allow to quantify the reduction of environmental footprint of the ship, for different plant configurations.

These simulators can be used as a tool to design or operate ships able to meet the present and future energy efficiency requirements.

The next step of the research could be the adoption of all the proposed solutions in a single ship.

Decarbonisation and environmentally friendly innovations are the real challenges of our century. Therefore, the future of research is strongly linked to the improvement of the energy efficiency and the reduction of environmental impact.

A Appendix: Ro-ro ferry diesel engines characteristics.

Here the characteristics of all the diesel engine onboard of the Ro-ro ferry case study for sludge recycling are reported.

As diesel generators 4 Wärtsilä 6R32LN are installed. Their load diagram is reported in Figure.
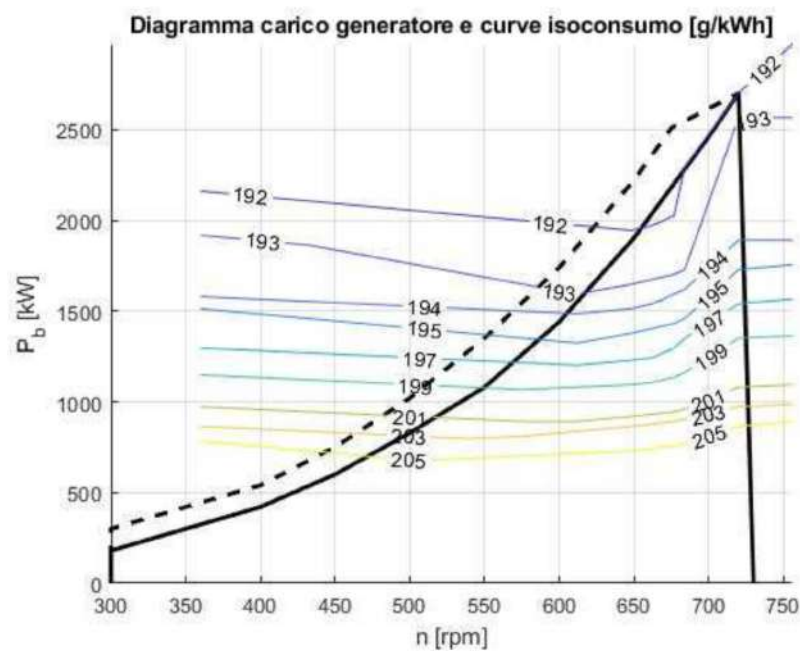

FIGURE A.1: Ro-ro ferry diesel engine Wärtsilä 6R32LN for electric generation

4 Wärtsilä 16V46C are the main propulsion engines. The propulsive power of each engine and the total fuel consumption (for 4 engines) are reported in Table A.1, one value for each combination of ship speed and propeller P/D.
Table A.1 is referred to the design draft of 7.4m.

TABLE A.1: Total Propulsion power (4 main diesel engines) and fuel consumption

	Ship speed	20	21	22	23	24	25	26	27	28	29	29.6	30	30.5
1 Engine PB [kW]	P/D													
	8.84	4549.8	5282.2	6004.4	6881.2	7744.3	8757.1	9825.2	11226.2	12605.5	14959.3	16452.1	17479.1	18800.4
	7.10	4559.6	5293.6	6017.5	6895.6	7761.0	8775.8	9846.3	11248.4	12629.6	14980.3	16471.3	17496.9	18816.5
	5.29	4559.7	5293.3	6017.6	6895.2	7760.8	8775.3	9845.7	11245.6	12625.5	14967.0	16452.1	17473.7	18788.0
	3.39	4554.8	5287.1	6011.0	6887.1	7752.0	8764.9	9834.0	11229.7	12606.6	14935.1	16411.6	17427.7	18734.4
	1.42	4551.1	5282.1	6005.8	6880.6	7745.0	8756.5	9824.4	11216.0	12589.9	14904.3	16371.6	17381.5	18680.1
	-0.62	4556.2	5287.6	6012.6	6887.6	7753.4	8765.5	9834.6	11224.2	12597.7	14900.3	16360.1	17364.9	18656.8
	-2.74	4581.0	5316.5	6045.8	6924.6	7795.9	8813.3	9888.6	11281.6	12660.4	14958.3	16415.5	17418.2	18707.9
	-4.94	4641.6	5388.0	6127.1	7016.2	7900.5	8931.7	10022.2	11428.9	12823.3	15130.7	16594.9	17601.5	18897.3
	-7.21	4765.2	5533.2	6291.9	7203.1	8113.5	9173.4	10295.1	11733.0	13161.7	15504.3	16992.4	18015.1	19330.8
Total FC [kg/h]	P/D													
	8.84	3603.5	4141.3	4659.4	5284.7	5885.7	6585.3	7356.8	8388.5	9328.1	11097.5	12174.5	12934.6	NaN
	7.10	3611.2	4150.1	4673.7	5295.9	5898.4	6599.4	7365.5	8409.3	9345.9	11111.7	12204.1	12947.7	NaN
	5.29	3611.3	4149.9	4676.4	5295.5	5898.2	6599.0	7373.1	8413.4	9344.1	11100.1	12201.8	12945.4	NaN
	3.39	3607.4	4145.1	4670.9	5289.3	5891.5	6591.2	7380.7	8409.2	9365.2	11110.6	NaN	NaN	NaN
	1.42	3604.5	4141.1	4667.7	5284.3	5886.2	6584.9	7389.9	8407.6	9391.4	NaN	NaN	NaN	NaN
	-0.62	3608.5	4145.5	4680.6	5289.6	5892.6	6623.4	7418.1	8422.7	NaN	NaN	NaN	NaN	NaN
	-2.74	3628.1	4168.2	4728.5	5322.7	5961.2	6714.8	NaN	NaN	NaN	NaN	NaN	NaN	NaN
	-4.94	3676.1	4228.7	4793.9	5416.3	6084.7	NaN	NaN	NaN	NaN	NaN	NaN	NaN	NaN
	-7.21	3774.1	4357.9	4918.1	NaN	NaN	NaN	NaN	NaN	NaN	NaN	NaN	NaN	NaN

B Appendix: Fuel consumption of hybrid propulsion.

B.1 Main engines fuel consumption

In Figure B.1 the project guide [79] values are reported for LNG mode and in Figure B.2 for HFO mode.

Engine MAN 51/60DF – Mechanical propulsion with CPP

975 kW/cyl., 500 rpm or 1,000 kW/cyl., 514 rpm

		L engine					V engine			
% Load		100	85	75	50	25	100	85	75	50	25
		Spec. fuel consumption in gas mode without attached pumps[1,2,3]									
Speed		constant = 514 rpm or 500 rpm									
a) Natural gas	kJ/kWh	7,385	7,422	7,855	8,432	10,238	7,435	7,472	7,895	8,462	10,238
b) Pilot fuel	g/kWh	2.0	2.3	2.7	4.4	12.0	2.0	2.3	2.7	4.4	12.0
	kJ/kWh	85	98	115	188	512	85	98	115	188	512
c) Total = a + b[4]	kJ/kWh	7,470	7,520[5]	7,970	8,620	10,750	7,520	7,570[5]	8,010	8,650	10,750
Speeds (±5 rpm)		514 (500)	514 (500)	501 (488)	462 (450)	402 (391)	514 (500)	514 (500)	501 (488)	462 (450)	402 (391)
a) Natural gas	kJ/kWh	7,385	7,422	7,455	7,562	8,038	7,435	7,472	7,455	7,572	8,038
b) Pilot fuel	g/kWh	2.0	2.3	2.7	4.4	12.0	2.0	2.3	2.7	4.4	12.0
	kJ/kWh	85	98	115	188	512	85	98	115	188	512
c) Total = a + b[4]	kJ/kWh	7,470	7,520[5]	7,570	7,750	8,550	7,520	7,570[5]	7,570	7,760	8,550

FIGURE B.1: SFOC MAN 51/60 in LNG mode

		L engine					V engine			
% Load		100	85	75	50	25	100	85	75	50	25
Speeds (±5 rpm)		514 (500)	514 (500)	501 (488)	462 (450)	402 (391)	514 (500)	514 (500)	501 (488)	462 (450)	402 (391)
		Spec. fuel oil consumption with HFO/MDO (DMB) without attached pumps[1,2,3]									
a) Main fuel	g/kWh	178.1	176.8	180.0	182.4	179.5	178.1	176.8	180.0	182.4	179.5
b) Pilot fuel	g/kWh	1.9	2.2	2.5	4.1	7.5	1.9	2.2	2.5	4.1	7.5
	kJ/kWh	81	94	107	175	320	81	94	107	175	320
c) Total = a + b[4]	g/kWh	180.0	179.0[5]	182.5	186.5	187.0	180.0	179.0[5]	182.5	186.5	187.0
	kJ/kWh	7,686	7,643	7,793	7,964	7,985	7,686	7,643	7,793	7,964	7,985

FIGURE B.2: SFOC MAN 51/60 in HFO mode

From this tables, it was possible to obtain the fuel mass flow rate for each engine working point, as reported in Table B.1.

	25%	50%	75%	85%	100%
Gas mode LNG	0.205	0.386	0.571	0.648	0.759
Gas mode pilot fuel MDO	0,015	0,011	0,010	0,010	0,010
Diesel mode HFO	0,224	0,456	0,675	0,751	0,891
Diesel mode pilot fuel HFO	0,009	0,010	0,009	0,009	0,010

TABLE B.1: Fuel mass flow rate for 1 main DF engine [kg/s]

B.2   Diesel generators fuel consumption

For the two main diesel generators Wärtsilä-Vasa 6R32LNE the precise fuel consumption was known in every load condition thanks to the curve reported in Figure B.3, evaluated by [95].
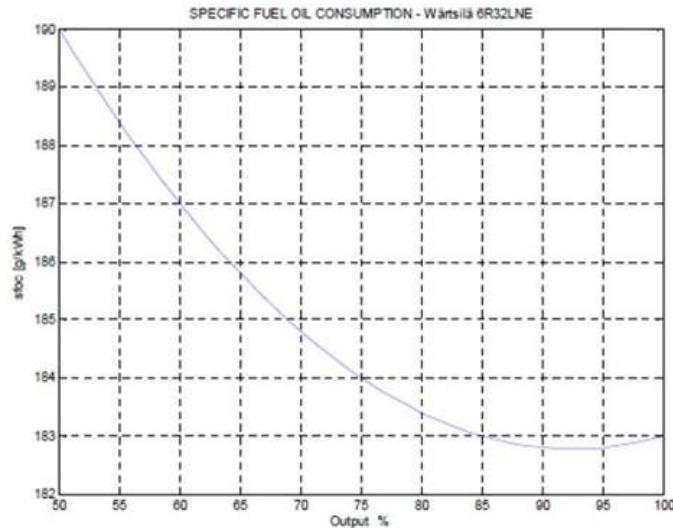

FIGURE B.3: SFOC DG Wärtsilä-Vasa 6R32LNE

Another small diesel generator was considered, the MAN 6L16/24 660kW, to work at low electric loads (for when recovery systems supply the majority of the request). From the manufacturers project guide, the fuel consumption were obtained, as reported in Figure.

L16/24 at 1200 rpm

5L16/24: 100 kW/cyl., 6-9L16/24: 110 kW/cyl.

% Load	100	85[1]	75	50	25
Spec. fuel consumption (g/kWh) with HFO/MDO without attached pumps [2] [3]	191	190[1]	189	194	213

[1] Fuel consumption at 85% MCR
[2] Tolerance +5%. Please note that the additions to fuel consumption must be considered before the tolerance is taken into account.
[3] Based on reference conditions, *see "Reference conditions"*

FIGURE B.4: SFOC DG MAN 6L16/24 660kW

B.3   Lower heat value

For the calculation of efficiency of Equations 3.1 and 3.2, the lower heat value (H_{ME} and H_{DG}) of each fuel is needed. The values used are reported in Table B.2.

H_{ME} LNG	49000 kJ/kg
H_{ME} HFO	42700 kJ/kg
H_{DG} MDO	42700 kJ/kg

TABLE B.2: Lower heat values

C Appendix: Rotor-engine integration.
Example of results.

In Section 6.4.2 the results of the numerical simulation of rotor-propeller-engine integration at the design ship speed are stated. In this Appendix some examples are reported for the selected case study for the engine Wärtsilä 6L26.

The rotor is in function in every case tested.

The Superimposition of the engine load diagram with propeller working points, calculated with the rotor ON, is reported in Figure C.1 for the most unfavorable (C.1a) and favorable (C.1b) wind.

(A) $V_{True} = 15 m/s$ from 0° (head wind).

(B) $V_{True} = 15 m/s$ from 100°
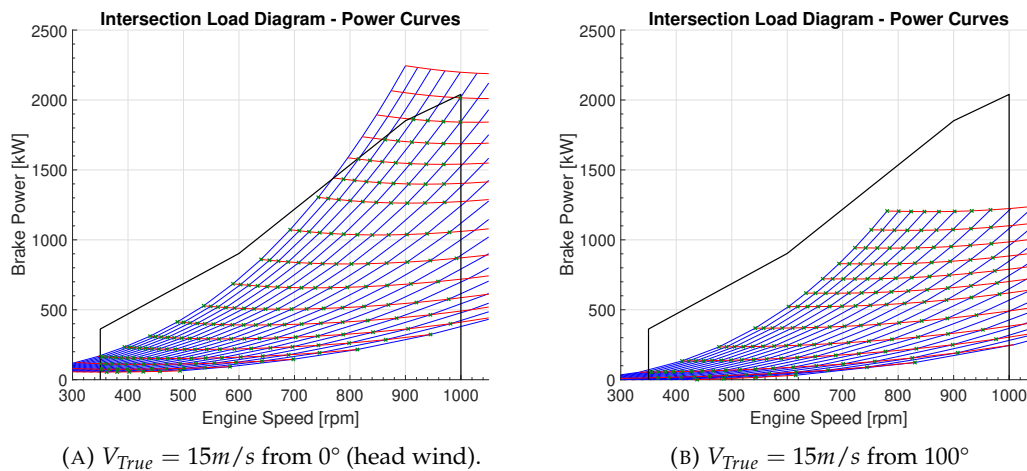
FIGURE C.1: Engine load diagram with propeller working points for V_{ship}=14 kn.

In Figure C.2 the curves of the hourly fuel consumption at the design ship speed, for fixed engine speed and variables P/D are reported. In Figure C.2a for the most unfavorable wind and in Figure C.2b for the most favorable wind.

In Figure C.3 the curves of the hourly fuel consumption at the design ship speed, for fixed propeller P/D and variable engine speed are reported. In Figure C.3a for the most unfavorable wind and in Figure C.3b for the most favorable wind.

(A) $V_{True} = 15m/s$ from $0°$

(B) $V_{True} = 15m/s$ from $100°$
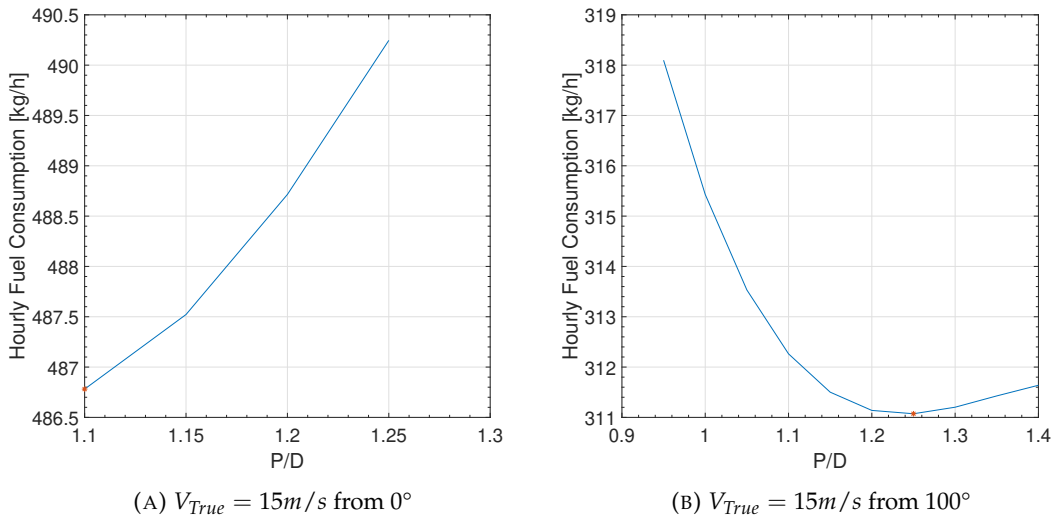
FIGURE C.2: Hourly fuel consumption curves at V_{ship}=14 knots and fixed n_e.

(A) $V_{True} = 15m/s$ from $0°$
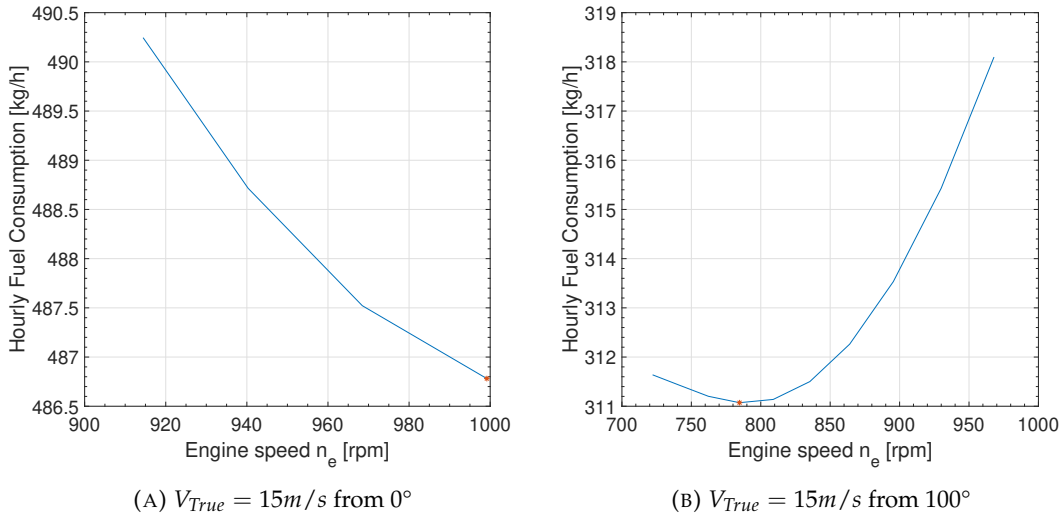

(B) $V_{True} = 15m/s$ from $100°$

FIGURE C.3: Hourly fuel consumption curves at V_{ship}=14 knots and fixed P/D.

In Figure C.4 the curves of the total propulsive power P_{TOT} are reported, in Figure C.4a for the most unfavorable wind and in Figure C.4b for the most favorable wind. The green line show the power when the rotor is ON and the red line is for the rotor OFF.

It can be observed that the rotor is beneficial in the cross wind condition and, on the contrary, it should be switched off in presence of head wind.

(A) $V_{True} = 15m/s$ from $0°$

(B) $V_{True} = 15m/s$ from $100°$
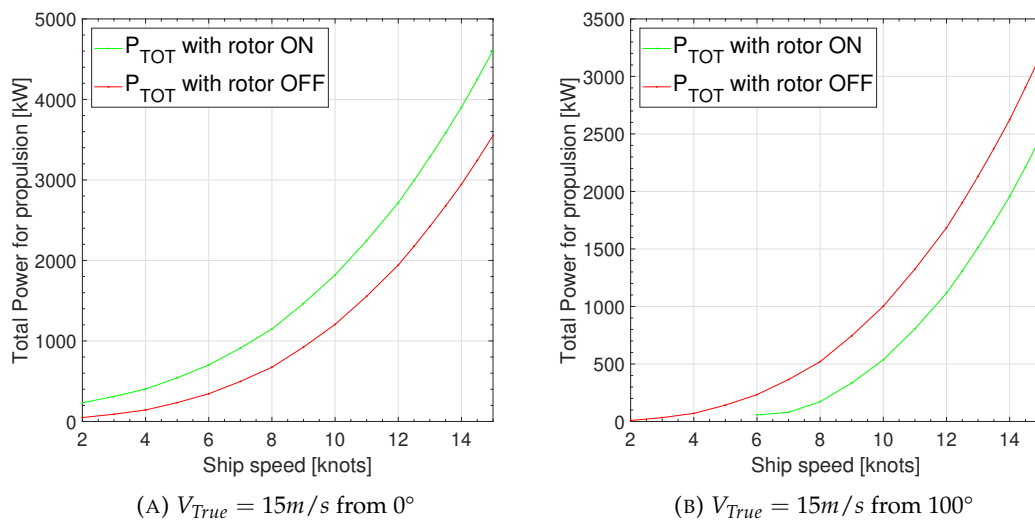
FIGURE C.4: Total Propulsion Power curves with and without rotor.

Bibliography

[1] M. Altosole, M. Figari, and F. Piastra. "Numerical modelling of high-speed diesel engines for small craft energy efficiency prediction". In: *Proceedings of HSMV 2014 - 10th Symposium on High Speed Marine Vehicles*. 2014.

[2] M. Altosole and Massimo Figari. "Effective simple methods for numerical modelling of marine engines in ship propulsion control systems design". In: *Journal of Naval Architecture and Marine Engineering* 8.2 (2011), 129–147. DOI: 10.3329/jname.v8i2.7366. URL: https://www.banglajol.info/index.php/JNAME/article/view/7366.

[3] M. Altosole et al. "Hybrid propulsion by gas engines for an ASD harbour tug". In: *Proceedings of 17th International Conference on Ships and Shipping Research, NAV 2012*. 2012.

[4] M. Altosole et al. "Real-time simulation of a COGAG naval ship propulsion system". In: *Proceedings of the Institution of Mechanical Engineers Part M: Journal of Engineering for the Maritime Environment* 223 (1 Jan. 2009), pp. 47–61. ISSN: 14750902. DOI: 10.1243/14750902JEME121.

[5] M. Altosole et al. "Simulation and performance comparison between diesel and natural gas engines for marine applications". In: *Journal of Engineering for the Maritime Environment* 231 (2 2017), pp. 690–704.

[6] M. Altosole et al. "Waste heat recovery from dual-fuel marine engines". In: *Maritime Transportation and Harvesting of Sea Resources* 1 (2016). Ed. by C. Guedes Soares and A.P. Teixeira, pp. 79–86.

[7] M. Altosole et al. "Waste heat recovery from marine gas turbines and diesel engines". In: *Energies* 10 (718 2017).

[8] M. Altosole et al. "Waste heat recovery systems from marine diesel engines: comparison between new design and retrofitting solutions". In: *Maritime Technology and Engineering - Proceedings of MARTECH 2014*. 2015, pp. 735–742.

[9] Marco Altosole, Ugo Campora, and Veronica Vigna. "Energy efficiency analysis of a flexible marine hybrid propulsion system". In: *2020 International Symposium on Power Electronics, Electrical Drives, Automation and Motion, SPEEDAM 2020*. 2020. DOI: 10.1109/SPEEDAM48782.2020.9161873.

[10] Marco Altosole et al. "Efficiency improvement of a natural gas marine engine using a hybrid turbocharger". In: *Energies* 11 (8 Aug. 2018). ISSN: 19961073. DOI: 10.3390/en11071924.

[11]   Marco Altosole et al. "High efficiency waste heat recovery from dual fuel marine engines". In: IOS Press, Jan. 2018, pp. 21–28. ISBN: 9781614998693. DOI: 10.3233/978-1-61499-870-9-21.

[12]   Marco Altosole et al. "Simulation study on the interaction between sailing and motor propulsion to optimize performance and control of the tall ship "Amerigo Vespucci"". In: *Developments in Maritime Transportation and Exploitation of Sea Resources - Proceedings of IMAM 2013, 15th International Congress of the International Maritime Association of the Mediterranean* (Oct. 2014), pp. 575–582.

[13]   Anemoi. URL: https://anemoimarine.com/flettner-rotor-efficiency/#example-saving-assessments (visited on 01/16/2022).

[14]   Anemoi. URL: https://anemoimarine.com/rotor-sail-technology/#technical-equipment (visited on 01/16/2022).

[15]   BBC. *COP26: US and EU announce global pledge to slash methane*. 2021. URL: https://www.bbc.com/news/world-59137828.

[16]   Marco Beccali and Fulvio Ardente. *Fisica tecnica - Esercizi*. Università degli Studi di Palermo, 2007.

[17]   Robert D Blevins. *Applied fluid dynamics handbook*. Van Nostrand Reinhold Company, 1984, p. 334.

[18]   G. Bordogna et al. "Experiments on a Flettner rotor at critical and supercritical Reynolds numbers". In: *Journal of Wind Engineering and Industrial Aerodynamics* 188 (2019). ISSN: 01676105. DOI: 10.1016/j.jweia.2019.02.006.

[19]   Jochim E. Brix. *Manoeuvering Technical Manual*. Seehafen Verlag GmbH, 1993, pp. 147, 243. ISBN: 3-87743-902-0.

[20]   *Bunkerindex*. URL: https://bunkerindex.com/. (accessed: May 2020).

[21]   *Bunkerindex*. URL: https://www.bunkerindex.com/. (accessed: April 2020).

[22]   Elisa Cadenasso and Arianna Fabbri. *Valorizzazione energetica a bordo nave di differenti tipologie di rifiuti (Master's degree thesis)*. Università degli Studi di Genova, 2017.

[23]   Ugo Campora and Massimo Figari. *Numerical simulation of ship propulsion transients and full-scale validation*. 2003.

[24]   C. Capasso, E. Notti, and O. Veneri. "Design of a hybrid propulsion architecture for midsize boats". In: *Energy Procedia* 158 (2019), pp. 2954–2959.

[25]   C. Capasso et al. "Preliminary design of the hybrid propulsion architecture for the research vessel "G. Dallaporta"". In: *Proceedings of ESARS-ITEC 2016, International Conference on Electrical Systems for Aircraft, Railway, Ship Propulsion and Road Vehicles and International Transportation Electrification Conference, Article number 7841342*. 2017.

[26] Ching Yuan Chang et al. "Major Products Obtained from the Pyrolysis of Oil Sludge". In: *Energy and Fuels* 14 (6 2000), pp. 1176–1183. ISSN: 08870624. DOI: 10.1021/ef0000532.

[27] Kin Wai Cheah et al. "Process simulation and techno economic analysis of renewable diesel production via catalytic decarboxylation of rubber seed oil – A case study in Malaysia". In: *Journal of Environmental Management* 203 (Dec. 2017), pp. 950–961. ISSN: 10958630. DOI: 10.1016/j.jenvman.2017.05.053.

[28] Shuo Cheng et al. "Pyrolysis of oil sludge with oil sludge ash additive employing a stirred tank reactor". In: *Journal of Analytical and Applied Pyrolysis* 120 (July 2016), pp. 511–520. ISSN: 01652370. DOI: 10.1016/j.jaap.2016.06.024.

[29] Emily Chou et al. "International policy, recommendations, actions and mitigation efforts of anthropogenic underwater noise". In: *Ocean and Coastal Management* 202 (Mar. 2021). ISSN: 09645691. DOI: 10.1016/j.ocecoaman.2020.105427.

[30] Todd Chou et al. "A Comeback of Wind Power in Shipping: An Economic and Operational Review on the Wind-Assisted Ship Propulsion Technology". In: *Sustainability* 13.4 (2021). ISSN: 2071-1050. DOI: 10.3390/su13041880. URL: https://www.mdpi.com/2071-1050/13/4/1880.

[31] B.R. Clayton. "Wind-assisted ship propulsion". In: *Physics in Technology* 18 (Nov. 2002), pp. 53–60. DOI: 10.1088/0305-4624/18/2/301.

[32] Carmen Colarusso. *Wind assisted propulsion optimization. Master Degree Thesis, University of Genoa*. Ed. by Massimo Figari and Veronica Vigna. 2021.

[33] T. Coppola, L. Micoli, and M. Turco. "Application of high temperature fuel cell powered by LNG on ferry boat: a case study". In: *Sustainable Developement Innovations in Marine Technologies* (2020). Ed. by P. Georgiev and C.G Soares, pp. 277–284.

[34] Hasan Islam Copuroglu and Emre Pesman. "Analysis of Flettner Rotor ships in beam waves". In: *Ocean Engineering* 150 (2018). ISSN: 00298018. DOI: 10.1016/j.oceaneng.2018.01.004.

[35] Costa Crociere. *Sea you tomorrow. On course for the future. Sustainability report 2015 Results and outlook*. 2015.

[36] Nastia Degiuli et al. "The impact of slow steaming on reducing CO2 emissions in the Mediterranean Sea". In: *Energy Reports* 7 (2021), pp. 8131–8141. ISSN: 2352-4847. DOI: https://doi.org/10.1016/j.egyr.2021.02.046. URL: https://www.sciencedirect.com/science/article/pii/S235248472100144X.

[37] A. DeMarco et al. "Flettner rotor concept for marine applications: A systematic study". In: *International Journal of Rotating Machinery* 2016 (2016). ISSN: 15423034. DOI: 10.1155/2016/3458750.

[38] *eConowind VentiFoil*. URL: https://www.econowind.nl/#about. (accessed: January 2022).

[39] EMSA European Maritime Safety Agency. *Preventing Pollution from Ships (2008, Lisboa).*

[40] Mahmoud Mohamed Eslam. "Recycling Marine Used Oil Using Green Ship Conversion Technique". In: SPE, Oct. 2019. DOI: 10.2118/198543-MS. eprint: https://onepetro.org/SPEGOTS/proceedings-pdf/19GOTS/1-19GOTS/D011S002R002/1181516/spe-198543-ms.pdf.

[41] EU. *Air emissions from maritime transport*. URL: https://ec.europa.eu/environment/air/sources/maritime.htm.

[42] EU. *European Climate Law*. URL: https://eur-lex.europa.eu/legal-content/EN/TXT/?uri=CELEX:32021R1119.

[43] EU. *MSFD Descriptor 11: Energy incl. Underwater Noise*. URL: https://ec.europa.eu/environment/marine/good-environmental-status/descriptor-11/index_en.htm.

[44] European Commission. *Full-length report Accompanying the document Report from the Commission 2020 Annual Report on CO2 Emissions from Maritime Transport.* 2021.

[45] Thor I. Fossen. *Handbook of Marine Craft Hydrodynamics and Motion Control*. 2011. DOI: 10.1002/9781119994138.

[46] Christos Frangopoulos. "Recent developments and trends in optimization of energy systems". In: *Energy* 164 (Sept. 2018). DOI: 10.1016/j.energy.2018.08.218.

[47] *Global Footprint Network*. URL: https://www.overshootday.org. (accessed: 22.07.2021).

[48] Eric Hanell. "Stena Bulk is presenting a prototype of the next-generation product and chemical tanker". In: *Press Release 2020-06-10* www.stenabulk.com (2020).

[49] Julia Hansson et al. "Alternative marine fuels: Prospects based on multi-criteria decision analysis involving Swedish stakeholders". In: *Biomass and Bioenergy* 126 (July 2019), pp. 159–173. ISSN: 18732909. DOI: 10.1016/j.biombioe.2019.05.008.

[50] Guangji Hu, Jianbing Li, and Guangming Zeng. "Recent development in the treatment of oily sludge from petroleum industry: A review". In: *Journal of Hazardous Materials* 261 (Oct. 2013), pp. 470–490. ISSN: 0304-3894. DOI: https://doi.org/10.1016/j.jhazmat.2013.07.069. URL: https://www.sciencedirect.com/science/article/pii/S0304389413005487.

[51] "Hybrid Turbocharger with Integrated High Speed Motor-generator". In: *Mitsubishi Heavy Industries* 44 (1 2007), pp. 1–3.

[52] IMO. *Addressing climate change - a decade of action to cut GHG emissions from shipping*. 2021. URL: https://wwwcdn.imo.org/localresources/en/MediaCentre/Documents/Addressing\%20climate\%20change\%20-\%20a\%20decade\%20of\%20action\%20to\%20cut\%20GHG\%20emissions\%20from\%20shipping_FINAL_(14-07-21)_Large.pdf.

[53] IMO. *Anti-fouling systems*. URL: https://www.imo.org/en/OurWork/Environment/Pages/Anti-fouling.aspx.

[54] IMO. *Ballast water management, the control of harmful invasive species*. URL: https://www.imo.org/en/MediaCentre/HotTopics/Pages/BWM-default.aspx.

[55] IMO. "Fourth Greenhouse Gas Study 2020". In: (2020). URL: https://www.imo.org/en/OurWork/Environment/Pages/Fourth-IMO-Greenhouse-Gas-Study-2020.aspx.

[56] IMO. *Further shipping GHG emission reduction measures adopted*. 2021.

[57] IMO. *Guidelines and relevant information under MARPOL Annex VI*. Note: Guideline 2014 MEPC 866, 30/01/17, pp 136-137 for conversion factors from fuel consumption to CO2 emissions. 2017.

[58] IMO. *IMO Train the Trainer (TTT) Course on Energy Efficient Ship Operation. Module 2: Ship Energy Efficiency Regulations and Related Guidelines*. 2016. URL: https://wwwcdn.imo.org/localresources/en/OurWork/Environment/Documents/Air\%20pollution/M2\%20EE\%20regulations\%20and\%20guidelines\%20final.pdf.

[59] IMO. *International Convention for the Prevention of Pollution from Ships (MARPOL)*. URL: https://www.imo.org/en/About/Conventions/Pages/International-Convention-for-the-Prevention-of-Pollution-from-Ships-(MARPOL).aspx.

[60] IMO. *MARPOL 73/78: articles, protocols, annexes, unified interpretations of the International Convention for the Prevention of Pollution from Ships, 1973, as modified by the protocol of 1978 relating thereto*. English. Consolidated ed., 2017. IMO London, 2017.

[61] IMO. *Recycling of ships*. URL: https://www.imo.org/en/OurWork/Environment/Pages/Ship-Recycling.aspx.

[62] IMO. *Ship noise*. URL: https://www.imo.org/en/MediaCentre/HotTopics/Pages/Noise.aspx#:~:text=IMO\%20adopted\%2C\%20in\%202012\%2C\%20a,noise\%20levels\%20on\%20board\%20ships..

[63] IMO Marine Environment Protection Committee. *Guidelines for voluntary use of the ship energy efficiency operational indicator (EEOI), MEPC.1/Circ.684*. IMO, 2009.

[64] IMO MEPC. *Resolution, MECP 212 (63/23), Annex 8. 2012. Guidelines to the Method of Calculation of the Attained Energy Efficiency Design Index (EEDI) for New Ships*.

[65] IMO MEPC 77/6/1. *Report of fuel oil consumption data submitted to the IMO Ship Fuel Oil Consumption Database in GISIS (Reporting year: 2020)*. 2021.

[66] Omer Berkehan Inal, Jean Frédéric Charpentier, and Cengiz Deniz. *Hybrid power and propulsion systems for ships: Current status and future challenges*. Mar. 2022. DOI: 10.1016/j.rser.2021.111965.

[67] *ISO 8217 2010 Fuel Standard for marine distillate fuel*. URL: https://www.standard.no/en/webshop/.

[68] S S Kim and S H Kim. "Pyrolysis kinetics of waste automobile lubricating oil". In: *Fuel* 79 ([15] Dec 2000), pp. 1943–1949. URL: www.elsevier.com/locate/fuel.

[69] Lukas Kistner et al. "Techno-economic and Environmental Comparison of Internal Combustion Engines and Solid Oxide Fuel Cells for Ship Applications". In: *Journal of Power Sources* 508 (Oct. 2021). ISSN: 03787753. DOI: 10.1016/j.jpowsour.2021.230328.

[70] K. Kume et al. "Evaluation of aerodynamic characteristics of a ship with Flettner rotors by wind tunnel tests and RANS-based CFD". In: *Ocean Engineering under review* (2022).

[71] Akshay Lele and K. V.S. Rao. "Net power generated by flettner rotor for different values of wind speed and ship speed". In: 2017. DOI: 10.1109/ICCPCT.2017.8074170.

[72] G. A. Livanos, G. Theotokatos, and D.N. Pagonis. "Techno-economic investigation of alternative propulsion plants for Ferries and RoRo ships". In: *Energy Conversion and Management* (2014), pp. 640–651.

[73] Lloyd's Register. *CII – Carbon Intensity Indicator*. URL: https://www.dnv.com/maritime/insights/topics/CII-carbon-intensity-indicator/implementation.html.

[74] Lloyd's Register. *Ship recycling. New regulatory requirements for owners*. URL: https://www.lr.org/en/insights/articles/ship-recycling-new-regulatory-requirements/.

[75] Lloyd's Register. "Ship Recycling. Practice and regulation today". In: (2011).

[76] Ruihua Lu and Jonas W. Ringsberg. "Ship energy performance study of three wind-assisted ship propulsion technologies including a parametric study of the Flettner rotor technology". In: *Ships and Offshore Structures* 15 (3 2020). ISSN: 17445302. DOI: 10.1080/17445302.2019.1612544.

[77] W. Addy Majewski and Hannu Jääskeläinen. *Exhaust Particulate Matter*. URL: https://dieselnet.com/tech/dpm.php#:~:text=Abstract\%3A\%20Exhaust\%20particulate\%20matter\%20(PM,diluted\%20and\%20cooled\%20exhaust\%20gases.&text=PM\%20contains\%20a\%20large\%20portion,PAH)\%20found\%20in\%20engine\%20exhaust.. (accessed: 20.01.2022).

[78]   MAN. *L16/24 Project Guide – Marine, Four stroke GenSet, compliant with IMO Tier II*. 2019.

[79]   MAN. *MAN 51/60DF Project Guide – Marine, Four stroke dual fuel engine, IMO Tier II / IMO Tier III*. 2014. URL: https://marine.man-es.com/four-stroke/engines/51-60df/features.

[80]   M. Martelli and M. Figari. "Numerical and experimental investigation for the performance assessment of full electric marine propulsion plant". In: *Maritime Transportation and Harvesting of Sea Resources* 1 (2018). Ed. by C. Guedes Soares and A.P. Teixeira, pp. 87–93.

[81]   M. Martelli and M. Figari. "Real-Time model-based design for CODLAG propulsion control strategies". In: *Ocean Engineering* 141 (2017), pp. 265–276. ISSN: 00298018. DOI: 10.1016/j.oceaneng.2017.06.029.

[82]   Michele Martelli et al. "Numerical modelling of propulsion, control and ship motions in 6 degrees of freedom". In: *Proceedings of the Institution of Mechanical Engineers Part M: Journal of Engineering for the Maritime Environment* 228 (4 Nov. 2014), pp. 373–397. ISSN: 20413084. DOI: 10.1177/1475090214544181.

[83]   Michela Mazzoccoli et al. "Marine Pollution Mitigation by Waste Oils Recycling Onboard Ships: Technical Feasibility and Need for New Policy and Regulations". In: *Frontiers in Marine Science* 7 (2020), p. 1057. ISSN: 2296-7745. DOI: 10.3389/fmars.2020.566363. URL: https://www.frontiersin.org/article/10.3389/fmars.2020.566363.

[84]   S. Michetti et al. "Ship control system wide integration and the use of dynamic simulation techniques in the FREMM project". In: *Proceedings of ESARS 2010, International Conference on Electrical Systems for Aircraft, Railway and Ship Propulsion. Article number 5665266*. 2010, pp. 1–6. DOI: 10.1109/ESARS.2010.5665266.

[85]   L. Mocerino et al. "A methodology for the design of an effective air quality monitoring network in port areas". In: *Scientific Reports* 10 (1 2020).

[86]   Norsepower. URL: https://www.norsepower.com/tankers (visited on 01/16/2022).

[87]   Norsepower. URL: https://www.norsepower.com/passenger/ (visited on 01/16/2022).

[88]   Norsepower. *Ro-ro vessel SC Connector*. 2021. URL: https://www.norsepower.com/sc-connector/ (visited on 10/05/2021).

[89]   Emilio Notti et al. "Experimental assessment of the fouling control coating effect on the fuel consumption rate". In: *Ocean Engineering* 188 (2019), p. 106233. ISSN: 0029-8018. DOI: https://doi.org/10.1016/j.oceaneng.2019.106233. URL: https://www.sciencedirect.com/science/article/pii/S0029801818309867.

[90]   OceanCare. *Underwater Noise: Consequences*. URL: https://www.oceancare.org/en/our-work/ocean-conservation/underwater-noise/underwater-noise-consequences/.

[91] Oceanco. *Oceanco delivers the 106.7m Black Pearl the largest dynarig sailing yacht in the world*. 2018. URL: https://www.oceancoyacht.com/oceanco-delivers-the-106-7m-black-pearl-the-largest-dynarig-sailing-yacht-in-the-world/ (visited on 10/05/2021).

[92] Yoshihisa Ono, Keiichi Shiraishi, and Yukio Yamashita. "Application of a Large Hybrid Turbocharger for Marine Electric-power Generation". In: *Mitsubishi Heavy Industries Technical Review* 49 (1 2012), pp. 29–33.

[93] Lorenzo Ottonello. *Impianto di propulsione non convenzionale per nave traghetto. Master Degree Thesis, University of Genoa*. Ed. by Ugo Campora, Marco Altosole, and Veronica Vigna. 2019.

[94] M. Petković et al. "Wind Assisted Ship Propulsion Technologies – Can they Help in Emissions Reduction?" In: *NAŠE MORE* 68 (2021), pp. 102–109. DOI: 10.17818/NM/2021/2.6. URL: https://doi.org/10.17818/NM/2021/2.6.

[95] Tazio Pieri. *Recupero del calore di scarto dei motori Dual-Fuel di una nave traghetto, Master's degree thesis, University of Genova*. 2016.

[96] M. Prussi et al. "Potential and limiting factors in the use of alternative fuels in the European maritime sector". In: *Journal of Cleaner Production* 291 (Apr. 2021). ISSN: 09596526. DOI: 10.1016/j.jclepro.2021.125849.

[97] Prame Punnaruttanakun et al. "Pyrolysis of API separator sludge". English. In: *Journal of Analytical and Applied Pyrolysis* 68-69.Complete (2003), pp. 547 –560. DOI: 10.1016/S0165-2370(03)00033-0.

[98] Dekeling R et al. *Monitoring Guidance for Underwater Noise in European Seas- Part II: Monitoring Guidance Specifications*. Technical guidance LB-NA-26555-EN-N. Luxembourg (Luxembourg), 2014. DOI: 10.2788/27158. URL: https://publications.jrc.ec.europa.eu/repository/handle/JRC88045.

[99] M Ringer, V Putsche, and J Scahill. *Large-Scale Pyrolysis Oil Production: A Technology Assessment and Economic Analysis*. 2006. URL: http://www.osti.gov/bridge.

[100] M. J.A. Romero et al. "Deoxygenation of waste cooking oil and non-edible oil for the production of liquid hydrocarbon biofuels". In: *Waste Management* 47 (Jan. 2016), pp. 62–68. ISSN: 18792456. DOI: 10.1016/j.wasman.2015.03.033.

[101] George N. Sakalis and Christos A. Frangopoulos. "Intertemporal optimization of synthesis, design and operation of integrated energy systems of ships: General method and application on a system with Diesel main engines". In: *Applied Energy* 226 (2018), pp. 991–1008.

[102] Agoes Santoso, Muhammad Badrus Zaman, and Arrijal Yudha Prawira. "Techno-economic Analysis of Rotor Flettner in Container Ship 4000DWT". In: *International Journal of Marine Engineering Innovation and Research* 1 (3 2017). ISSN: 2541-5972. DOI: 10.12962/j25481479.v1i3.2074.

[103] Harsh Sapra et al. "Integration of solid oxide fuel cell and internal combustion engine for maritime applications". In: *Applied Energy* 281 (Jan. 2021). ISSN: 03062619. DOI: 10.1016/j.apenergy.2020.115854.

[104] Ibrahim S. Seddiek and Nader R. Ammar. "Harnessing wind energy on merchant ships: case study Flettner rotors onboard bulk carriers". In: *Environmental Science and Pollution Research* (2021). ISSN: 16147499. DOI: 10.1007/s11356-021-12791-3.

[105] Jost Seifert. *A review of the Magnus effect in aeronautics*. 2012. DOI: 10.1016/j.paerosci.2012.07.001.

[106] Je Lueng Shie et al. "Pyrolysis of oil sludge with additives of catalytic solid wastes". In: *Journal of Analytical and Applied Pyrolysis* 71 (2 2004), pp. 695–707. ISSN: 01652370. DOI: 10.1016/j.jaap.2003.10.001.

[107] Je Lueng Shie et al. "Use of inexpensive additives in pyrolysis of oil sludge". In: *Energy and Fuels* 16 (1 Jan. 2002), pp. 102–108. ISSN: 08870624. DOI: 10.1021/ef0100810.

[108] SkySails Marine. *SkySails Propulsion Systems*. URL: https://skysails-marine.com/products.html (visited on 10/05/2021).

[109] Brandon L. Southall et al. "Marine mammal noise exposure criteria: Updated scientific recommendations for residual hearing effects". In: *Aquatic Mammals* 45 (2 2019), pp. 125–232. ISSN: 01675427. DOI: 10.1578/AM.45.2.2019.125.

[110] D. Stapersma and Hk Woud. "Matching propulsion engine with propulsor". In: *Journal of Marine Engineering and Technology* 4 (2 2005), pp. 25–32. ISSN: 20568487. DOI: 10.1080/20464177.2005.11020189.

[111] Marcin Stec et al. "Reducing the energy efficiency design index for ships through a post-combustion carbon capture process". In: *International Journal of Greenhouse Gas Control* 108 (2021), p. 103333. ISSN: 1750-5836. DOI: https://doi.org/10.1016/j.ijggc.2021.103333. URL: https://www.sciencedirect.com/science/article/pii/S1750583621000852.

[112] M. Tadros, M. Ventura, and C. Guedes Soares. "Optimization procedure to minimize fuel consumption of a four-stroke marine turbocharged diesel engine". In: *Energy* 168 (2019), pp. 897–908. ISSN: 0360-5442. DOI: https://doi.org/10.1016/j.energy.2018.11.146. URL: https://www.sciencedirect.com/science/article/pii/S0360544218323570.

[113] L. Talluri, D. K. Nalianda, and E. Giuliani. "Techno economic and environmental assessment of Flettner rotors for marine propulsion". In: *Ocean Engineering* 154 (2018). ISSN: 00298018. DOI: 10.1016/j.oceaneng.2018.02.020.

[114] Prapisala Thepsithar. *Alternative Fuels for International Shipping*. 2020.

[115] Michael Traut et al. "Propulsive power contribution of a kite and a Flettner rotor on selected shipping routes". In: *Applied Energy* 113 (2014). ISSN: 03062619. DOI: 10.1016/j.apenergy.2013.07.026.

[116] Andrew Turner. "Marine pollution from antifouling paint particles". In: *Marine Pollution Bulletin* 60.2 (2010), pp. 159–171. ISSN: 0025-326X. DOI: `https://doi.org/10.1016/j.marpolbul.2009.12.004`. URL: `https://www.sciencedirect.com/science/article/pii/S0025326X09005050`.

[117] Mihail Vlad Vasilescu et al. "Influence of four modern Flettner rotors, used as wind energy capturing system, on container ship stability". In: vol. 180. 2020. DOI: `10.1051/e3sconf/202018002003`.

[118] V. Vigna et al. "A ship energy efficiency analysis by considering trim influence and waste recycling". In: *Georgiev, P., Soares, C.G. (Eds.). (2019). Sustainable Development and Innovations in Marine Technologies (1st ed.). CRC Press.* (2019).

[119] Wallenius Wilhelmsen. *Orcelle Wind – introducing the world's first wind-powered RoRo vessel*. 2021. URL: `https://www.walleniuswilhelmsen.com/news-and-insights/highlighted-topics/orcelle` (visited on 10/05/2021).

[120] Huaiyu Wang et al. "Emission and Performance Optimization of Marine Four-Stroke Dual-Fuel Engine Based on Response Surface Methodology". In: *Mathematical Problems in Engineering* 2020 (Jan. 2020), pp. 1–9. DOI: `10.1155/2020/5268314`.

[121] Zhiqi Wang et al. "Low temperature pyrolysis characteristics of oil sludge under various heating conditions". In: *Energy and Fuels* 21 (2 Mar. 2007), pp. 957–962. ISSN: 08870624. DOI: `10.1021/ef060628g`.

[122] WHO World Health Organisation. "Ambient (outdoor) air pollution". In: (2021). URL: `https://www.who.int/news-room/fact-sheets/detail/ambient-(outdoor)-air-quality-and-health`.

[123] Windy forecast. URL: `https://windy.app/forecast2/spot/261440/Marina+Messina\%2C+Italy/statistics` (visited on 11/20/2020).

[124] Qingji Zhou et al. "Factors influencing green ship recycling: A conceptual framework and modeling". In: *Journal of Cleaner Production* 322 (Nov. 2021). ISSN: 09596526. DOI: `10.1016/j.jclepro.2021.129155`.